

University of Central Florida

STARS

Graduate Thesis and Dissertation 2023-2024

2024

Opto-Electronic Oscillator driven Electro-Optic Modulator based Optical Frequency Comb

Lawrence Trask

University of Central Florida

Find similar works at: <https://stars.library.ucf.edu/etd2023>

University of Central Florida Libraries <http://library.ucf.edu>

This Doctoral Dissertation (Open Access) is brought to you for free and open access by STARS. It has been accepted for inclusion in Graduate Thesis and Dissertation 2023-2024 by an authorized administrator of STARS. For more information, please contact STARS@ucf.edu.

STARS Citation

Trask, Lawrence, "Opto-Electronic Oscillator driven Electro-Optic Modulator based Optical Frequency Comb" (2024). *Graduate Thesis and Dissertation 2023-2024*. 461.

<https://stars.library.ucf.edu/etd2023/461>

OPTO-ELECTRONIC OSCILLATOR DRIVEN ELECTRO-OPTIC MODULATOR BASED
OPTICAL FREQUENCY COMB

by

LAWRENCE ROBERT TRASK

B.S. Electrical Engineering, University of California San Diego, 2016

M.S. Optics and Photonics, University of Central Florida, 2020

A dissertation submitted in partial fulfilment of the requirements
for the degree of Doctor of Philosophy
in the College of Optics and Photonics
at the University of Central Florida
Orlando, Florida

Spring Term
2024

Major Professor: Peter J. Delfyett

© 2024 Lawrence Robert Trask

ABSTRACT

Optical frequency combs (OFC) are now a well-known tool for utilizing broad optical bandwidths with electronic resolution. Several applications including spectroscopy, metrology, ultra-wideband signal processing, and communications are being propelled forward by optical frequency combs. The advent of high repetition rate optical frequency combs for use in astrophotonics has elucidated the need for newer architectures. This dissertation discloses a self-oscillating, self-stabilizing, and self-referenced opto-electronic oscillator (OEO) driven electro-optic modulated (EOM) based optical frequency comb. We demonstrate a new path towards high repetition rate OFCs with two major developments. The use of a photonicly filtered OEO simultaneously stabilizes the optical carrier frequency and generates a spectrally pure & stable ~ 10 GHz RF signal. The generated oscillation signal is then used to drive a cascade of electro-optic modulators to create a ~ 10 GHz repetition rate EOM comb. A new all-fiber based nonlinear pulse compressor for conditioning picosecond pulses, with pico-Joule pulse energies where 60% of the energy lies in the pedestal. The compressor can produce pulses under 200 fs in duration with nanojoule pulse energies and high contrast. This all-fiber approach removes the need for expensive pulse-shapers and operates solely on nonlinear fiber dynamics. Finally, we detect the carrier-envelope-offset frequency (f_0) of the OEO EOM OFC through f-2f interferometry. This represents the first time a self-oscillating ~ 10 GHz repetition rate comb source has been self-referenced.

To my wife, Meixi, who continues to knock some sense into me.

ACKNOWLEDGMENTS

I would like to acknowledge my advisor, Prof. Peter J. Delfyett, for giving me the opportunity to conduct world class science and a space to let my ideas flourish. I would also like to acknowledge the current and past members of the UP group during my time. Amongst them, Srinivas Varma Pericherla, Dr. Ricardo Bustos Ramirez, and Dr. Chinmay Shirpurkar who I have had the pleasure of working together with. Especially Srinivas Varma Pericherla, who's aid allowed me to finish this work. In addition, I would like to acknowledge Dr. Stefan Gausman, Dr. Matthew Cooper, Joseph Wahlen, and Caleb Dobias for teaching me all about fiber optics. To my friends and family, for listening to my incessant complaints about the difficulties in science and their continued support. Finally, I would like to acknowledge CREOL as a whole for giving me a chance at turning my life around.

TABLE OF CONTENTS

LIST OF FIGURES	x
CHAPTER 1: INTRODUCTION	1
Optical Frequency Combs	1
Generation of Optical Frequency Combs in telecom band	4
EOM Combs	4
Mode-locked laser based frequency combs	6
Fiber based mode-locked lasers	7
Semiconductor based mode-locked lasers	8
Kerr-ring resonator based frequency combs	11
Thesis Outline	12
CHAPTER 2: GENERATION OF A LOW NOISE AND STABLE 10 GHZ COMB SOURCE	
14	
Construction of an EOM comb	14
CW laser	16
Electro-optic modulation	17

Compressed pulses	18
External RF source	20
EOM comb experiment	22
Pound-Drever-Hall locking	24
Modified Pound-Drever-Hall locking using a tunable etalon	28
Pound-Drever-Hall locking on an EOM comb	31
Optoelectronic Oscillators	34
Photonically filtered opto-electronic oscillators	36
Optically filtered and stable electro-optic modulated comb without an external RF source	38
Opto-electronic oscillator driven electro-optic modulated comb	44
CHAPTER 3: OPTICAL FILTERING USING A TUNABLE ETALON	48
Optical Cavity Dispersion and FSR walk-off	48
Tunable etalon background	53
Construction of a tunable etalon (3k finesse)	55
Construction of a tunable etalon (600 finesse)	59
CHAPTER 4: HIGH CONTRAST NONLINEAR PULSE COMPRESSION	65
Self-Phase Modulation	66

Self phase modulation in fiber	67
Linear Pulse Shaping	76
Saturable Absorption	80
Nonlinear Loop Mirrors	81
CHAPTER 5: ULTRASHORT PULSE AMPLIFICATION	94
Ultrashort pulse amplification in Erbium doped fiber amplifiers	94
Watt Class EDFAs	99
Gain narrowing	103
Pulse-picking	105
Pulse-pick by 64	107
Pulse-pick by 8	109
CHAPTER 6: COHERENT OCTAVE SPANNING SUPERCONTINUUM GENERATION FOR CARRIER-ENVELOPE-OFFSET FREQUENCY DETECTION	115
Theoretical background: Supercontinuum Generation	115
Experimental Work: Supercontinuum generation	120
Carrier-Envelope-Offset Frequency Detection	124
Nonlinear waveguides for coherent octave spanning supercontinuum generation	131

CHAPTER 7: CARRIER ENVELOPE OFFSET FREQUENCY EXPERIMENTS	134
Pulse-picking By 64 Experiments	134
Pulse-picking by 8 Experiments	138
CHAPTER 8: CONCLUSION	141
Future work	142
LIST OF REFERENCES	144

LIST OF FIGURES

1.1	(a) Time domain representation of an optical frequency comb, (b) frequency domain representation of an optical frequency comb	2
1.2	Schematic of a simple EOM comb driven by a single external RF source. CW: continuous-wave laser, PM: electro-optic phase modulator, IM: electro-optic intensity modulator, RF: external RF oscillator.	4
1.3	Passive mode-locking in a FMLL using a NALM (a) figure-of-eight laser (b) figure-of-nine laser	8
1.4	A schematic of an external cavity HML SCMLL where SA: saturable absorber, PBS: polarization beam splitter, SOA: semiconductor optical amplifier, Dispersion 1 and Dispersion 2 are dual grating compressors	9
1.5	Schematic of a fully integrated SCMLL with a saturable absorber and metal pads to enable HML. Where SA: saturable absorber.	10
1.6	Frequency domain picture of pumping a Kerr microring resonator	11
2.1	Simulated EOM comb consisting of four phase modulators (assuming $V_{\pi} = 4V$) using a noiseless external RF source with 3 W RF power into each phase modulator showing the a) normalized spectral intensity and b) the temporal waveform	18

2.2	<p>Simulated EOM comb consisting of four phase modulators (assuming $V_{\pi} = 4V$) using a noiseless external RF source with 3 W of RF into the phase modulators power showing the a) pulse profile after linear chirp (blue) with the transform limited pulse (red), b) the autocorrelation of the pulse profile after linear chirp (blue) with the transform limited autocorrelation of the pulse (red).</p>	19
2.3	<p>Sample 10 GHz RF synthesizer phase noise breakdown, taken from "Keysight Technologies Solutions for Reducing Phase Noise at RF and Microwave Frequencies Application Note".</p>	21
2.4	<p>a) Schematic of an EOM comb using 2 phase modulators and one intensity modulator driven by a common RF synthesizer at 12 GHz. PDH: Pound-Drever-Hall locking, PC: polarization controller, PM: phase modulator, MZM: intensity modulator, PS: RF phase shifter, RF Amps: RF amplifiers, Finisar Waveshaper: Liquid Crystal on Silicon pulse-shaper. b) Measured optical spectrum, c) Measured intensity autocorrelation</p>	23
2.5	<p>a) Experimental schematic of an EOM comb using four phase modulators and one intensity modulator driven by a common RF synthesizer at 10.5 GHz. PC: polarization controller, PM: phase modulator, MZM: intensity modulator, PS: RF phase shifter, AOM: acousto-optic modulator, VCO: voltage controlled oscillator, PID: proportional-integral-derivative controller. b) Measured optical spectrum, c) Measured compressed intensity autocorrelation</p>	25
2.6	<p>a) Transmission response of an etalon with respect to optical frequency, b) transmission and reflection profile of a single etalon resonance, c) reflected phase profile of a single etalon resonance.</p>	26

2.7	PDH error signal when a phase modulated CW laser sweeps across an etalon resonance.	27
2.8	Schematic for locking a CW laser to a 100k finesse etalon through PDH. AOM: acousto-optic modulator, PM: phase modulator, FPE: Fabry-Perot etalon, ISO: fiber pigtailed isolator, VCO: voltage-controlled oscillator, PID: proportional-integral-derivative controller, LPF: low pass filter, PD: photodiode, RF Amp: RF amplifier, RF Synth: RF synthesizer.	28
2.9	Schematic for measuring residual phase noise before and after a haphazardly built tunable etalon. EOM: cascade of electro-optic modulators, SOA: semiconductor optical amplifier, PS: RF phase shifter, ATT: RF variable attenuator, PDH:-Pound-Drever-Hall locking, EDFA: erbium doped fiber amplifier, WS: Finisar waveshaper, RFSA: RF spectrum analyzer, Phase Noise test set: HP carrier noise test set for measuring phase noise.	29
2.10	Residual phase noise measurement (blue) before locking tunable etalon to EOM comb, (red) after locking tunable etalon to EOM comb, (black) noise floor dictated by phase noise of synthesizer and amplifier	30
2.11	Architecture for generating filtered EOM combs via PDH locking of the EOM comb to a 100k finesse etalon. AOM: acousto-optic modulator, ISO: fiber pigtailed isolator, PC: polarization controller, SOA: semiconductor optical amplifier, PM: phase modulator, MZM: intensity modulator, EDFA: Erbium doped fiber amplifier, FPE: 100k finesse Fabry-Perot etalon, VCO: voltage controlled oscillator, RF Amps: RF amplifiers, PS: RF phase shifter, Att: optical attenuator, LPF: low pass filter, PID: proportional-integral-derivative controller.	32

2.12	Transmission response of a single resonance of the 100k finesse etalon in dB scale. 100k finesse etalon specs: 100k finesse, ~ 1.5 GHz FSR, FWHM: ~ 15 kHz.	33
2.13	Diagnostic traces of PDH locked EOM comb employing two phase modulators and one intensity modulator: a) Optical spectrum before etalon (black) and after etalon (red), b) photodetected RF beat note after the etalon, c) intensity autocorrelation externally compressed and measured after the etalon.	34
2.14	Schematic representation of a basic OEO using optical fiber as the high Q optical cavity and an RF filter as a high Q electronic cavity.	35
2.15	a) Schematic diagram of an RF filtered OEO, b) RF frequency spectrum of an RF filtered OEO, c) schematic diagram of a photonically filtered OEO, d) optical spectrum of the photonically filtered OEO, e) RF spectrum of the photonically filtered OEO.	37
2.16	Schematic of the optically filtered OEO EOM comb employing 4 phase modulators and 1 intensity modulator for comb generation. AOM: acousto-optic modulator; PM: phase modulator; MZM: intensity modulator; EDFA: erbium doped fiber amplifier; FPE: 100k finesse ULE quartz spaced Fabry Perot etalon; att: adjustable attenuator; PD: photodetector; ISO: isolator; BPF: bandpass filter; PS: phase shifter; VCO: voltage-controlled oscillator; PID: servo controller; LPF: low pass filter	39
2.17	Normalized acousto-optic modulator response with respect to input drive frequency (black) and normalized output power response after EDFA 2 with respect to frequency (red).	40

2.18	(a) Optical spectrum of the optically filtered OEO EOM comb before (black) and after the etalon (red). (b) Optical spectrum of the OEO EOM comb after the etalon with high 2 sensitivity. (c) RF spectrum at RF output 1 (red) and RF output 2 (black) of the optically filtered OEO EOM comb. (d) Externally compressed and measured SHG Intensity autocorrelation of optically filtered OEO EOM comb (black), calculated transform limited pulse autocorrelation from optical spectrum (red), and calculated transform limited pulse from optical spectrum (blue).	42
2.19	(a) Measured absolute phase noise at RF output 1 of the optically filtered OEO EOM comb. (b) Measured fractional frequency stability at RF output 1 of the optically filtered OEO EOM comb.	44
2.20	OEO EOM comb schematic diagram with 4 phase modulators placed after the etalon. AOM: acousto-optic modulator, EDFA: Erbium doped fiber amplifier, MZM: intensity modulator, PM: phase modulator, FPE: Fabry-Perot etalon, Att.: attenuator, RF Amp: RF amplifier, LPF: low pass filter, PID: proportional-integral-derivative controller, VCO: voltage controlled oscillator, RF Amp: RF amplifier, ISO: RF isolator, BPF: RF bandpass filter center frequency of 10.486 GHz and 10 MHz passband, PS: RF phase shifter, RF switch: RF absorptive switch.	46
2.21	Diagnostic traces of the OEO EOM comb: a) optical spectrum, b) RF spectrum measured at the RF output, externally compressed and measured second harmonic intensity autocorrelator.	47

3.1	a) Schematic for testing optical bandwidth limitation of 100k finesse etalon. AOM: acousto-optic modulator, ISO: fiber pigtailed isolator, PC: polarization controller, SOA: semiconductor optical amplifier, PM: phase modulator, MZM: intensity modulator, EDFA: erbium doped fiber amplifier, HNLF: 100 m of normal dispersion highly nonlinear fiber, FPE: 100k finesse Fabry-Perot etalon, VCO: voltage controlled oscillator, RF Amps: RF amplifiers, PS: RF phase shifter, LPF: low pass filter, PID: proportional-integral-derivative controller. b) Normalized optical spectrum of the nonlinearly broadened EOM comb before (black) and after the 100k finesse etalon (red). c) Normalized optical spectrum of the etalon throughput for different repetition rates: 11.9851414 GHz (black) and 11.9851415 GHz (red)	49
3.2	Reflected phase data of ultrahigh reflectivity crystalline mirrors provided by Thorlabs. Top: Reflected phase with respect to wavelength. Middle: Calculated group delay with respect to wavelength, Bottom: Calculated group delay dispersion with respect to wavelength.	51
3.3	Theoretical Fabry-Perot etalon free-spectral range with respect to wavelength using Thorlabs crystalline mirrors assuming a cavity with designed FSR=14.986 GHz and Finesse=200,000.	52
3.4	Theoretical transmission of a tunable etalon with FSR=14.9896229 GHz. In blue, the etalon resonances with no mirror translation. In red, the etalon resonances when the front mirror has translated backward by 100 nm. In magenta, the etalon resonances when the front mirror has translated forward by 100 nm.	53

3.5	Schematic of a tunable etalon employing a flat-curved mirror configuration and a brass block as an anchor. M: mirror, KC1T: Thorlabs 30 mm cage compatible mount.	55
3.6	Front, rear, and top view of the CAD file of the metallic block used as an anchor for the tunable etalon.	55
3.7	Photograph of the newly constructed $\sim 3k$ finesse tunable etalon employing flat-curved mirror configuration and mirror reflectivities of 99.97% and FSR ~ 10.5 GHz.	56
3.8	a) Schematic for testing the performance of the tunable etalon. PM: phase modulator, Tetalon: Tunable etalon, Att: RF attenuator, PD: photodiode, PZT: High voltage piezo driver, RF Amp: RF amplifier, RF Amp: RF amplifier, LPF: Low pass filter, PID: proportional-integral-derivative controller. b) Optical spectrum of the OEO EOM comb before passing through the tunable etalon (black) and after locking the tunable etalon to the OEO EOM comb.	58
3.9	Schematic of a ~ 600 finesse tunable etalon employing a curved-curved mirror configuration anchored by a steel block. M: mirror, KC1T: thorlabs 30 mm cage compatible mount.	60
3.10	Photodetected ASE beat note of the ~ 600 finesse etalon.	61

3.11	Schematic for measuring the FSR of ~ 600 finesse tunable etalon using an EOM comb with spectral broadening. AOM: acousto-optic modulator, ISO: fiber pigtailed isolator, PC: polarization controller, EDFA: Erbium doped fiber amplifier, PM: phase modulator, FPE: 100k finesse Fabry-Perot etalon, RF Amp: RF amplifier, PD: photodiode, LPF: low pass filter, PID: proportional-integral-derivative controller, VCO: voltage controlled oscillator, MZM: intensity modulator, RF synth: RF synthesizer, Att: RF attenuator, PZT: high voltage piezo controller.	62
4.1	Conceptual diagram of self phase modulation. Top: input intensity profile of an optical pulse in nonlinear medium. Bottom: instantaneous frequency of pulse after undergoing SPM.	67
4.2	Intensity autocorrelation traces showing soliton compression in single mode fiber.	68
4.3	Simulated parabolic pulse propagation by nonlinearly propagating a Gaussian pulse in a normal dispersion fiber.	70

4.4	<p>Experimental work of spectral broadening an EOM comb (consisting of two phase modulators and one intensity modulator driven by a common RF synthesizer at 10 GHz) using 100 m of anomalous dispersion HNLF from OFS.</p> <p>a) Schematic representation of spectrally broadening an EOM comb using anomalous dispersion HNLF. PDH: Pound-Drever-Hall locking, FPE: Fabry-Perot etalon, EOM: cascade of electro-optic modulators, SOA: semiconductor optical amplifier, β_2: linear chirp for compressing EOM comb pulses, EDFA: erbium doped fiber amplifier, HNLF: anomalous dispersion HNLF.</p> <p>b) Optical spectrum of EOM comb before broadening, c) compressed intensity autocorrelation of EOM comb, d) optical spectrum of EOM comb after amplification to 100 mW and spectral broadening in 100 m of HNLF, e) intensity autocorrelation of spectrally broadened EOM comb with average power 100 mW, f) optical spectrum of EOM comb after amplification to 300 mW and spectrally broadened by HNLF, g) intensity autocorrelation of spectrally broadened EOM comb with average power 300 mW.</p>	72
-----	-----------------------------------------------------------------------------------------------------------------------------------------------------------------------------------------------------------------------------------------------------------------------------------------------------------------------------------------------------------------------------------------------------------------------------------------------------------------------------------------------------------------------------------------------------------------------------------------------------------------------------------------------------------------------------------------------------------------------------------------------------------------------------------------------------------------------------------------------------------------------------------------------------------------------------------------------------------------------------------------------------------------------------------------------------------------------------------------------------------------------------------------	----

4.5	<p>Experimental work of spectral broadening an EOM comb (consisting of two phase modulators and one intensity modulator driven by a common RF synthesizer at 10 GHz) using 100 m of zero dispersion HNLF from OFS. a) Schematic representation of spectrally broadening an EOM comb using zero dispersion HNLF. PDH: Pound-Drever-Hall locking, FPE: Fabry-Perot etalon, EOM: cascade of electro-optic modulators, SOA: semiconductor optical amplifier, β_2: linear chirp for compressing EOM comb pulses, EDFA: erbium doped fiber amplifier, HNLF: zero dispersion HNLF. b) Optical spectrum of EOM comb before broadening, c) compressed intensity autocorrelation of EOM comb, d) optical spectrum of EOM comb after amplification to 100 mW and spectral broadening in 100 m of HNLF, e) intensity autocorrelation of spectrally broadened EOM comb with average power 100 mW, f) optical spectrum of EOM comb after amplification to 300 mW and spectrally broadened by HNLF, g) intensity autocorrelation of spectrally broadened EOM comb with average power 300 mW.</p>	73
-----	------------------------------------------------------------------------------------------------------------------------------------------------------------------------------------------------------------------------------------------------------------------------------------------------------------------------------------------------------------------------------------------------------------------------------------------------------------------------------------------------------------------------------------------------------------------------------------------------------------------------------------------------------------------------------------------------------------------------------------------------------------------------------------------------------------------------------------------------------------------------------------------------------------------------------------------------------------------------------------------------------------------------------------------------------------------------------------------------------------	----

4.6	Experimental work of spectral broadening an EOM comb (consisting of two phase modulators and one intensity modulator driven by a common RF synthesizer at 10 GHz) using 100 m of normal dispersion HNLF from OFS. a) Schematic representation of spectrally broadening an EOM comb using normal dispersion HNLF. PDH: Pound-Drever-Hall locking, FPE: Fabry-Perot etalon, EOM: cascade of electro-optic modulators, SOA: semiconductor optical amplifier, β_2 : linear chirp for compressing EOM comb pulses, EDFA: erbium doped fiber amplifier, HNLF: normal dispersion HNLF. b) Optical spectrum of EOM comb before broadening, c) compressed intensity autocorrelation of EOM comb, d) optical spectrum of EOM comb after amplification to 100 mW and spectral broadening in 100 m of HNLF, e) intensity autocorrelation of spectrally broadened EOM comb with average power 100 mW, f) optical spectrum of EOM comb after amplification to 300 mW and spectrally broadened by HNLF, g) intensity autocorrelation of spectrally broadened EOM comb with average power 300 mW.	75
4.7	Schematic of a commercially available grating based pulse shaper from Finisar (now Coherent).	77
4.8	Schematic representation of an EOM comb spectrally broadened by HNLF, reshaped using a linear pulse shaper, and then amplified again. MZM: intensity modulator, PM: phase modulator, PDH: Pound-Drever-Hall lock, β_2 : linear chirp for compressing EOM comb, EDFA: erbium doped fiber amplifier, HNLF: 100 m of highly nonlinear fiber, pulse-shaper: grating based pulse shaper.	78

4.9	Associated data of an EOM comb spectrally broadened and shaped using pulse shaper. a) Optical spectrum of the 33 GHz EOM comb using 2 phase modulators and 1 intensity modulator, b) optical spectrum of EOM comb after amplification to .5 W and subsequent nonlinear spectral broadening in 100 m of HNLF before shaping (green) and after spectral flattening in 5 nm increments (black), c) intensity autocorrelation trace of spectrally broadened EOM without shaping (green) and with shaping in 5 nm increments (black), d) optical spectrum of spectrally broadened EOM after full line by line shaping, e) intensity autocorrelation of spectrally broadened EOM comb after full line by line shaping (black) and transform limited autocorrelation (red). . . .	79
4.10	Simplified diagram of a nonlinear amplifying loop mirror.	82
4.11	Experimental work of nonlinear pulse compression using a 40/60 NOLM on an EOM comb (with 2 phase modulators driven by an external RF synthesizer at 10.5 GHz) locked and filtered by our 100k finesse etalon. a) AOM: acousto-optic modulator, ISO: fiber pigtailed isolator, PC: polarization controller, SOA: semiconductor optical amplifier, PM: phase modulator, MZM: intensity modulator, EDFA: Erbium doped fiber amplifier, FPE: 100k finesse Fabry-Perot etalon, SMF: 540 m of standard single mode fiber, VCO: voltage controlled oscillator, RF Amps: RF amplifiers, PS: RF phase shifter, Att: optical attenuator, LPF: low pass filter, PID: proportional-integral-derivative controller, 40/60: 40/60 fiber optic coupler, D<0 HNLF: 100 m of normal dispersion HNLF with low loss splices SMF28 pigtails, b) Optical spectrum of EOM comb (black) and NOLM output (red), c) Intensity autocorrelation of EOM comb (black) and NOLM output (red).	83

4.12 Experimental work of nonlinear pulse compression using a 50/50 NALM on an EOM comb (with 4 phase modulators driven by an external RF synthesizer at 10.5 GHz) locked and filtered by our 100k finesse etalon. a) AOM: acousto-optic modulator, ISO: fiber pigtailed isolator, PC: polarization controller, PM: phase modulator, MZM: intensity modulator, EDFA: Erbium doped fiber amplifier, FPE: 100k finesse Fabry-Perot etalon, SMF: 250 m of standard single mode fiber, VCO: voltage controlled oscillator, RF Amps: RF amplifiers, PS: RF phase shifter, Att: optical attenuator, LPF: low pass filter, PID: proportional-integral-derivative controller, 50/50: 50/50 fiber optic coupler, DSF: 110 m of dispersion shifted fiber, EDF: 12 m of M12-980-125 Erbium doped fiber bi-directionally pumped by two 1 W 976 nm laser diodes, b) Optical spectrum of EOM comb (black) and NALM output (red), c) Intensity autocorrelation of EOM comb (black) and NALM output (red). . 85

4.13 Experimental work of nonlinear pulse compression by cascading a 40/60 NOLM and a 50/50 NALM on an EOM comb (with 2 phase modulators driven by an external RF synthesizer at 10.5 GHz) locked and filtered by our 100k finesse etalon. a) Schematic diagram using an EOM comb followed by a 40/60 NOLM and a 50/50 NALM. AOM: acousto-optic modulator, SOA: semiconductor optical amplifier, ISO: fiber pigtailed isolator, PC: polarization controller, PM: phase modulator, MZM: intensity modulator, EDFA: Erbium doped fiber amplifier, FPE: 100k finesse Fabry-Perot etalon, SMF: 540 m of standard single mode fiber, VCO: voltage controlled oscillator, RF Amps: RF amplifiers, PS: RF phase shifter, Att: optical attenuator, LPF: low pass filter, PID: proportional-integral-derivative controller, 40/60: 40/60 fiber optic coupler, D<0 HNLF: 100 m of normal dispersion HNLF with low loss splices to SMF28 pigtails, HX-PP: high extinction electro-optic pulse-picker, 50/50: 50/50 fiber optic coupler, EDF: 2.6 m of Er40-4/125 erbium doped fiber pumped by a 1 W 976 nm laser diode, b) Optical spectrum of EOM comb (dark blue), after NOLM (light blue), after NALM (red), c) Intensity autocorrelation of EOM comb (dark blue), after NOLM (light blue), and after NALM (red), d) sampling scope trace after pulse-picking (black) and after NALM (blue). 87

4.14 Experimental work of nonlinear pulse compression by using a short length 50/50 NALM on an EOM comb (with 4 phase modulators driven by an external RF synthesizer at 10.5 GHz) locked and filtered by our 100k finesse etalon. a) Schematic diagram of an EOM comb followed by a short length 50/50 NALM. AOM: acousto-optic modulator, ISO: fiber pigtailed isolator, PC: polarization controller, PM: phase modulator, MZM: intensity modulator, EDFA: Erbium doped fiber amplifier, FPE: 100k finesse Fabry-Perot etalon, SMF: 250 m of standard single mode fiber, VCO: voltage controlled oscillator, RF Amps: RF amplifiers, PS: RF phase shifter, Att: optical attenuator, LPF: low pass filter, PID: proportional-integral-derivative controller, HX-PP: high extinction electro-optic pulse-picker, 50/50: 50/50 fiber optic coupler, EDF: 2.6 m of Er40-4/125 erbium doped fiber pumped by a 1 W 976 nm laser diode, b) Optical spectrum of EOM comb (black), after NALM (red), c) Intensity autocorrelation of EOM comb (black), and after NALM (red). 89

4.15	<p>Experimental work of nonlinear pulse compression by using cascaded 50/50 NALMs on an OEO EOM comb (EOM comb is generated by 4 phase modulators and one intensity modulator driven by the OEO loop at ~ 10.5 GHz).</p> <p>a) Schematic diagram of OEO EOM comb followed by cascade of 50/50 NALMs. OEO EOM: OEO EOM comb employing 1 intensity modulator and 4 phase modulators (phase modulators placed after the etalon), β_2: linear chirp from finisar waveshaper, ISO: fiber pigtailed isolator, PC: polarization controller, EDFA: Erbium doped fiber amplifier, 50/50: 50/50 fiber optic coupler, EDF: 2.6 m of Er40-4/125 erbium doped fiber pumped by a 1 W 976 nm laser diode, HNLF1: 100 m of zero dispersion HNLF with low loss splices to SMF28 on each side, HNLF2: 100 m of normal dispersion HNLF with low loss splices to SMF28 on each side, b) Optical spectrum of EOM comb (black), after NALM 1(red), and after NALM 2 (blue), c) Intensity autocorrelation of EOM comb (black), after NALM 1(red), and after NALM 2 (blue).</p>	91
5.1	<p>Measured output powers using an input of 1 mW CW at 1550 nm and a 1 W 976 nm pump laser for various Erbium doped fibers.</p>	95
5.2	<p>Various pump configurations in fiber. From top to bottom: co-propagating pump, counter propagating pump, and bi-directional pump.</p>	97
5.3	<p>Fiber pump combining architectures. From top to bottom: Polarization beam combining, spectral beam combining, and polarization plus spectral beam combining.</p>	98
5.4	<p>Conceptual diagram of chirped pulse amplification.</p>	100

5.5	Schematic for a cascaded Raman fiber laser. RIG: Raman cavity input grating, HR: high reflector, ROG: Raman cavity output grating.	101
5.6	Schematic diagram for testing home-built EDFA using RFL. ISO: 5 W power handling fiber isolator, WDM: 1480/1550 wavelength division multiplexer, Er40-4/125: 4.5 m of Liekki Erbium doped fiber Er-40-4/125.	103
5.7	Experimental data demonstrating gain narrowing in a commercial 2 W EDFA. a) Schematic for generating broad bandwidth pulses followed by an EDFA producing gain narrowed pulses. β_2 : linear chirp from finisar waveshaper, ISO: fiber pigtailed isolator, PC: polarization controller, EDFA: Erbium doped fiber amplifier, 50/50: 50/50 fiber optic coupler, EDF: 2.6 m of Er40-4/125 erbium doped fiber pumped by a 1 W 976 nm laser diode, HNLF1: 100 m of zero dispersion HNLF with low loss splices to SMF28 on each side, HNLF2: 100 m of normal dispersion HNLF with low loss splices to SMF28 on each side. b) optical spectrum after NALM 2 (red) and after final EDFA (black). . .	104
5.8	Conceptual diagram of pulse-picking in the time domain.	106
5.9	Sampling scope trace of our electrical gate signal with a repetition rate \sim 164 MHz.	108
5.10	a) Experimental setup for generating ultrashort high peak power pulses seeded by an EOM comb. EDFA: erbium doped fiber amplifier, ISO: fiber isolator, HX pulse-picker: high extinction electro optic pulse-picker, \div 64: divide by 64 countdown trigger box, EDF: 2.6 m of Liekki Er40-4/125 Erbium doped fiber, Att: adjustable optical attenuator. b) Optical spectrum after the final EDFA. c) Intensity autocorrelation after the final EDFA.	108

5.11	Sampling scope trace of newly acquired electrical pulse generator operating at a repetition rate of 1.3 GHz.	110
5.12	Experimental schematic for generating ultrashort high contrast pulses with pulse pick rate of 8. EDFA: erbium doped fiber amplifier, NALM 1: nonlinear amplifying loop mirror, PM: phase modulator, β_2 : linear chirp applied by Finisar waveshaper, DCF: 0.7 m dispersion compensating fiber, FPE: Tunable ~ 600 finesse etalon, ISO: fiber isolator, HX-PP: high extinction pulse-picker, Att: RF attenuator, synth: RF synthesizer operating at 900 MHz, RF Amp: RF amplifier, PD: photodiode, PZT: high voltage piezo driver, LPF: low pass filter, PID: proportional-integral-derivative controller, EPG: electrical pulse generator.	111
5.13	Diagnostic traces of the new all fiber approach to generating high contrast ultrashort pulses for supercontinuum generation. a) optical spectrum of OEO EOM comb output (green), NALM 1 output (blue), tunable etalon throughput (red), final EDFA output (black). b) Intensity autocorrelation traces of OEO EOM comb output (green), NALM 1 output (blue), tunable etalon throughput (red), final EDFA output (black). c) Sampling scope traces before pulse-picker (black) and after pulse-picker (red).	112
6.1	Supercontinuum generation simulation pumping .5 m of Thorlabs HN1550 with sech pulses of 10 kW peak power and ~ 70 fs. Left: Spectral evolution of pulse, middle: temporal evolution of pulse, right: spectrum of pulse after .5 m in HNLF.	118

6.2	Supercontinuum generation simulation pumping .5 m of Thorlabs HN1550P with sech pulses of 10 kW peak power and ~ 70 fs. Left: Spectral evolution of pulse, middle: temporal evolution of pulse, right: spectrum of pulse after .5 m in HNLF.	119
6.3	Supercontinuum generation simulation pumping .5 m of Thorlabs PMHN5 with sech pulses of 10 kW peak power and ~ 70 fs. Left: Spectral evolution of pulse, middle: temporal evolution of pulse, right: spectrum of pulse after .5 m in HNLF.	120
6.4	Setup for generating sub ~ 100 fs pulses for supercontinuum generation . . .	121
6.5	Diagnostic traces of amplified 20 MHz fiber laser used for supercontinuum generation experiments: a) intensity autocorrelation after the home-built EDFA, b) optical spectrum after the home-built EDFA	122
6.6	Optical spectrum of supercontinuum generation 10 cm of anomalous dispersion HNLF ($D = 1.25\text{ps/nm/km}$ and $S = .0093\text{ps/nm}^2/\text{km}$)	123
6.7	Optical spectrum of supercontinuum generation using 15 cm of anomalous dispersion ($D = 2.5\text{ps/nm/km}$ and $S = .017\text{ps/nm}^2/\text{km}$)	124
6.8	Optical spectrum of supercontinuum generation using 47 cm of anomalous dispersion ($D = 2.5\text{ps/nm/km}$ and $S = .017\text{ps/nm}^2/\text{km}$)	125
6.9	Optical spectrum of supercontinuum generation using 50 cm of anomalous dispersion PM-HNLF on one polarization axis	126
6.10	Optical spectrum of supercontinuum generation using 50 cm of anomalous dispersion PM-HNLF on a second polarization axis	127

6.11	a) Conceptual diagram of f-2f interferometry, b) non-common path f-2f interferometer schematic, c) quasi-common path f-2f interferometer schematic, d) common path (in line) f-2f interferometer schematic.	127
6.12	Calculated dispersion parameter for common materials used for f-2f interferometry	128
6.13	Experimental implementation of non-common path f-2f interferometer. PC: fiber polarization controller, PM-HNLF: 0.5 m of Thorlabs PMHN5, DM: dichroic mirror, $\frac{\lambda}{2}$: half waveplate, M: metallic mirror, $\frac{\lambda}{2}$: half waveplate, PPLN: periodically poled Lithium Niobate, PBS: polarizing beam splitter, BPF: 1030 nm optical bandpass filter, LNA: Wenzel low noise amplifier.	128
6.14	Carrier-envelope-offset frequency detection using commercial FMLL	129
6.15	Improved f_0 beat note for commercial fiber mode-locked laser.	130
6.16	a) Schematic for measuring the carrier-envelope-offset frequency of a 20 MHz repetition rate fiber mode-locked laser using the COSMO, b) Measured carrier-envelope-offset frequency without post amplification, c) Measured carrier-envelope-offset frequency with low noise Wenzel RF amplifier.	132
7.1	Optical spectrum of supercontinuum generated using 50 cm of PMHN5 seeded by the EOM comb downsampled by 64 and then amplified to 1.5 nJ.	135
7.2	Top: Schematic for measuring heterodyne beat notes in each part of our locked EOM comb system. Bottom: Measured heterodyne beat notes after the 100k finesse etalon, pulse-picker, and NALM using a <100 Hz linewidth laser.	136

7.3	Heterodyne beat measurement with Menlo fiber mode-locked laser and CW laser.	137
7.4	Experimental schematic of measuring f_0 using our OEO EOM comb using the COSMO. β_2 : linear chirp applied by waveshaper, EDFA: erbium doped fiber amplifier, NALM: nonlinear amplifying loop mirror, PM: phase modulator, DCF: 0.7 m dispersion compensating fiber, FPE: tunable ~ 600 finesse Fabry-Perot etalon, ISO: fiberized isolator, f-2f: COSMO, PZT: high voltage piezo driver, RF Amp: RF amplifier, LPF: low pass filter, PID: proportional-integral-derivative controller, EPG: electrical pulse generator.	138
7.5	Measured carrier-envelope-offset beat note using OEO EOM comb. a) Without Miteq RF amplifier, b) with Miteq RF amplifier.	140

CHAPTER 1: INTRODUCTION

Optical Frequency Combs

Optical frequency combs (OFC) are magnificent tools that have fostered the growth of technology in multiple fields such as ultra-wide band communications [1], metrology [2,3], spectroscopy [4,5], low noise microwave generation [6], LIDAR [7], and many more [8]. Many of these applications are made possible through viewing the OFC in either the time or frequency domain.

In the time domain, an OFC consists of a train of pulses that are temporally separated with period T_{rep} . The periodicity of the OFC is related to the length of the laser cavity (for mode-locked lasers) by equation 1.1, where l_c is the length of the laser cavity and v_g is the group velocity of the cavity medium. The pulse train can be thought of as an ultrafast oscillating optical carrier (on the order of 100's of THz) being modulated by a much slower signal (from the repetition period). If one were to track the optical carrier with respect to the peak of the pulse, one would observe that the optical carrier seems to be changing from pulse to pulse. This shift in the optical carrier phase and the envelope of the pulse train is known as the carrier envelope shift. This effect can be seen in Fig. 1.2a, where the optical carrier phase changes from pulse to pulse by $\Delta\phi$.

$$T_{rep} = l_c/v_g \quad (1.1)$$

The frequency domain picture of an OFC is related to the time domain picture by a Fourier transform of the pulse train. The periodic nature of the pulse train manifests itself as several delta functions centered at the optical frequency and spaced by $f_{rep} = 1/T_{rep}$; forming the shape of a comb. The comb lines are weighted by the Fourier transform of the envelope of a single pulse.

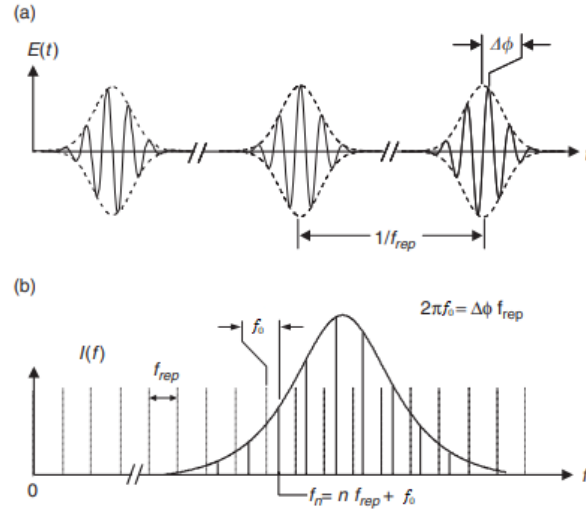


Figure 1.1: (a) Time domain representation of an optical frequency comb, (b) frequency domain representation of an optical frequency comb

By extrapolating the delta functions down to 0, one would typically measure an offset frequency ($f_0 = \nu_{opt} \% 2\pi$). The offset frequency f_0 is related to the carrier-envelope shift $\Delta\phi$ from pulse to pulse. The OFC in the frequency domain can be seen in Fig. 1.1b. Mathematically, we can express the frequency of each comb line in the OFC by equation 1.2.

$$f_n = f_0 + n f_{rep} \quad (1.2)$$

Many of the previously mentioned applications are made possible through the inherent properties of frequency combs such as coherent equidistant longitudinal modes and frequency stability. For example, dual comb spectroscopy requires the use of two coherent OFCs to effectively sample large optical bandwidths in a short amount of time. Optical frequency division uses the broad optical bandwidth and coherency as bridge to optical atomic clocks using spectrally distant wavelengths.

Some applications require knowledge and control of both f_0 & f_{rep} while others only require f_{rep} . For repetition rates within the bandwidth of photodetectors (typically < 70 GHz), f_{rep} can be measured by simply illuminating a photodetector and observing the combline on an RF spectrum analyzer (RFSA). On the other hand, measuring f_0 with precision requires a self-referencing interferometer. The most common self-referencing interferometer is known as an f-2f interferometer which requires a coherent octave of bandwidth and second harmonic generation (SHG). Various techniques have been employed to either compensate [9] for or eliminate its presence [10]. However, they all still require a coherent octave of bandwidth and SHG. Measuring f_0 with f-2f interferometry involves frequency doubling the low frequency end of the coherent octave and interfering the frequency doubled light with a set of comblines on the high frequency end. The mathematical operation of f-2f interferometry can be seen in 1.3.

$$2(f_0 + nf_{rep}) - f_0 + mf_{rep} = f_{beat} \quad (1.3)$$

When $m=2n$, $f_{beat} = f_0$, which f_0 to be attainable electronically. Once determined, a feedback loop can be used to compensate for f_0 ; yielding a stabilized optical frequency comb. The result is an OFC in which each combline frequency is known with several digits of precision.

In the next section, we will discuss different methods of generating frequency combs such as Electro-optic modulation (EOM), mode-locking, and microresonators. We will also discuss the types of frequency combs that have demonstrated self-referencing.

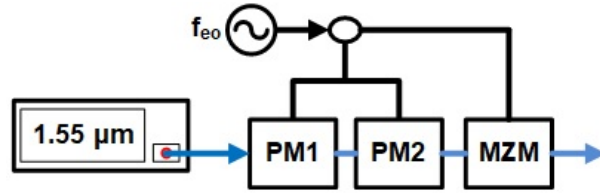


Figure 1.2: Schematic of a simple EOM comb driven by a single external RF source. CW: continuous-wave laser, PM: electro-optic phase modulator, IM: electro-optic intensity modulator, RF: external RF oscillator.

Generation of Optical Frequency Combs in telecom band

EOM Combs

An EOM comb is the simplest type of frequency comb in which a CW laser is passed through a cascade of phase and intensity modulators. Fig. 1.2 shows the schematic of a simple EOM comb. The spacing between comb lines, f_{rep} , is determined by the modulation frequency used to drive the modulators. This gives the EOM comb a large amount of flexibility in terms of adjusting f_{rep} , allowing for both wide and narrow spacing between comb lines. The number of generated comb lines is determined by the combination of the V_{π} and the RF power driving the modulator. The intensity modulator gives rise to the pulse like nature of the EOM comb while the phase modulators impress a sinusoidal temporal phase on the carrier frequency leading to the generation of additional frequency components and spectral phase. In this case, the phase modulators are the main driver for comb line generation. Phase modulators can produce significantly more comb lines due to the higher modulation index that can be achieved as a result of a lower V_{π} and higher RF power handling. A typical broadband EOM comb uses several phase modulators and a single intensity modulator.

Recent experiments have demonstrated pulse durations of 230 fs at 1552.52 nm (24 nm bandwidth with a repetition rate of 25 GHz), [11], with subsequent nonlinear broadening bringing the pulse duration to as short as 120 fs with a repetition rate of 1 GHz. This was accomplished by cascading three phase modulators and one intensity modulator that are all driven with the same 25 GHz RF drive signal. Then, the pulses from the EOM comb were compressed to a FWHM of 230 fs, amplified, and then sent through a glass block for nonlinear spectral broadening to reach a pulse duration of 100 fs. It has been also shown that EOM combs can be used to generate pulses as short as 550 fs at 514.5 nm (2 THz FWHM bandwidth with a repetition rate of 16.25 GHz) [12] using a single modulator. However, this requires the modulator to be placed in a cavity which allows for multiple passes. This requires the input light to not only spatially match the cavity modes but to also spectrally match the cavity modes. These works and many others use an external RF oscillator to drive the phase modulators at a constant frequency [13, 14].

An EOM comb using cascaded modulators is the simplest case in generating a frequency comb as it requires no optical cavity and f_{rep} can be tuned without having to match a cavity's resonances. EOM combs generated using an opto-electronic oscillator (OEO) have also been demonstrated, eliminating the need for an external RF oscillator [15]. However, by using an OEO loop to generate the RF signal, the EOM comb is no longer continuously tunable. Instead, the EOM comb would become discretely tunable due to the discrete resonance peaks displayed by the periodic filter in both f_{rep} & f_0 . Due to their simplicity in generation, EOM combs have been used for a variety of applications that can take advantage of their tunability and robustness. However, the tradeoff for robustness and tunability is high timing jitter. EOM combs typically possess more timing jitter than other comb sources because they lack a filter mechanism which is typically found in other frequency comb generators. This is because the phase noise of an EOM comb is dictated by the noise of the CW laser and RF driving signal. Comb lines generated through the modulation process can be interpreted as multiplication of the RF driving signal which results in background

noise multiplication [16]. This has also been confirmed in a more recent experiment in which an EOM comb was self-referenced via f-2f interferometry [17]. The authors of [17] note that they were unable to obtain a coherent beat note for f_{ceo} without an external filtering etalon.

Mode-locked laser based frequency combs

Another method of producing frequency combs is through mode-locking. Mode-locking is the process by which several near equidistant frequency components acquire a fixed phase relationship through gain, nonlinearity, and feedback. The feedback is accomplished by an optical resonator which provides the frequency spacing for the combs. The resonator modes are a result of a standing wave which is produced inside the cavity, allowing only frequencies which satisfy the Berkhausen condition (round trip phase of 2π) to sustain oscillation. The mode spacing is the result of several longitudinal modes which satisfy the round trip phase of 2π , which is called the free spectral range (FSR). For plane cavities, the $FSR = c/2l_c$ while for ring cavities $FSR = c/l_c$. Where c is the speed of light in vacuum, n is the index of refraction of the material, and l_c is the length of the cavity. A typical mode-locked laser contains a comb generating element (such as an electro-optic modulator or nonlinear element) and gain inside an optical resonator. The fixed phase relationship of an MLL occurs due to the energy exchange between comb lines from the comb generating element. MLLs come in three variants: active mode-locking (AML), passive mode-locking (PML), and hybrid mode-locking (HML). Typically, passively mode-locked lasers have been self-referenced due to superior pulse properties. Since we are mainly interested in high repetition rate (>10 GHz) self-referenced optical frequency combs in the telecommunications window, we will keep our discussion brief.

It is important to note that the combline spacing in a mode-locked laser (MLL) is an integer multiple of the FSR. Integers greater than 1 for a MLL are called harmonic mode-locked lasers and have

been shown to be noisy & unstable. MLLs with $FSR = f_{rep}$ are known as fundamentally mode-locked lasers and are significantly more stable than their harmonic counterparts. For applications that require high repetition rates of at least 10 GHz (such as photonic assisted ADC's and astronomical spectroscopy), the cavity length must be kept below 15 mm (assuming free space). In addition, PML requires nonlinearity for pulse formation to occur. Nonlinearity requires sufficient pulse energies to be available. Pulse energy is inversely proportional to repetition rate ($E_p \sim P_{av}/f_{rep}$). This means that higher repetition rate MLL not only require a smaller size cavity but also require even higher average powers to support pulse formation.

Fiber based mode-locked lasers

Mode-locked lasers using fibers doped with Erbium have been demonstrated with great success. Erbium can provide optical gain when optically pumped inside the fiber. This in combination with the low propagation loss of optical fiber (SMF28 $\alpha = .2dB/km @ 1550 \text{ nm}$) allows for a simplistic design of a laser. There are many examples of fiber mode-locked lasers (FMLL) that have achieved short pulses (<100 fs), low timing jitter, and carrier-envelope phase stabilization [18]. FMLL have demonstrated both active and passive mode-locking. However, PML is more common due to the long lifetime of the gain medium, resulting in ease of mode-locking with a saturable absorber. Common examples of passively mode-locked FMLL consist of using fast saturable absorbers such as the nonlinear optical loop mirror (NOLM), nonlinear amplifying loop mirror (NALM), and nonlinear polarization rotation (NPR). Typical FMLL employing fast saturable absorbers include the figure of eight [19] and figure of nine lasers [20] as shown in Fig. 1.3. FMLL with slow saturable absorbers have also been employed [21] & [22]. Typically, FMLL employing slow saturable absorbers can reach higher repetition rates due to the significantly lower saturation fluence compared to fast saturable absorbers (for the same length).

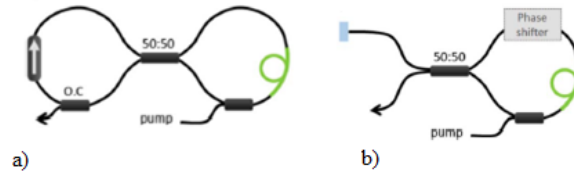


Figure 1.3: Passive mode-locking in a FMLL using a NALM (a) figure-of-eight laser (b) figure-of-nine laser

Passive FMLL employing the above fast saturable absorbers have demonstrated carrier-envelope phase stabilization due to their ability to generate high peak powers and short pulses. FMLL have attained ultralow noise operation through various schemes such as pump feedback control [23], dispersion management [18], and intracavity filtering [24] to name a couple.

Despite their high performance and simplistic design, FMLL generally have low f_{rep} (20 MHz to 1 GHz) due to the long lengths of fiber required to build the laser cavity. To circumvent this limitation, sometimes FMLL operate on a harmonic of the repetition rate (harmonic mode-locking). However, harmonic mode-locking alone gives rise to an increase in timing jitter as well as instabilities. Typically, harmonic mode-locked lasers display super-mode spurs which are noise spikes that appear in the photodetected pulse train. These spurs are a result of the uncorrelated noise between the multiple pulses circulating inside the cavity. Various methods have been employed for super-mode suppression utilizing injection-locking [25], intra-cavity filters [26], and other methods [27].

Semiconductor based mode-locked lasers

Semiconductor MLL (SCMLL) are an attractive option for generating optical frequency combs because of their small footprint, low cost, simplicity in pumping, and their efficiency. Since SCMLL can be made much smaller than other lasers, they can easily achieve repetition rates of 10 GHz

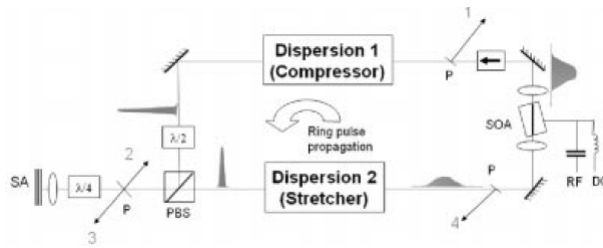


Figure 1.4: A schematic of an external cavity HML SCMLL where SA: saturable absorber, PBS: polarization beam splitter, SOA: semiconductor optical amplifier, Dispersion 1 and Dispersion 2 are dual grating compressors

and above. Semiconductors are capable of operating at various wavelengths through bandgap engineering. Unlike Erbium, semiconductors typically have a short upper state lifetime (ns-ps). As a result, they tend to have low pulse energies and longer pulse durations. These characteristics make it difficult to self-reference even with external amplification and broadening. However, SCMLL have demonstrated short pulse operation (fs) [28, 29], high peak power [30], and low noise [31].

Femtosecond pulses from SCMLL typically use an external cavity, a saturable absorber, and some form of dispersion compensation as shown in Fig. 1.4. External cavity operation is used to better control the laser operation and dispersion compensation is used to circumvent the nonlinear effects in semiconductor gain medium. Due to the low pulse energies available from semiconductors as a result of the short upper state lifetime, a slow saturable absorber with low saturation fluence must be used for PML or HML operation. At the same time, to reduce detrimental nonlinear effects in the gain medium, pulse stretching before the gain medium is required. Saturable absorbers such as multiple quantum well saturable absorbers [32] as well as a semiconductor saturable absorber mirror (SESAM) [33] have been used for SCMLL. Similarly, high peak power SCMLL use concepts such as an external cavity, saturable absorber, and dispersion compensation. External cavity SCMLL can also achieve high repetition rates if they use a nested cavity approach [34]. This entails using a Fabry-Perot etalon as a comb filter to suppress the low repetition rate fundamental cavity.

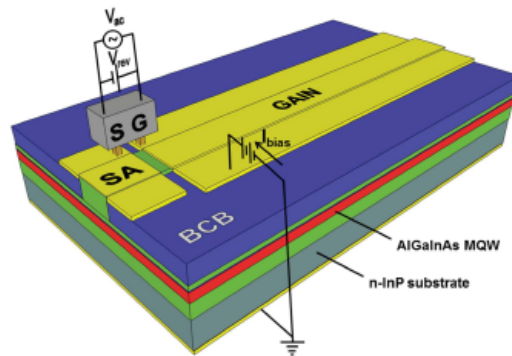


Figure 1.5: Schematic of a fully integrated SCMLL with a saturable absorber and metal pads to enable HML. Where SA: saturable absorber.

To date, an electrically pumped SCMLL has not been self-referenced through f-2f interferometry. The carrier-envelope-offset frequency for an electrically pumped SCMLL has been measured by interfering a stabilized comb source and measuring the beat signal [35].

Although a fully integrated SCMLL with a stabilized carrier envelope phase (such as Fig. 1.5) [36] has not been demonstrated yet, a self-referenced SCMLL based on the optically pumped vertical-external-cavity surface-emitting lasers (OP-VECSELs) has been shown [37]. Unlike the previously mentioned SCMLL, OP-VECSELs are not integrated lasers, require optical pumping, and are therefore not as energy efficient. However, OP-VECSELs are capable of generating significantly shorter pulses with greater pulse energies. Since their configuration is closer to an external cavity approach, repetition rates of 10 GHz and above are difficult due to cavity size. This shows that for self-referencing of 10 GHz mode-locked lasers is still challenging.

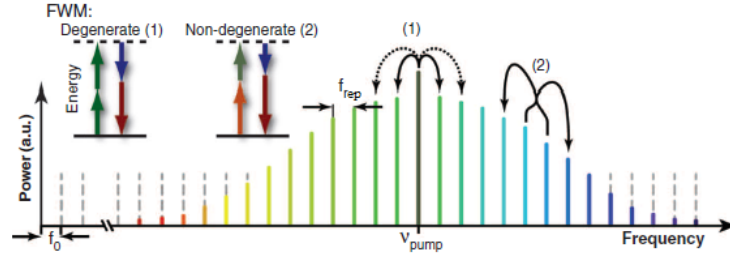


Figure 1.6: Frequency domain picture of pumping a Kerr microring resonator

Kerr-ring resonator based frequency combs

Another type of frequency comb generator that has gained prominence in recent years is the Kerr microring resonators. A microring resonator is a small ring like structure which has an extremely tight confinement on the order of $Q 10^6 - 10^{10}$ [38]. The combination of the tight confinement and high nonlinearity when pumped with large optical powers give rise to cascaded nonlinear effects seeded by parametric four-wave mixing. Furthermore, the ability to span wide spectra is made possible by dispersion engineering of the cavity [39]. Typically, ring resonators are pumped with a CW laser. Due to the tight confinement and material nonlinearity, four-wave mixing occurs where two pump photons are converted into an up converted signal photon and a down converted idler photon. When the generated photons match the cavity FSR, the process is enhanced and allows for a cascaded process to occur [40]. Non-degenerate FWM takes place as well, allowing for even further comb generation. Since the frequency components exchange energy through FWM, they all have a well-defined phase relationship, which makes the output of the ring resonator a frequency comb. This can be seen in Fig. 1.6, where a strong CW pump is used to seed the initial comb by degenerate FWM. Ring resonators have demonstrated coherent octave generation without external broadening for obtaining [41]. Compensation of f_0 has been done by tuning the wavelength of the CW laser while f_{rep} has been adjusted by thermal tuning of the cavity [42].

While ring resonators can obtain extremely large bandwidths with relatively low input powers, they have an extremely high f_{rep} due to the small footprint of these devices. Their f_{rep} often can exceed the bandwidth of fast photodetectors (100 GHz). The bandwidth is also tied to the f_{rep} , which necessitates high repetition rates to achieve an octave of bandwidth. To date, self-referenced Kerr micro-rings operating with a repetition rate within the bandwidth of commercial photodetectors has not been demonstrated. Since the f_{rep} exceeds the bandwidth of available photodetectors, a more complicated method of measuring f_{rep} was necessary. Again, optical frequency comb sources with a repetition rate of 10 GHz to 100 GHz are difficult to come by.

Thesis Outline

Several candidate comb sources in the telecom region have been introduced. The goal of this thesis is to measure and stabilize the carrier-envelope-offset frequency for a comb source with comb spacing of 10 GHz and above. However, few comb sources in the telecom range with repetition rates between 10 GHz and 100 GHz have measured the carrier-envelope-offset frequency. This is primarily due three factors: few viable comb sources (difficulty in reaching high repetition rates and relatively low spectral coverage), poor spectral broadening options (stringent requirements on coherent octave spanning supercontinuum generation), and poor pulse amplification options (lack of low distortion and high power amplifiers). Few comb sources can be constructed with cavity sizes of 15 mm (10 GHz spaced modes in a linear cavity). Micro-rings are capable of obtaining high repetition rate comb sources but the comb power is extremely low, necessitating additional amplification and supercontinuum generation. Even after generating a 10 GHz spaced comb, coherent octave spanning supercontinuum generation imposes difficult requirements on pulse parameters; sub-100 fs pulse durations with decent pulse quality and over 1 nJ of pulse energy for fiber based supercontinuum. This entails an output average power of at least 10 W while still being able

to support ultrashort pulses. Waveguide based supercontinuum generation imposes less stringent requirements such as sub-200 fs pulse duration and over 200 pJ of pulse energy. However, 200 pJ of pulse energy at a repetition rate of 10 GHz is still 2 W. Commercial pulsed optical amplifiers typically achieve a few hundred mW as opposed to the Watt class needed. These challenges will be addressed in the following chapters. The rest of the thesis is outlined as follows: Chapter 2 describes our 10 GHz comb source realized through a combination of an OEO and an EOM comb. Chapter 3 describes our work for constructing an external tunable Fabry-Perot etalon for additional noise suppression. Chapter 4 details our work for conditioning the pulses from our oscillator through saturable absorption. Chapter 5 details our work for high power amplification and pulse compression. Chapter 6 describes our work in measuring the carrier-envelope-offset frequency through coherent octave spanning supercontinuum generation. Chapter 7 presents our work in measuring the carrier-envelope-offset frequency using our 10 GHz comb source. Finally, chapter 8 concludes our work and gives future directions for research.

CHAPTER 2: GENERATION OF A LOW NOISE AND STABLE 10 GHz COMB SOURCE

As previously mentioned, many comb sources in the telecom wavelength have measured f_0 with $f_{rep} < 1GHz$ or $f_{rep} > 200GHz$. However, few comb sources with repetition rates between 10 GHz - 100 GHz have measured f_0 . This is because mode-locked comb sources with GHz repetition rates and above are extremely challenging due to limited pulse energies and a small cavity size. On the other hand, micro-ring resonators operate with excessively high repetition rates. This section will cover EOM combs in detail and discuss our work on generating a low noise 10 GHz spaced optical frequency comb that does not require an external clock.

Construction of an EOM comb

In this section we will provide detailed background on how EOM combs work and then discuss the components that we used for our EOM comb along with simple simulations to further explain. As previously mentioned, a basic EOM comb consists of a CW laser, cascade of electro-optic modulators, and an external RF source. By applying an RF signal to all of the modulators and tuning their phases to align, combs are generated at the repetition rate of the RF signal. The generation of frequency components by sinusoidal modulation and the addition of spectral phase can be seen in Eq. 2.1 & 2.2.

$$e^{i\beta\cos(\omega_mt)} = \sum_{n=-\infty}^{\infty} i^n J_n(\beta) e^{in\omega_mt} \quad (2.1)$$

$$\cos(\omega_m t) \approx 1 - (\omega_m t)^2/2! + (\omega_m t)^4/4! - (\omega_m t)^6/6! \quad (2.2)$$

Where β is the depth of modulation, J_n is the Bessel function of order n , and ω_m is the modulation frequency. Using the Jacobi-Anger expansion, we find that sinusoidal phase modulation generates frequency components separated by the modulation frequency and that the amplitude of the components is dictated by the Bessel function. By decomposing the sinusoidal drive signal with a Taylor series expansion, we obtain the spectral phase of the generated comb lines. The result of the sinusoidal phase modulation gives rise to even orders of spectral phase. The sign of the quadratic spectral phase can be changed by adjusting the phase of the driving sinusoid. Typically, the majority of the spectral phase is quadratic, which can easily be compensated for using a grating pair compressor [43] or SMF28. As previously mentioned, the number of comb lines generated by an EOM comb is determined by the V_π and the power of the RF drive signal. The optical bandwidth is determined by the number of comb lines multiplied by the drive frequency. The pulse like nature of an EOM comb comes into play when an intensity modulator is used to carve out the CW light. Despite the simple comb formation and simplicity in pulse compression, EOM combs also exhibit high temporal sidelobes. It is important to note that the sidelobes mentioned here are not a result of the spectral shape. The spectral shape of an EOM comb is a rect function which entails that the transform limited pulse is that of a sinc (which has sidelobes built in). When the quadratic spectral phase is eliminated (whether by a grating compressor or single mode fiber), the sidelobe height is significantly higher than that of a sinc function. The poor pulse characteristics of the EOM comb are a result of the sinusoidal chirp impressed upon the optical carrier. Although the intensity modulator effectively acts as a 50% duty cycle gate, there is still a significant portion of higher order polynomial terms in the phase that are not extinguished. As a result, temporal sidelobes are apparent when compensating for only linear chirp for compressing the EOM comb pulses. This effect will be further explained with simulations later in this chapter. Next, we will discuss the

individual components in detail.

CW laser

The CW laser acts as the seed source for the EOM comb. For simulation purposes, one can represent the CW laser as a delta function centered at a particular frequency with some power. In practice, the side mode suppression ratio, output power, spectral width, and the wavelength of the laser are important. The side mode suppression ratio gives the effective optical signal to noise ratio (OSNR) of the laser. The output power, spectral width, and wavelength of the laser are self explanatory. Without optical filtering, the OSNR of the EOM comb is limited by the CW laser. Every additional component after the laser that is not a filter will serve to reduce the OSNR of the comb. In our experiment, the side mode suppression ratio of our laser is 50 dB, center wavelength of 1550 nm, linewidth of 7 Hz, and output power of 20 mW. Additional important factors and options with the laser are the optical frequency fluctuation, the linewidth, a fast-tuning PZT option, and the bandwidth of the PZT. The frequency fluctuation is directly linked to f_0 fluctuations. Selecting a laser with low drift would significantly simplify locking f_0 . Unfortunately, laser manufacturers do not spec the optical frequency fluctuation of a laser and therefore this parameter can only be selected based off of experience. In our experiments, we use a CW laser that consists of a semiconductor gain medium that is self-injection locked to a high Q whispering gallery mode resonator (WGMR) made by OEwaves. We have found that this type of CW laser offers extremely low optical frequency fluctuation compared to other options. Other types of lasers include, external cavity tunable semiconductor laser, DFB lasers, and fiber lasers. Although these other lasers can be used to generate an EOM comb, we have found that their inherent optical frequency fluctuations are significantly wider (in frequency extent) and faster than the OEwaves laser. Even when a laser has an integrated piezo for quickly sweeping the laser frequency, we have found that their natural frequency fluctuation is fast faster than the bandwidth of the piezo. This gives rise to an issue where

the inherent frequency fluctuations of the laser cannot easily be overcome through modulation of the laser cavity. This issue will be further discussed later on in this chapter. It is sufficient to say that our EOM comb OSNR is limited to a maximum of 50 dB without optical filtering due to the side mode suppression ratio.

Electro-optic modulation

The practical parameters of interest in an electro-optic modulator (both phase and amplitude) are: the V_π , insertion loss, RF bandwidth, RF power handling, and optical power handling capabilities. The V_π dictates how much RF power is needed to change the optical carrier phase by π radians. As previously mentioned, the insertion loss is important because it dictates the OSNR reduction of the comb after passing through each modulator. The rest of the parameters are self-explanatory. The main goal associated with the modulators is to generate as many comb lines as possible with as much spacing as possible. This is accomplished by 1) selecting phase modulators with the lowest V_π , 2) driving the modulators at as high an RF frequency as possible (dictated by availability of components), and 3) driving the modulators with as much RF power as possible. The expression that relates these parameters together for phase modulation is shown in Eq. 2.3. Where V_{eo} is the amplitude of the RF drive signal, f_{eo} is the frequency of the RF drive signal, ϕ is the phase of the RF drive signal, and V_π is the amplitude required to produce a π phase shift.

$$E_{out} = E_{in} e^{j\pi \frac{V_{eo} \cos(2\pi f_{eo} t + \phi)}{V_\pi}} \quad (2.3)$$

Assuming a noiseless external RF source with 3 W RF power into each phase modulator and $V_\pi = 4V$ at 10 GHz, we simulate an EOM comb with four electro-optic phase modulators and one intensity modulator (with 20 dBm of RF power). The normalized spectral intensity, temporal

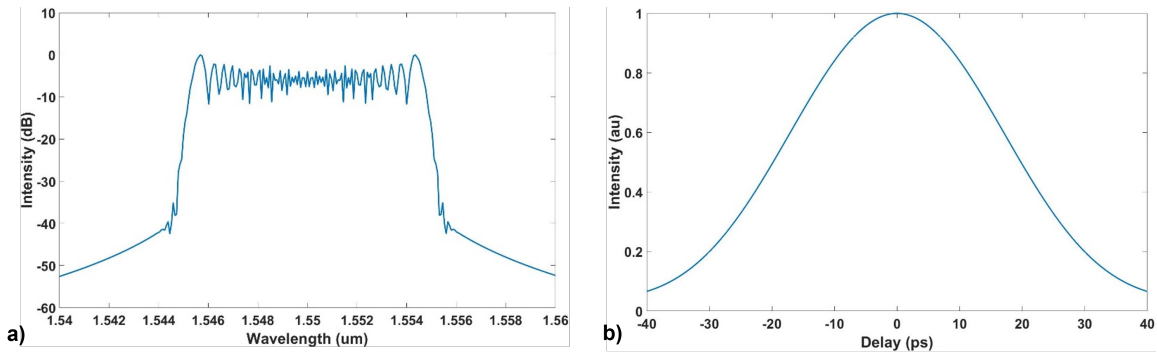


Figure 2.1: Simulated EOM comb consisting of four phase modulators (assuming $V_{\pi} = 4V$) using a noiseless external RF source with 3 W RF power into each phase modulator showing the a) normalized spectral intensity and b) the temporal waveform

waveform, and optical phase after each modulator can be seen in Fig. 2.1.

From Fig. 2.1a, we observe the shape of the optical spectrum to be relatively flat in the center and large spectral oscillations on the edges of the spectrum. The spectrum also sharply rolls off after the spectral oscillations. The temporal waveform in Fig. 2.1b simply shows a sinusoid. It is important to note that we assumed the phase of the driving signal entering each modulator had the exact same phase. In practice, one would require RF phase shifters to ensure that the phases are aligned to constructively interfere. If the phases of each RF signal entering each modulator are π out of phase, each generated combline would destructively interfere. This would cancel out any generated combines and reduce the generated optical bandwidth.

Compressed pulses

From the preceding simulations shown in Fig. 2.1, we observe a significant amount of chirp on the optical spectrum. By reducing the chirp, it is possible to compress the pulse. As mentioned before, the majority of the chirp in an EOM comb is linear. By applying a strong linear chirp (using 250

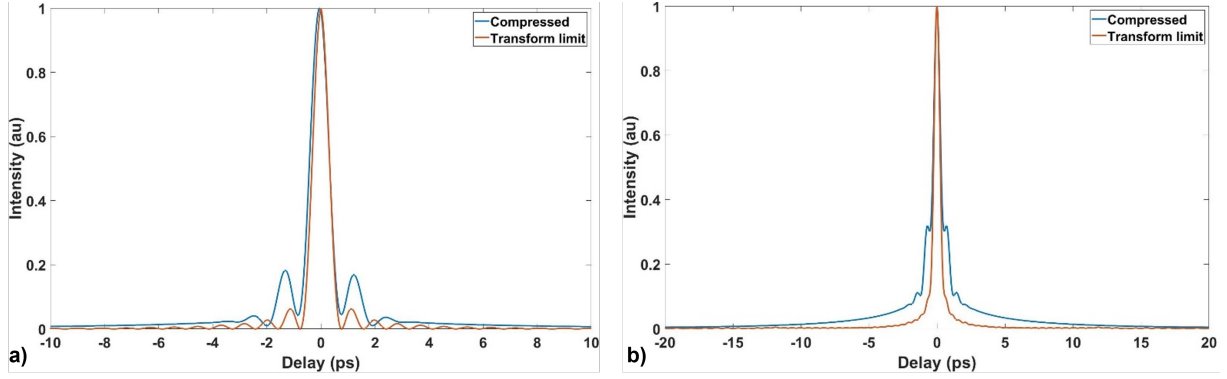


Figure 2.2: Simulated EOM comb consisting of four phase modulators (assuming $V_\pi = 4V$) using a noiseless external RF source with 3 W of RF into the phase modulators power showing the a) pulse profile after linear chirp (blue) with the transform limited pulse (red), b) the autocorrelation of the pulse profile after linear chirp (blue) with the transform limited autocorrelation of the pulse (red).

m of SMF28 equivalent dispersion), we observe a significant reduction in the pulse duration. The simulated pulse intensity profile after the linear chirp is applied is shown in Fig. 2.2a while the intensity autocorrelation is shown in Fig. 2.2b.

We find that the pulse full width at half maximum (FWHM) is close to the transform limit after compensating for the linear chirp. However, we observe the sidelobe level to be much higher in the compressed version compared to the transform limit of the pulse. The transform limited EOM comb pulse exhibits sidelobes due to the square like spectrum, but the compressed pulse's sidelobe height is at least 2x higher. The asymmetry in the sidelobe height is due to the third order dispersion of the simulated fiber. The increased sidelobe height manifests itself in the autocorrelation trace as a pulse riding on a background. From our previous analysis of the phase in an EOM comb and the literature [13], we find that the heightened sidelobes are a result of uncompensated higher order dispersion terms. This structure within the pulse is another common issue in EOM combs that will be further discussed. The key takeaway is that although the majority of the EOM chirp is linear,

the remainder of the chirp imposes pulse sidelobes. These sidelobes reduce the peak power of the pulse.

External RF source

At this point, we have mentioned the optical portion of an EOM comb such as the laser and the modulators. Although we have mentioned the OSNR of the comb and what are its limitations, we have not yet mentioned the noise characteristics of each generated combline. For simulations, typically the linewidth and RF noise information is ignored because it would require significant computational resources to simultaneously observe Hz resolution noise processes for THz bandwidths. Instead, we focus on the phase noise of each combline by using pre-measured RF phase noise data from a synthesizer. With the known RF phase noise data, we use known noise relations that relate the RF phase noise to each combline. Typically, the external RF signal used in an EOM comb is an RF synthesizer. This is because the output RF frequency and amplitude can be easily adjusted for any application. An RF synthesizer consists of several low noise reference oscillators, phase-locked loops, a YIG oscillator and many more. A comprehensive discussion on the design of RF synthesizers can be found in [44]. For our purposes, we are generally more interested in the phase noise of the external RF source. A sample plot of the phase noise can be seen in Fig. 2.3.

Fig. 2.3 shows a sample phase noise plot for an output frequency of 10 GHz using an Agilent E8257D RF synthesizer. The plot is broken up into four distinct sections: reference section, synthesizer section, YIG oscillator, and output section. The reference section starts off at a high phase noise and trends downwards from an offset frequency of 1 Hz to 1 kHz. The synthesizer section from 1 kHz to about 100 kHz shows a plateau effect at a phase noise of $-115 \frac{dBc}{Hz}$. The YIG oscillator section starts at about 100 kHz and ends at a few MHz and trends downwards again to a final value of about $-155 \frac{dBc}{Hz}$. Finally, the output section of the phase noise, starting from a few

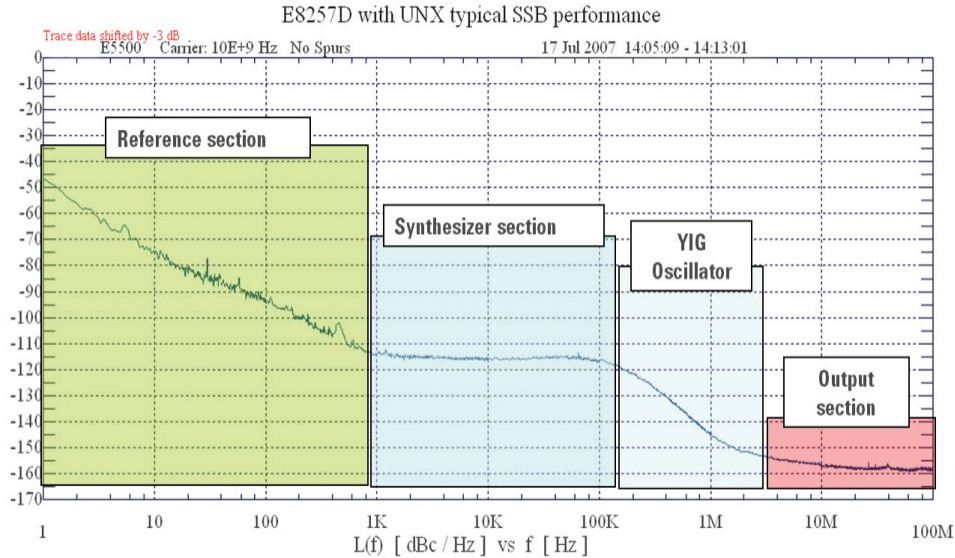


Figure 2.3: Sample 10 GHz RF synthesizer phase noise breakdown, taken from "Keysight Technologies Solutions for Reducing Phase Noise at RF and Microwave Frequencies Application Note".

MHz to 100 MHz, is relatively flat again at a phase noise of about $-160 \frac{dBc}{Hz}$. This reveals to us that the phase noise profile of an RF synthesizer is far from being a perfect delta function in the frequency domain. For low noise operation, it is critical to use an RF source with the lowest phase noise possible. Unfortunately, low noise and high frequency RF sources are extremely expensive.

The noise trend with respect to combline number in an EOM comb also multiplies up quadratically. The noise of each combline is determined by the addition of the optical linewidth of the CW laser with the combline number times the RF source phase noise. Eq. 2.4 gives the phase of each combline in an EOM comb, where θ_m is the phase of the combline, θ_L is the phase of the CW laser, m is the mode number, and θ_{RF} is the phase of the RF source. To obtain the phase noise, one must convert the phase fluctuation to power. This conversion gives rise to the quadratic nature of the noise multiplication.

$$\theta_m = \theta_L + m\theta_{RF} \quad (2.4)$$

From this discussion, the noise of each combline in an EOM comb can be determined by knowing the phase noise of the CW laser, the combline number of the EOM comb, and the phase noise of the external RF source. RF Amplifiers simply add phase noise depending on the noise figure of the amplifier. Clearly, the noise of a broadband EOM comb is of significant concern. In our simulated EOM comb, we generate over 100 comblines (50 on each side of the CW laser). Therefore, the phase noise of the comblines on the end of the spectrum are roughly ($20\log_{10}50 \sim 34\text{dB}$) 34 dB higher than the phase noise of the external RF signal. For an octave of bandwidth ($\sim 200\text{ THz}$), this implies a phase noise increase of $20\log_{10}\frac{200\text{THz}}{10\text{GHz}} = 86\text{ dB}$! The increase in phase noise broadens the optical linewidth of the comblines on the edges of the spectrum. This linewidth broadening has been shown to obscure the f_0 beat note [45], [14].

EOM comb experiment

As previously mentioned, an EOM comb is a flexible comb source with f_0 and f_{rep} being completely tunable. However, the advantages that EOM combs present are not useful in measuring f_0 . In fact, EOM combs are at a significant disadvantage for measuring f_0 because of the following properties: 1) excessive noise (optical and RF) due to the lack of a filtering cavity, 2) relatively long pulse durations, and 3) poor pulse quality. Throughout this work, we will explain and address each of these issues.

Fig. 2.4a shows a schematic of an EOM comb. The system starts with a CW laser centered at 1550 nm that is frequency locked to a 100k finesse etalon (free spectral range: $\sim 1.5\text{ GHz}$, FWHM= $\sim 15\text{ kHz}$) by PDH (this will further be discussed in the next section). The frequency locked CW laser is

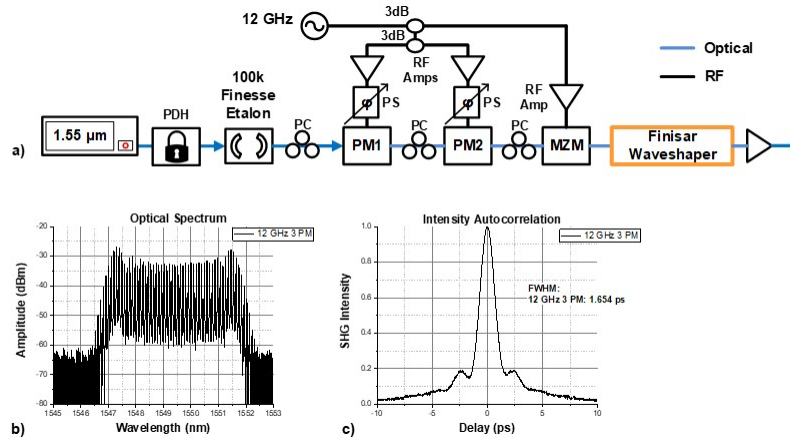


Figure 2.4: a) Schematic of an EOM comb using 2 phase modulators and one intensity modulator driven by a common RF synthesizer at 12 GHz. PDH: Pound-Drever-Hall locking, PC: polarization controller, PM: phase modulator, MZM: intensity modulator, PS: RF phase shifter, RF Amps: RF amplifiers, Finisar Waveshaper: Liquid Crystal on Silicon pulse-shaper. b) Measured optical spectrum, c) Measured intensity autocorrelation

then modulated by two electro-optic phase modulators and one electro-optic intensity modulator. The modulators are driven by a common RF synthesizer at 12 GHz. The RF amplifiers amplify the synthesizer signal to 3 W while the RF phase shifters are used to ensure the phase of the generated comblines constructively interfere for maximum optical bandwidth. The finisar waveshaper is used as a tunable dispersive delay line where only quadratic spectral phase is applied. Fig. 2.4b,c show the measured optical spectrum and nearly compressed intensity autocorrelation trace of the EOM comb. The EOM comb exhibits ~ 50 comblines within a 10 dB deviation that are spaced 12 GHz apart and an OSNR ~ 35 dB. The optical spectrum in the center portion is relatively flat while the edges of the spectrum exhibit 'ears'. The compressed intensity autocorrelation also exhibits a temporal pedestal. The 'ears' on the optical spectrum and the temporal pedestal are a result of the sinusoidal modulation, which gives rise to higher order dispersion components. The higher orders of dispersion give rise to the large pedestal. Exotic dispersion management techniques are required to reduce the pedestal.

We have also constructed an EOM comb consisting of four phase modulators and one intensity modulator driven by a common RF synthesizer at ~ 10.5 GHz. This is shown in Fig. 2.5a while the diagnostic traces are shown in Fig. 2.5b & c. We observe similar spectral features on the optical spectrum with a much greater spectral extent (from 50 to at least 100 combines). This is due to the usage of four high RF power handling phase modulators as opposed to two. We also observe similar temporal features in the autocorrelation with the presence of sidelobes being apparent when only second order dispersion is applied. From this, we observe that each phase modulator provides ~ 25 combines. To reach an octave of bandwidth using only electro-optic modulation at a repetition rate of 10 GHz, we would need 800 phase modulators! If we were to instead seek enough bandwidth to support 300 fs pulses, we would need 8 phase modulators. It is important to note that each phase modulator costed us $\sim \$5k$ while each RF amplifier we used costed us $\sim \$2.1k$ (mini-circuits ZVE-3W-183+). If we obtained higher power RF amplifiers (Pasternack PE15A5049: $\sim \$10k$), operated at higher repetition rates, or used even lower V_π phase modulators, we could reduce the number of phase modulators needed. Unfortunately, we are still looking at $\sim \$7k$ minimum to generate an additional 25 combines.

From the previously mentioned data, we observe the OSNR of the EOM comb is limited due to the lack of a filtering cavity. Improvements to the typical EOM comb must be made to allow for a coherent octave through supercontinuum generation. To improve the noise performance of the EOM comb, we resort to optical filtering using an optical cavity.

Pound-Drever-Hall locking

From the previous discussion regarding CW lasers, EOM combs not only exhibit a low OSNR but also random frequency translations of the entire comb. This is caused by the frequency drift of the CW laser. The frequency translation of the entire comb manifests itself as a change in f_0 .

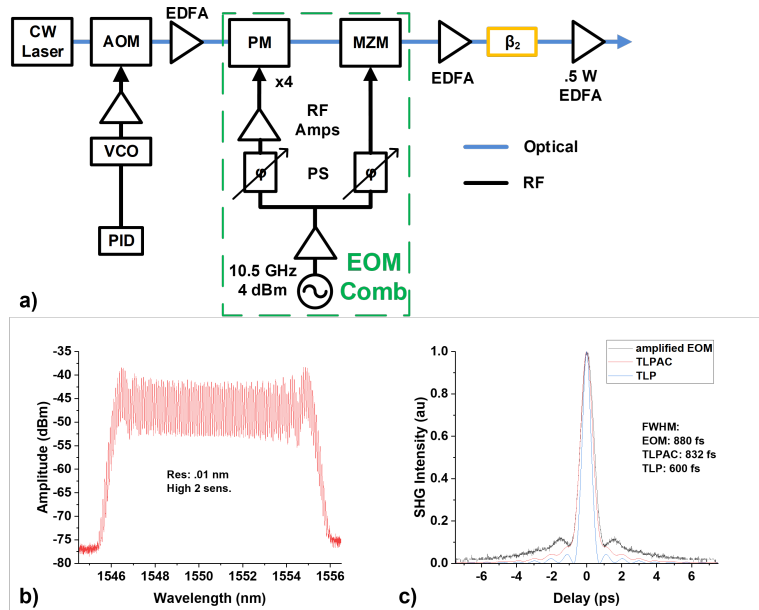


Figure 2.5: a) Experimental schematic of an EOM comb using four phase modulators and one intensity modulator driven by a common RF synthesizer at 10.5 GHz. PC: polarization controller, PM: phase modulator, MZM: intensity modulator, PS: RF phase shifter, AOM: acousto-optic modulator, VCO: voltage controlled oscillator, PID: proportional-integral-derivative controller. b) Measured optical spectrum, c) Measured compressed intensity autocorrelation

Depending on the laser, this could be an issue. One solution is to lock the CW laser frequency to a secondary reference (such as a Fabry-Perot etalon) and then use an additional single sideband suppressed carrier modulator. As of right now, ultra-stable etalons have been made by utilizing ultra-low expansion quartz as a spacer. Fig. 2.6 shows the transmission, reflection, and reflected phase profile of a Fabry-Perot etalon. Fig. 2.6a shows the reflection and transmission power of the etalon over multiple resonances while fig. 2.6b shows the transmitted and reflected power of a single etalon resonance. Finally fig. 2.6c shows the transmitted power and reflected phase profile of a single resonance.

Pound-Drever-Hall (PDH) laser stabilization is a common technique in which a CW laser fre-

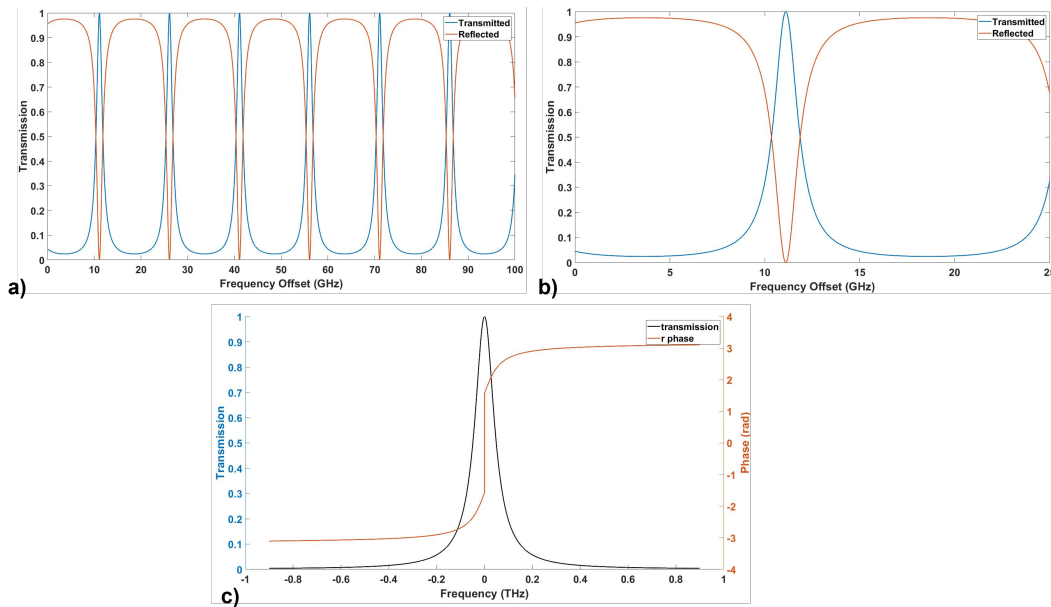


Figure 2.6: a) Transmission response of an etalon with respect to optical frequency, b) transmission and reflection profile of a single etalon resonance, c) reflected phase profile of a single etalon resonance.

frequency is stabilized to a reference cavity [46, 47]. The technique utilizes the reflected phase profile of an etalon to lock the CW laser frequency to the center of the passband. This is done by phase modulating the CW laser to produce sidebands that have opposing phase to each other. By sweeping the CW laser and sidebands across a resonance, the reflected light acquires a phase shift depending on the spectral location of each component of the light. From Fig. 2.6c, if the CW laser frequency is at the center of the resonance, the sidebands will cancel each other when photodetected. When the CW laser sweeps the passband of a resonance with a large modulation frequency, an error signal is produced which can be seen in Fig. 2.7. By decreasing the span of the frequency sweep, the center portion of the error signal is magnified. This results in a nearly linear error signal which can be compensated for with a simple PID lock. This allows for the CW laser frequency to be locked to the passband of an FPE. This is assuming the frequency sweep of the laser dominates

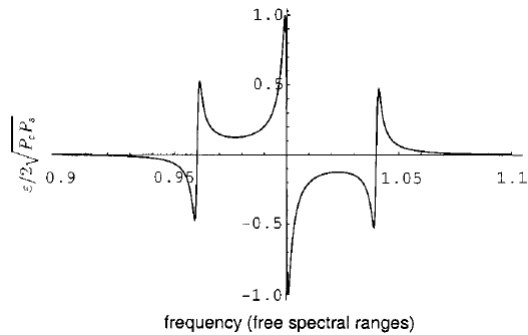


Figure 2.7: PDH error signal when a phase modulated CW laser sweeps across an etalon resonance.

over the laser's natural frequency drift, hence the previous discussion on selecting a low drift CW laser. It is important to note that the sidebands can be placed far from the carrier, allowing for higher suppression of the sidebands on the throughput of the etalon.

By locking the CW laser frequency to an etalon resonance, the extent of the frequency fluctuations has been significantly diminished. This results in a significant reduction in the laser phase noise. However, the CW laser frequency will still fluctuate within the passband of the etalon. This combined with the fact that a single etalon resonance has a non-flat transfer function contributes to amplitude noise.

In our experiments, we typically lock our ultra-narrow linewidth and frequency stable CW laser to an ultra-stable FP etalon with a finesse of 100,000 (FSR = 1.5 GHz and FWHM = 15 kHz). The setup used to perform PDH locking is shown in Fig. 2.8. The acousto-optic modulator (AOM) is used to quickly sweep the laser frequency and a separate analog proportional-integral-derivative controller (PID) is used to tune the laser frequency close to an etalon resonance. The phase modulator is used to imprint sidebands for the lock while the circulator is used to retrieve the reflected signal. In our PDH laser stabilization setup, we use one feedback loop using the AOM to quickly

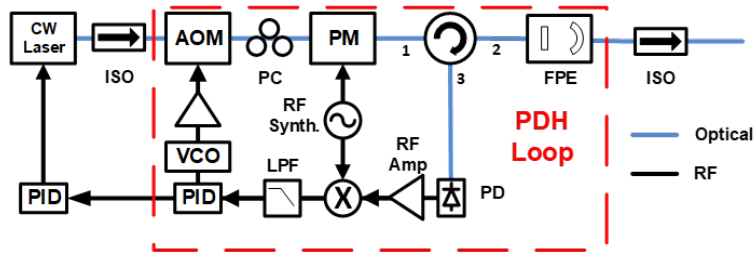


Figure 2.8: Schematic for locking a CW laser to a 100k finesse etalon through PDH. AOM: acousto-optic modulator, PM: phase modulator, FPE: Fabry-Perot etalon, ISO: fiber pigtailed isolator, VCO: voltage-controlled oscillator, PID: proportional-integral-derivative controller, LPF: low pass filter, PD: photodiode, RF Amp: RF amplifier, RF Synth: RF synthesizer.

tune the laser frequency to account for fast fluctuations in the laser frequency. A secondary feedback loop can be employed if the laser has a built in piezo for tuning the frequency. It is important to note that AOMs are a resonant device and exhibit high insertion loss when driven at frequencies offset from the resonant frequency. This gives rise to an unwanted change in power with respect to drive frequency. When locking the laser to the etalon using the AOM, it is common to observe frequency fluctuations of 10 MHz over the span of a couple hours.

With this in mind, we have significantly reduced the frequency fluctuations of our CW laser (and consequently, the f_0 drift of our future comb source). We have also increased the OSNR of the CW laser. The next section will discuss filtering noise between comblines in an EOM comb.

Modified Pound-Drever-Hall locking using a tunable etalon

In the previous section, it was mentioned that the OSNR of an EOM comb is limited by the lack of a filtering cavity. Optical filtering with a bandpass filter would indeed increase the OSNR of the comb, but the noise in between the comblines would still be present. This issue would be obscured when using a normal OSA, but would be revealed when performing a heterodyne beat

measurement with sufficient resolution. The result of noise in between comb lines consists of added noise (amplitude and phase) within the optical pulse train. An ideal filter for a comb source would be something that can filter the noise in between comb lines. A Fabry-Perot etalon would be an ideal type of filter if the resonances and the EOM comb lines were to perfectly match (both f_0 & f_{rep}). However, all lasers have an inherent frequency drift. For a Fabry-Perot etalon to properly filter an EOM comb, the comb lines must lie within the passband of the etalon. The filtering effect would not work if the comb were to drift outside of the filter passband. Pound-Drever-Hall locking has just been introduced as a method for locking a CW laser to an FPE. However, our goal requires us to not only stabilize the comb but also to filter the noise in between the comb lines. An alternative option is to design an FPE with an FSR equal to f_{rep} . In this section, we discuss using a poorly built tunable Fabry-Perot etalon to filter the noise between comb lines in an EOM comb. A schematic of this experiment can be seen in Fig. 2.9 and associated residual phase noise data in Fig. 2.10.

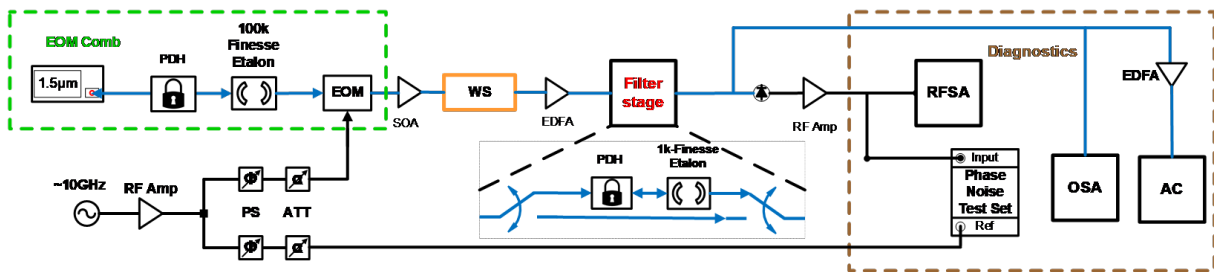


Figure 2.9: Schematic for measuring residual phase noise before and after a haphazardly built tunable etalon. EOM: cascade of electro-optic modulators, SOA: semiconductor optical amplifier, PS: RF phase shifter, ATT: RF variable attenuator, PDH:-Pound-Drever-Hall locking, EDFA: erbium doped fiber amplifier, WS: Finisar waveshaper, RFSA: RF spectrum analyzer, Phase Noise test set: HP carrier noise test set for measuring phase noise.

In Fig. 2.9, a CW laser is locked to a 100k finesse etalon by PDH, then modulated at 10 GHz to produce an EOM comb. An RF synthesizer is used to simultaneously drive an EOM comb and the reference branch of a carrier noise test set. The residual phase noise of the EOM comb before after the tunable etalon was measured by photodetecting the light, and amplifying it prior to the

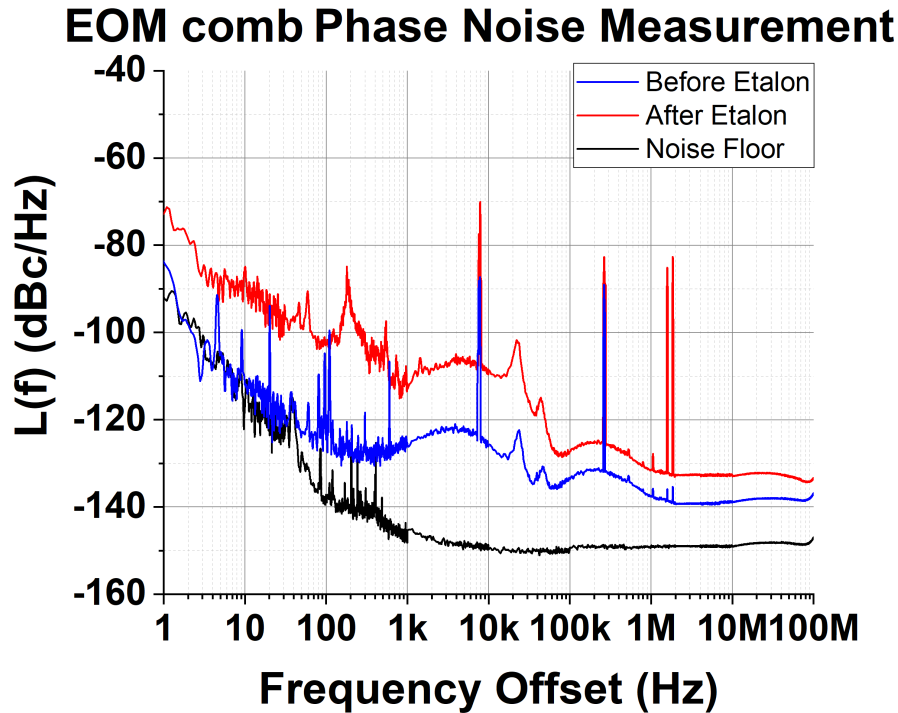


Figure 2.10: Residual phase noise measurement (blue) before locking tunable etalon to EOM comb, (red) after locking tunable etalon to EOM comb, (black) noise floor dictated by phase noise of synthesizer and amplifier

input port of the carrier noise test set. The residual phase noise measurement was used to test the change in phase noise after each component such as RF amplifier, EOM comb, and tunable etalon. It can be seen in Fig. 2.10 that the phase noise increases after passing through the tunable etalon at lower frequency offsets. Not shown here, we also measured the residual phase noise of an EOM comb seeded by a free-running CW laser. We observed the phase noise before the tunable etalon to be similar to the PDH locked CW laser based EOM comb before the tunable etalon. We also observed a significant increase in phase noise when the EOM comb seeded by the free-running CW laser was sent through the tunable etalon. We attribute this effect to issues regarding the build quality of the tunable etalon [48]. First, a tunable etalon is subject to environmental disturbances.

Environmental disturbances such as air currents, temperature fluctuations, and vibrations at the base cause the resonances to fluctuate. These fluctuations cause rapid changes in both the cavity spacing and the position of each individual resonance with respect to the next. This gives rise to noise coupling between f_{rep} and f_{ceo} . In addition, the piezo-electric material has a finite response time. This means that if the frequency fluctuations of the comb source are too quick for the etalon to respond, the comb source would experience a random phase shift in time due to the motion of the tunable etalon. The random fluctuations cause the passband of the etalon to modulate the incoming pulse train in both amplitude and phase. The modulation occurs because the amplitude and phase response of the etalon are not flat with respect to frequency. We also later discovered that the front mirror was not glued to the piezo! This means that as the piezo was pushing the front mirror forward, there was no way for it to retract! The etalon was essentially free-running with respect to the pulse train. The idea of the etalon was to reduce noise! However, we observe an increase in noise because of the etalon construction. All of these things together are an issue for coherent octave spanning supercontinuum generation. Significant effort is required to reduce additional noise from the tunable etalon. This motivates us to find a different method for filtering the noise in our EOM comb. A common option for building extremely stable etalons is to instead use Ultra-Low-Expansion (ULE) quartz spacers instead of mounting the mirrors on optical mounts. Tunable Fabry-Perot etalons will be further discussed in a later chapter.

Pound-Drever-Hall locking on an EOM comb

In the previous section, we discussed how using a haphazardly built tunable etalon could result in an increase in phase noise close to the carrier; creating issues in generating low noise EOM comb sources. However, we still need a method to filter the noise in between comb lines in our EOM comb. Last but not least, amplitude fluctuations caused by the AOM are still an issue for

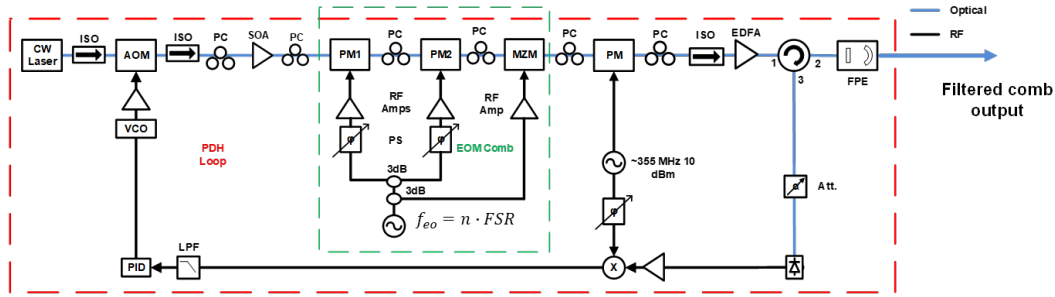


Figure 2.11: Architecture for generating filtered EOM combs via PDH locking of the EOM comb to a 100k finesse etalon. AOM: acousto-optic modulator, ISO: fiber pigtailed isolator, PC: polarization controller, SOA: semiconductor optical amplifier, PM: phase modulator, MZM: intensity modulator, EDFA: Erbium doped fiber amplifier, FPE: 100k finesse Fabry-Perot etalon, VCO: voltage controlled oscillator, RF Amps: RF amplifiers, PS: RF phase shifter, Att: optical attenuator, LPF: low pass filter, PID: proportional-integral-derivative controller.

generating low noise combs. In this section, we present an alternative method to producing filtered and stabilized EOM combs. Fig. 2.11 shows the architecture we use to produce locked and filtered EOM combs [49].

The operation of Fig. 2.11 is like the EOM comb in the previous chapter. First, the EOM comb is generated by applying a ~ 12 GHz RF signal. The anti-phase symmetric sidebands required for PDH locking are impressed upon all of the comb lines. The synthesizer frequency is then adjusted to match an integer multiple of the cavity FSR. The comb is then locked to the PDH locked to the etalon, allowing for each comb line to be simultaneously locked and filtered to the etalon. Optical amplifiers in between are used to compensate for losses and to eliminate for power fluctuations due to various components such as the AOM or intensity modulator. The EOM comb is first generated before completing the PDH loop. The advantages to this approach are that each comb line will be simultaneously filtered and stabilized by the FPE. As mentioned before, the FPE uses ULE quartz spacers and features a finesse of 100k, 15 kHz passband, and a 1.5 GHz FSR. The filtering capabilities should provide for a $-20\text{dB}/\text{dec}$ slope on the phase noise plot starting at 15 kHz. The

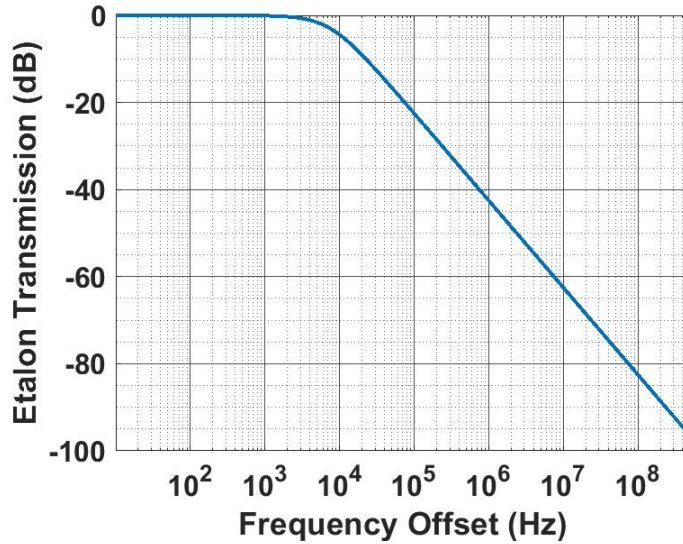


Figure 2.12: Transmission response of a single resonance of the 100k finesse etalon in dB scale. 100k finesse etalon specs: 100k finesse, ~ 1.5 GHz FSR, FWHM: ~ 15 kHz.

transmission of a single resonance of the 100k finesse etalon is shown in Fig. 2.12. Each combline should be placed at the center of the passband with minimal attenuation as long as the cavity FSR and f_{rep} drift sufficiently slowly with respect to each other.

This technique requires that the etalon FSR must be known to as many digits of precision as possible. The etalon FSR was measured using a modified PDH technique of adjusting the frequency of the PM sidebands used to sweep the cavity resonance. This ensures that the output power of the system remains constant, despite the AOMs frequency response. Optical spectrum, RF spectrum, and intensity autocorrelation measurements are shown in Fig. 2.13.

From Fig. 2.13a, the optical spectrum's OSNR is shown to increase by at least a factor of at least 20 dB. The enhancement in the OSNR demonstrates the feasibility of this technique to improve the noise performance of EOM combs. The RF spectrum shown in Fig. 2.13b also exhibits an SNR > 60 dB. The intensity autocorrelation in Fig. 2.13c was measured using an SHG autocorrelator. The

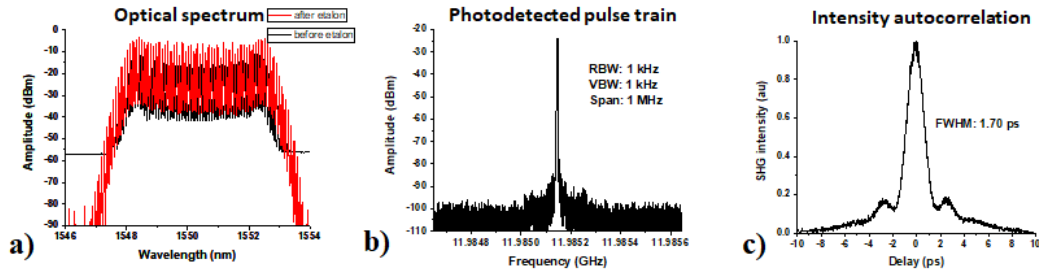


Figure 2.13: Diagnostic traces of PDH locked EOM comb employing two phase modulators and one intensity modulator: a) Optical spectrum before etalon (black) and after etalon (red), b) photodetected RF beat note after the etalon, c) intensity autocorrelation externally compressed and measured after the etalon.

compressed pulses again exhibit temporal sidelobes characteristic of EOM combs. Although this approach solves the issue of filtering noise in between comb lines, there is still an issue of ensuring the RF drive frequency matches the FPE FSR to Hz level precision. Despite being extremely stable to thermal fluctuations, ULE quartz still ages over time. This gives rise to a small change in the FSR of the cavity with respect to the RF synthesizer's clock. Ideally, we would like to replace the RF synthesizer with a lower noise RF source, continuously filter the EOM comb, and eliminate the drift of the etalon FSR with respect to an external RF source.

Optoelectronic Oscillators

OEOs are a photonic-electronic oscillator that uses an optical and an RF cavity together to generate an RF signal. An OEO consists of a CW laser, electro-optic intensity modulator, photodetector, RF amplifier, and some type of high Q element such as a filter [50]. OEO's have become an alternative method to generating higher frequency RF oscillator signals and are still being investigated today. OEO's can oscillate at high electrical frequencies (up to 70 GHz) without as much degradation in the quality of the signal compared to purely electrical means of generating high frequency signals.

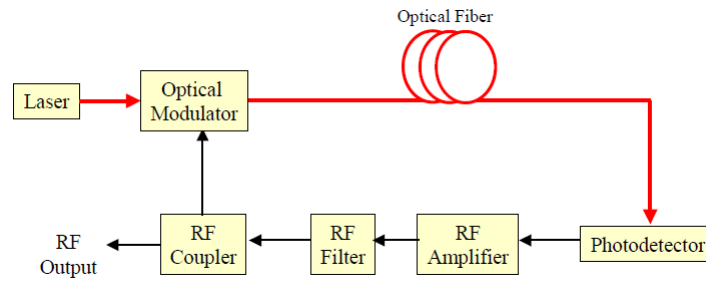


Figure 2.14: Schematic representation of a basic OEO using optical fiber as the high Q optical cavity and an RF filter as a high Q electronic cavity.

The oscillation frequency and noise properties mainly depend on the high Q element. The most basic OEO uses a long length of SMF28 for the high Q cavity and a RF bandpass filter (BPF) to select the oscillating frequency. The Q of an optical fiber delay is $\sim 2\pi f\tau$, where f is the OEO oscillation frequency and τ is the round trip time [51]. Although the Q of the delay line can be made extremely high, the frequency spacing of the oscillation modes is inversely proportional to the length. Longer lengths of fiber yields higher Q's but narrower frequency spacing of the modes. This requires the use of extremely high Q RF filters to suppress adjacent oscillating modes for steady operation. A sample schematic of a simple OEO can be found in Fig. 2.14.

Many improvements on their noise performance have been thoroughly investigated [52–54]. Some approaches have used multiloop OEO where two different loops of SMF28 of different lengths are used so that the peaks of each fiber loop are cancelled by the nulls of the other one. However, a drawback is that the effective Q of the multiloop OEO is an average of the two loops, resulting in suboptimal performance. Another approach is to combine the multiloop approach with injection locking, which can circumvent the issue of the Q averaging effect.

Photonicly filtered opto-electronic oscillators

An alternative method to circumvent the challenges with RF filtering (passband width and high extinction) is to use an optical filter such as a Fabry-Perot etalon (FPE) or whispering gallery mode (WGM) resonator [55] and [56]. The optical resonator provides transmission peaks that filter the optical noise from the previous components such as amplifiers and the CW laser. Photodetection of the transmission peaks gives rise to RF beat notes commensurate with the FSR of the cavity. The RF beat notes can then be fed back to the modulator to form an OEO feedback loop. The benefit to using an optical filter compared to long lengths of fiber are 1) a lack of noise spurs in the OEO RF tone and 2) improved RF and environmental stability. Schematically, the difference between an RF filtered OEO and a photonicly filtered OEO can be seen in Fig. 2.15.

Fig. 2.15 shows the difference between an RF filtered OEO and a photonicly filtered OEO. In Fig. 2.15b, several RF modes are shown oscillating while the RF filter is used to sustain a single RF mode. To sustainably oscillate, the RF filter must have a sufficiently narrow passband and a sufficiently high rejection of the adjacent modes. In contrast, the photonicly filtered OEO, shown in Fig. 2.15c, optically filters the light and then photodetects the filtered light. This gives rise to a comb filtered optical spectrum, shown in Fig. 2.15d, where light only oscillates within the transmission peaks of the filter and is rejected outside of the filter passband. This gives rise to farther spaced RF modes in the RF frequency domain (shown in Fig. 2.15e). FPE's and WGMR can easily be made with extremely large mode spacings (30 GHz) and high Q's (10^{10}). In addition, FPE's can employ Ultra-low expansion (ULE) quartz as a spacer between the mirror cavities and have significantly less nonlinearity compared to fiber. The use of ULE quartz as a spacer significantly enhances both the thermal and vibrational stability of the cavity.

Although photonicly filtered OEO's can easily achieve greater frequency stability compared to their RF filtered counterpart, significantly less research has been done on low noise photonicly

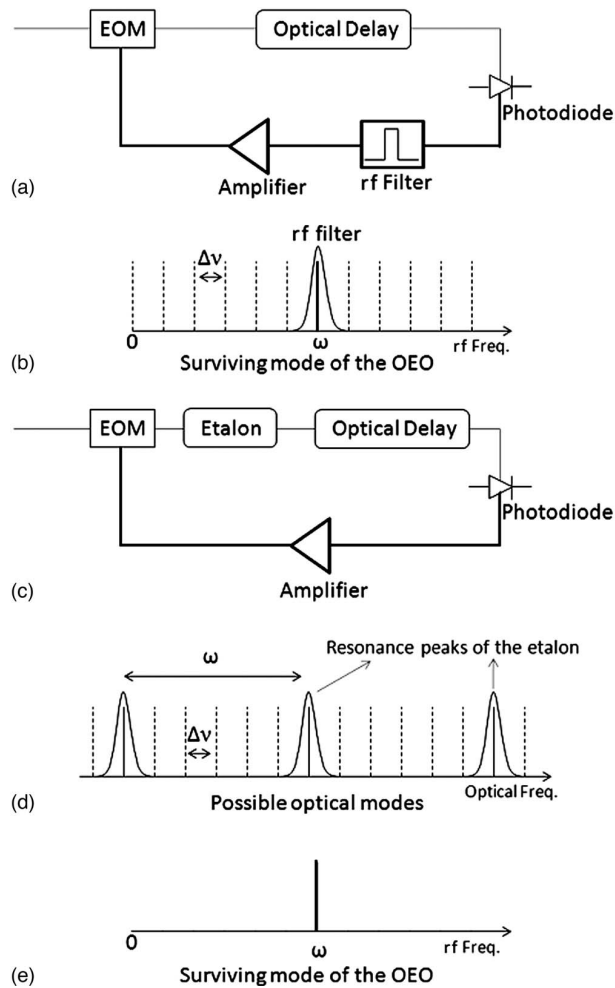


Figure 2.15: a) Schematic diagram of an RF filtered OEO, b) RF frequency spectrum of an RF filtered OEO, c) schematic diagram of a photonic filtered OEO, d) optical spectrum of the photonic filtered OEO, e) RF spectrum of the photonic filtered OEO.

filtered OEO's. This can be attributed to several issues including: coupling into the optical cavity, ensuring the laser stays within the passband of the cavity, and the cost of a high Q cavity. Coupling into an optical cavity requires spatial mode matching which requires the use of free space optics and is not easily portable. Fiber coupled FPE enclosures can be purchased but are still expensive. A significant technical issue is ensuring the laser frequency does not drift out of the passband of the cavity. This typically requires using a phase locked loop to lock the laser to the cavity. We

typically employ PDH locking to ensure the CW laser frequency stays locked to a single resonance of the FPE.

For our purposes, a photonicly filtered OEO better suits our needs for a low noise RF signal generator. A combined approach of using an OEO and a frequency comb generator has been demonstrated in other works [15, 55]. This allows for a cost-effective approach in generating high repetition rate frequency combs by removing the RF source and replacing it with a high speed photodetector. Although we mentioned that a high finesse FPE is expensive, we draw attention to the fact that stabilizing the CW laser in an EOM comb greatly helps with reducing the drift of f_0 . In this sense, we are generating the RF signal to drive the EOM comb (just by adding a photodetector). It has also been shown that OEOs exhibit lower phase noise than RF synthesizers at the same output frequency. As previously mentioned, RF synthesizers employ a 10 MHz reference oscillator and multiply the frequency to generate the output. This results in severe phase noise degradation as a result of the multiplication process. Unlike an RF synthesizer, OEOs do not employ frequency multiplication and naturally oscillate at the output frequency. This potentially allows for the OEO to produce a lower phase noise RF signal.

Optically filtered and stable electro-optic modulated comb without an external RF source

As previously mentioned, an OEO can generate an RF source that can be used to drive an EOM comb. However, in previous works, the etalon used to complete the OEO loop was not used to its full potential. Typically, PDH locking is employed to ensure that the CW laser stays within the etalon resonance and forces the OEO oscillation at a single frequency. Since an OEO oscillates at integer multiples of the FSR of the cavity, the correct modulation frequency to allow the EOM comb lines to pass through the etalon is already being generated. When generating RF signals via integer multiples of the FSR, an RF bandpass filter can be used to ensure oscillation at only one

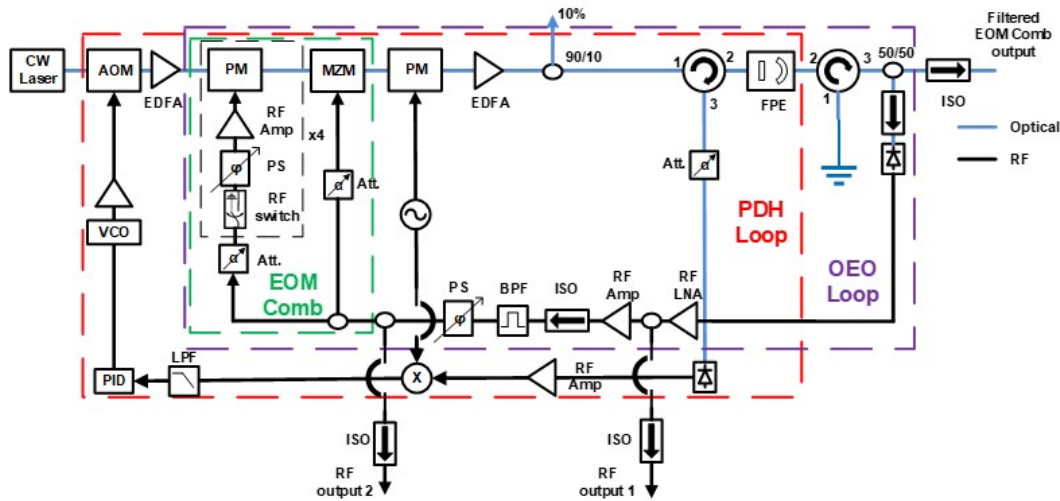


Figure 2.16: Schematic of the optically filtered OEO EOM comb employing 4 phase modulators and 1 intensity modulator for comb generation. AOM: acousto-optic modulator; PM: phase modulator; MZM: intensity modulator; EDFA: erbium doped fiber amplifier; FPE: 100k finesse ULE quartz spaced Fabry Perot etalon; att: adjustable attenuator; PD: photodetector; ISO: isolator; BPF: bandpass filter; PS: phase shifter; VCO: voltage-controlled oscillator; PID: servo controller; LPF: low pass filter

frequency. By simply moving the phase modulators in the OEO EOM comb before the etalon, it is possible to simultaneously generate, stabilize, and filter all the comb lines. However, unlike mode-locking, there would be no interplay between the gain medium, roundtrip time of the cavity, and nonlinearity (saturable absorption for passive mode-locking and time gating for active mode-locking). This allows for the OEO EOM comb to oscillate at integer multiples of the FSR without the high noise from harmonic mode-locking (unlike traditional mode-locking) [57]. A schematic of the demonstrated OEO EOM comb is shown in Fig 2.16.

The OEO EOM comb schematic shown in Fig. 2.16 can be broken up into three distinct portions, PDH locking (red), EOM comb generation (green), and the OEO loop (purple), which are outlined in the dashed boxes. The main idea of the schematic is to first lock the CW laser to an FPE resonance by PDH, photodetect a portion of the filtered light, and then feed the RF signal into a set

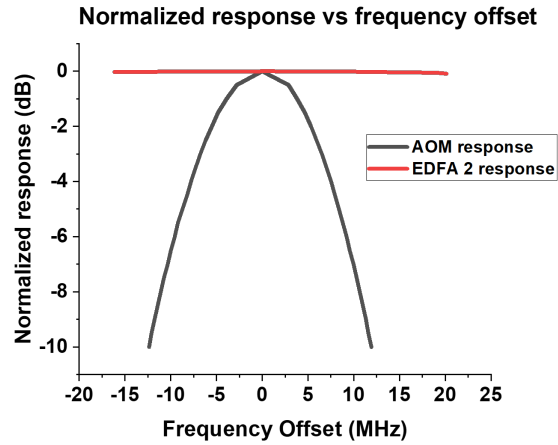


Figure 2.17: Normalized acousto-optic modulator response with respect to input drive frequency (black) and normalized output power response after EDFA 2 with respect to frequency (red).

of modulators placed before the etalon. Since the OEO can only oscillate at integer multiples of the cavity FSR, the generated comb lines will naturally fit inside the cavity passbands. The setup starts with a CW laser (OEwaves4028 with optical linewidth < 7 Hz) that is frequency swept by an acousto-optic modulator (AOM). The AOM is used to lock to an FPE resonance. An EDFA is operated in saturation to simultaneously amplify the light up to 280 mW and dampen the amplitude fluctuations caused by the AOM. Fig. 2.17 shows the normalized amplitude response of the AOM with respect to VCO frequency and the normalized output response of the AOM after amplification using the EDFA.

From Fig. 2.17, we observe significant changes in output power with respect to input frequency after the AOM (shown in black). By operating multiple amplifiers in deep saturation after the AOM, we observe almost no change in output power with respect to input frequency (red).

A cascade of four low V_{π} high RF power handling Lithium Niobate phase modulators and a single intensity modulator are used to produce the EOM comb. Another phase modulator is used to pro-

duce the anti-phase symmetric sidebands necessary for PDH locking. Another EDFA is operated in saturation to amplify and clamp the signal to 55 mW. The FPE in this work features an ultra-low expansion (ULE) quartz spaced etalon with a ~ 15 kHz passband and a ~ 1.5 GHz FSR. Unlike other OEO architectures, long lengths of fiber to increase the Q of the cavity are not used. The FPE is mounted in a chamber to reduce air current fluctuations but is not vacuum pumped nor temperature controlled. For PDH locking, the reflected phase modulated sidebands are photodetected and mixed down to produce an error signal for frequency correcting the CW laser by the AOM. At the output of the etalon, an additional fiber circulator is used as an isolator to prevent any back reflections from passing through the FPE. We measure an output power after the circulator of 11 dBm. Better coupling into the cavity and fusion splicing connectors could increase the output power by at least 3 dB.

A 50/50 coupler is used for the optical output (7 dBm) while the other output (7 dBm) is photodetected for the OEO loop. Fusion splicing the circulator, coupler, and isolator would reduce the losses by ~ 1 dB. The photodetector output is amplified by two RF amplifiers; one low noise amplifier (P1dB=10 dBm) and one power amplifier (P1dB=35 dBm). The RF amplifiers are followed by an RF isolator, a 10 MHz bandpass filter centered at 10.5 GHz, an RF phase shifter, and a series of couplers. The bandpass filter is used to ensure the OEO can only oscillate at the 7th harmonic of the FPE while the RF phase shifter is used to ensure a full 2π phase necessary for the OEO oscillation of 10.5 GHz. The first coupler after the phase shifter is used to drive the intensity modulator. An adjustable attenuator is used to ensure the intensity modulator does not exceed the maximum RF power rating. The other end of the coupler is fed into an adjustable attenuator to ensure the input power into the following RF amplifiers is below the maximum rating. Each phase modulator has an RF switch, RF phase shifter, and RF power amplifier. For maximum comb bandwidth generation, the phase of each RF signal driving the phase modulator is matched in phase with the phase of the signal in the intensity modulator. The RF switch and RF phase shifter allow

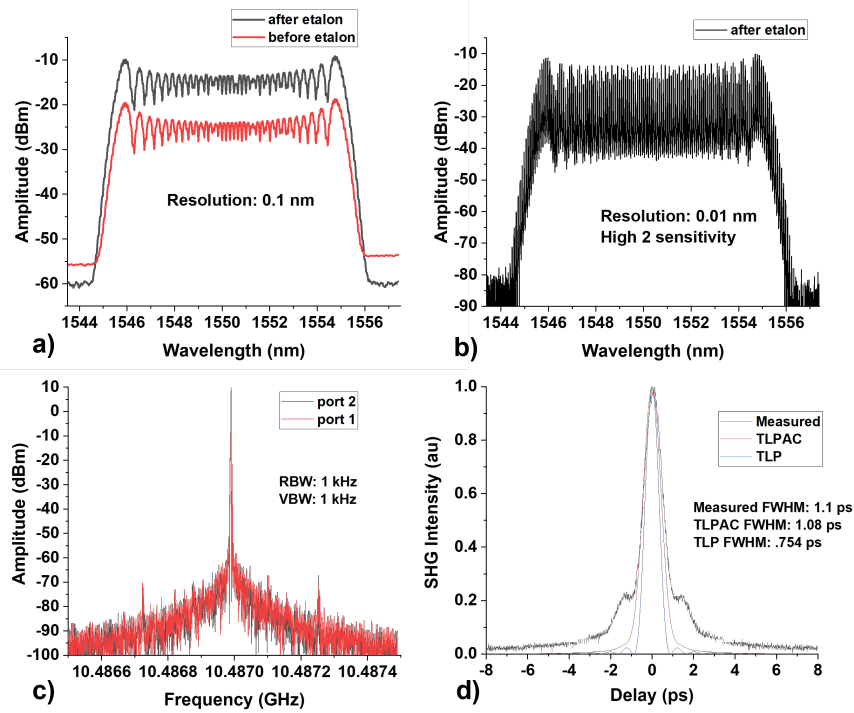


Figure 2.18: (a) Optical spectrum of the optically filtered OEO EOM comb before (black) and after the etalon (red). (b) Optical spectrum of the OEO EOM comb after the etalon with high 2 sensitivity. (c) RF spectrum at RF output 1 (red) and RF output 2 (black) of the optically filtered OEO EOM comb. (d) Externally compressed and measured SHG Intensity autocorrelation of optically filtered OEO EOM comb (black), calculated transform limited pulse autocorrelation from optical spectrum (red), and calculated transform limited pulse from optical spectrum (blue).

simple adjustment of the phase to ensure maximum comb generation. The RF amplifier connected to each phase modulator has a P1dB=35 dBm.

OEO comb generation is initiated by connecting one end of the 50/50 coupler to the photodetector, adjusting the RF phase, and attenuators to allow for the OEO EOM comb to oscillate. Fig 2.18 shows the optical spectrum, RF beat note (from RF output 2), and compressed intensity autocorrelation of the OEO EOM comb. The optical spectrum before the FPE was measured using the 10% output port while the optical spectrum after the FPE was measured at the filtered EOM comb

output port. Before the FPE, the OSNR of the comb is ~ 35 dB. After the FPE, the OSNR of the comb increases by ~ 15 dB and is limited by the resolution and sensitivity of the OSA. The same optical spectrum after the etalon was measured with .01 nm resolution and increased sensitivity at the filtered EOM comb output port in Fig. 2.18b, demonstrating the generation of over 100 comb lines with OSNR > 65 dB and a noise floor of -80 dBm, which is limited by the noise floor of the OSA.

A 6 dB attenuator and 1 meter long SMA cable are used to direct the RF output 2 signal into the RF spectrum analyzer. Back calculating the losses results in an RF output power of ~ 28 dBm. The resulting RF spectrum is shown in Fig. 2.18c. The RF beat note exhibits an SNR > 90 dB at a resolution bandwidth of 1 kHz. The RF beat note exhibits noise spurs that are offset from the carrier in integer multiples of 7.5 kHz. Typically, a CW laser locked to an FPE by PDH would exhibit sidebands that are commensurate with the FWHM of the etalon passband. This is because the CW laser frequency is dithered within the passband of the FPE. The amplitude response of the FPE is not flat within the frequency range of the laser's fluctuation, giving rise to an amplitude modulation sideband. We observe a spur that is 260 kHz offset from the carrier on the RF spectrum, which only appears after comb generation is initiated. We believe this is due to the noise of the switching power supplies that are used to drive the RF amplifiers.

At the filtered EOM comb output port, the pulse train has a 50% duty-cycle. The SHG intensity autocorrelation was measured by using a Finisar waveshaper to apply 4.2 ps/nm dispersion and amplifying the pulse train prior to the autocorrelator. The compressed autocorrelation trace in Fig. 2.18d shows a FWHM duration of 1.1 ps with temporal sidelobes which are common to EOM combs compressed by second order dispersion. The sidelobes can also be reduced by applying higher even order dispersion terms [13].

The phase noise of the 10.5 GHz signal and the Allan variance were also measured at RF output 1

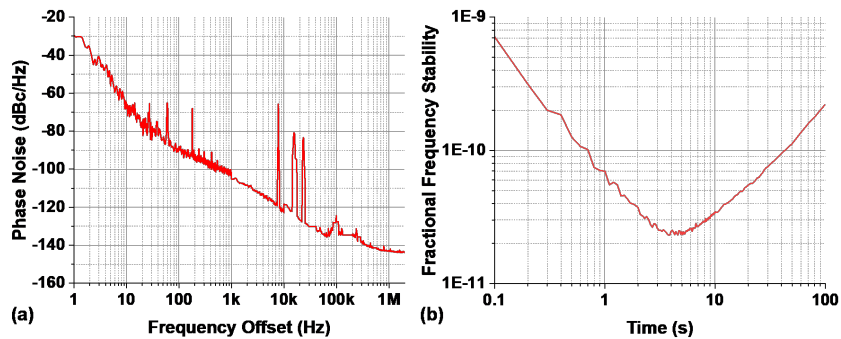


Figure 2.19: (a) Measured absolute phase noise at RF output 1 of the optically filtered OEO EOM comb. (b) Measured fractional frequency stability at RF output 1 of the optically filtered OEO EOM comb.

of the OEO EOM comb. The results of these measurements are shown in Fig. 2.19. We observed ~ 10 dB improvement in the phase noise at frequency offsets from 1 Hz to 10 kHz in Fig. 2.19a compared to previous works of using the same etalon for an OEO. At frequency offsets of 100 kHz and above, the measurement is limited by the noise floor of the measurement system. We attribute the improvement in phase noise to multiple factors such as: all optical amplifiers are placed before the etalon and more power on the photodetector. We also observed an order of magnitude improvement in the Allan variance in Fig. 2.19b. We attribute the improvement of the Allan variance to the optically filtered combs in that are photodetected and used for the OEO.

Opto-electronic oscillator driven electro-optic modulated comb

In the previous section, we discussed using a 100k finesse etalon to stabilize, generate, and filter an EOM comb. We also showed results of said system. Unfortunately, the system became difficult to work with for reasons unknown. We have noticed that the system in the previous section is extremely sensitive to fluctuations in the intensity modulator bias as well as the length of fiber

before the 100k finesse etalon. By increasing the length of fiber before the etalon, the PDH loop bandwidth decreases due to the additional transit time the correction signal must take. Although the CW laser stays locked to the cavity, the laser frequency begins to oscillate within the passband of the etalon. This issue is further amplified by the OEO loop and EOM comb generation. When the CW laser fluctuates within the passband of the etalon, the throughput of the etalon also experiences the same oscillation. The photodetector in the OEO loop would then convert this oscillation into an RF signal around the main OEO tone. The EOM comb is then driven by this noisy RF signal and generates noisy comb lines around the CW laser. Our EOM comb is capable of generating at least 100 comb lines when an RF signal is present. This means that the noisy RF tone driving the EOM comb branch produces 100 noisy comb lines. This affects the stability of the PDH lock and forces the PDH lock to break. Future iterations of the previous system may need to shorten the fiber lengths between components to ensure robustness on the PDH lock. Due to the issues of robustness in the previous system, we have modified the OEO EOM comb setup such that the phase modulators are placed after the 100k finesse etalon. Although we are unable to take advantage of the filtering effect of the 100k finesse etalon, we can still derive a high quality RF signal through the OEO loop. A schematic diagram of the new OEO EOM comb is shown in Fig. 2.20 with diagnostic traces in Fig. 2.21.

This chapter has demonstrated multiple improvements to a common EOM comb in terms of cost and performance. We have shown that a high finesse FPE can be used to simultaneously generate and stabilize an EOM comb without an external RF oscillator. Our EOM comb produces pulses that are compressible to under a picosecond with phase noise lower than an RF synthesizer. Although these improvements do not immediately solve the issues associated with coherent octave spanning supercontinuum generation, they provide important intermediate steps. The beginning of this chapter started with pulses as long as 1.6 ps (autocorrelation FWHM) and ended with pulses shorter than 1.0 ps (by use of additional phase modulators). We showed an architecture capable of

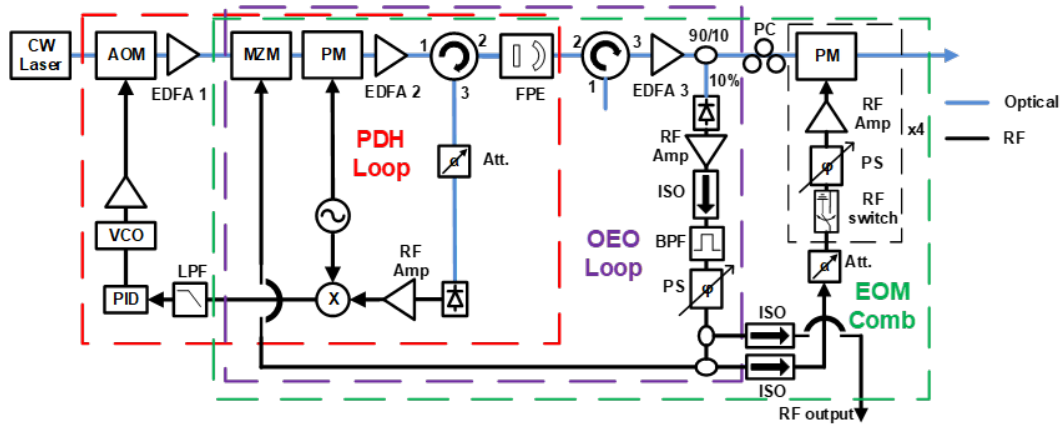


Figure 2.20: OEO EOM comb schematic diagram with 4 phase modulators placed after the etalon. AOM: acousto-optic modulator, EDFA: Erbium doped fiber amplifier, MZM: intensity modulator, PM: phase modulator, FPE: Fabry-Perot etalon, Att.: attenuator, RF Amp: RF amplifier, LPF: low pass filter, PID: proportional-integral-derivative controller, VCO: voltage controlled oscillator, RF Amp: RF amplifier, ISO: RF isolator, BPF: RF bandpass filter center frequency of 10.486 GHz and 10 MHz passband, PS: RF phase shifter, RF switch: RF absorptive switch.

locking and filtering f_0 and f_{rep} of an EOM comb.

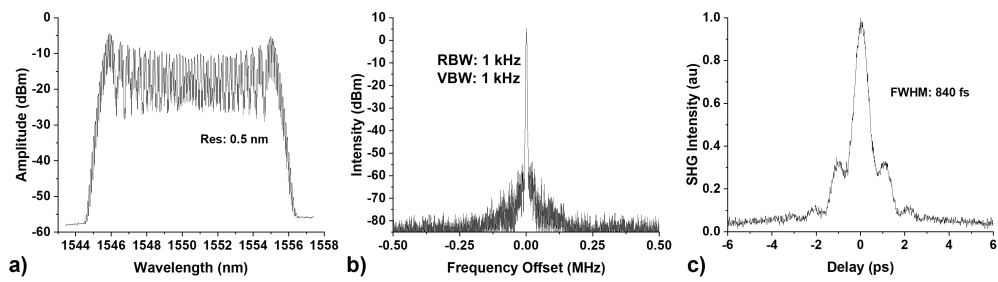


Figure 2.21: Diagnostic traces of the OEO EOM comb: a) optical spectrum, b) RF spectrum measured at the RF output, externally compressed and measured second harmonic intensity auto-correlator.

CHAPTER 3: OPTICAL FILTERING USING A TUNABLE ETALON

In the previous chapter, we discussed using an ultra-high finesse optical cavity as a means for generating, locking, and stabilizing a high repetition rate comb source. However, the generated optical bandwidth is insufficient for producing ultrashort fs pulses necessary for coherent octave spanning supercontinuum generation. To reach pulse durations of <200 fs, additional amplification and spectral broadening is needed. In addition to these phase noise multiplication of newly generated comb lines, amplification adds amplified spontaneous emission (ASE) noise which has been shown to degrade coherence in supercontinuum generation. This chapter seeks to solve the issues related to adding ASE noise and phase noise multiplication through optical filtering.

Optical Cavity Dispersion and FSR walk-off

As previously mentioned, the spectral bandwidth of the generated comb is only on the order of 1 THz. We require at least 4.4 THz of optical bandwidth (assuming a rect function) to generate pulses short enough in duration. To increase the generated optical bandwidth, we would need either more phase modulators or some form of nonlinear spectral broadening. Ideally, we would like to have all 8 THz of coherent optical bandwidth filtered by the 100k finesse etalon used for generating our OEO signal. This would simplify the setup by eliminating the need for an external etalon. To test the filtering capability of our 100k finesse etalon, we generate as much optical spectra as possible and try to lock it to the etalon. In Fig. 3.1a shows the setup schematic for testing the limits of optical filtering. This is done by first generating an EOM comb (driven by an external RF synthesizer), compressing the pulses, amplifying the pulses up to .5 W, and then sending the pulses into 100 m of normal dispersion highly nonlinear fiber for spectral broadening. Finally, the broadened spectrum is PDH locked to the 100k finesse etalon by driving the phase modulator

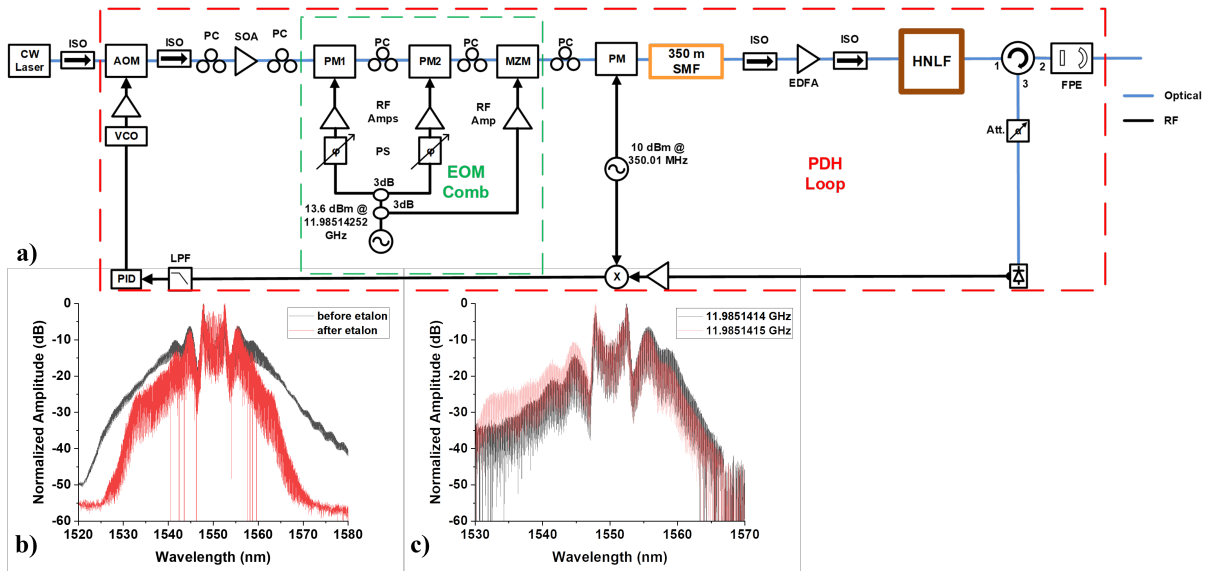


Figure 3.1: a) Schematic for testing optical bandwidth limitation of 100k finesse etalon. AOM: acousto-optic modulator, ISO: fiber pigtailed isolator, PC: polarization controller, SOA: semiconductor optical amplifier, PM: phase modulator, MZM: intensity modulator, EDFA: erbium doped fiber amplifier, HNFLF: 100 m of normal dispersion highly nonlinear fiber, FPE: 100k finesse Fabry-Perot etalon, VCO: voltage controlled oscillator, RF Amps: RF amplifiers, PS: RF phase shifter, LPF: low pass filter, PID: proportional-integral-derivative controller. b) Normalized optical spectrum of the nonlinearly broadened EOM comb before (black) and after the 100k finesse etalon (red). c) Normalized optical spectrum of the etalon throughput for different repetition rates: 11.9851414 GHz (black) and 11.9851415 GHz (red)

at 350 MHz and sweeping the entire comb (using the AOM) across the etalon resonances. We adjust the RF synthesizer frequency to match the cavity FSR. This should theoretically allow for the combs to pass through the etalon without attenuation. It is important to note that the PDH error signal also gives an indication for the detuning of the repetition rate of the EOM comb and the FSR. Details regarding nonlinear spectral broadening will be discussed in future chapters.

From Fig. 3.1b, the normalized optical spectrum before (shown in black) and after (shown in red) the etalon is shown. The difference in thickness between the two spectra are due to the measurements using different resolutions. In addition, the spectrum in red shows several dropped

combines which are artifacts from the OSA. We observe significant spectral broadening before the etalon (with respect to the seed EOM comb) and a significant roll off after the etalon. Fig. 3.1c shows the etalon throughput for different repetition rates. We observe that depending on the repetition rate of the EOM comb, the filtered comb leans in different directions. The lower repetition rate leans towards longer wavelengths while the higher repetition rate leans more towards the center of the spectrum. The difference in repetition rate between the vastly different optical spectra is only 100 Hz. It seems like the edges of the optical spectrum experience additional attenuation compared to the center regardless of the repetition rate. We also could not observe a broader throughput spectra by tuning the repetition rate with finer precision. These results entail an FSR changing with respect to wavelength. Unfortunately, high finesse etalons are extremely susceptible to this effect.

The change in FSR with respect to wavelength can be expressed as: $FSR \sim \frac{c}{2L + \frac{c}{\pi} \frac{\partial \phi}{\partial f}}$ [58]. Where $\frac{\partial \phi}{\partial f}$ is the change in reflected phase with respect to optical frequency of the mirrors used in the etalon. To achieve extremely high reflectivity mirrors, a distributed Bragg reflector (DBR) stack is deposited on a substrate. Reflected phase data that was provided from Thorlabs crystalline mirror coatings were used to compute the group delay and group delay dispersion. This is shown in Fig. 3.2. Using the reflected phase data from Fig. 3.2, we calculated the FSR of an etalon using these mirrors (shown in Fig. 3.3).

From Fig. 3.3, we observe the FSR of the etalon to sharply decrease from the center located at ~ 1546 nm. The mirrors used to calculate the cavity dispersion here are meant for a 200k finesse etalon with an FSR of 15 GHz, entailing a passband FWHM of 75 kHz. The orange line in Fig. 3.3 denotes the FSR of the highest value (GDD=0). The green line denotes where the FSR has changed by half the passband of a single resonance. With this particular etalon, we estimate a usable optical bandwidth of ~ 16 nm. Although the etalon used in our experiments is different than the one mentioned here, it is important to note that the same effect of cavity dispersion can be observed.

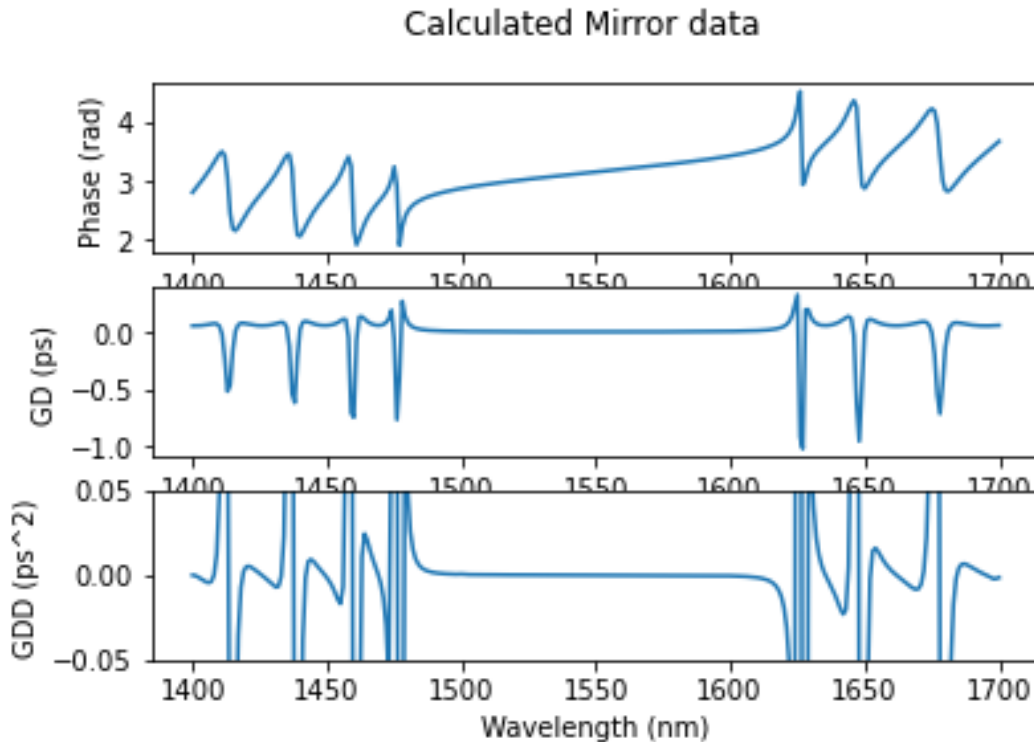


Figure 3.2: Reflected phase data of ultrahigh reflectivity crystalline mirrors provided by Thorlabs. Top: Reflected phase with respect to wavelength. Middle: Calculated group delay with respect to wavelength, Bottom: Calculated group delay dispersion with respect to wavelength.

From Fig. 3.1, we observe that the usable bandwidth of the ultra-high finesse etalon is only ~ 16 nm. Assuming a rect function with the theoretical maximum bandwidth of 16 nm centered at 1546 nm, we compute a transform limited pulse duration of ~ 440 fs. Why does this happen? From Fig. 3.2, we see that the reflected phase of these mirrors is far from flat in the operating band. Mirrors based on multiple interference exhibit high dispersion because different colors penetrate different depths on the DBR stack. The different depth gives rise to a difference in delay for different colors. This effect causes the mirror dispersion which causes the cavity FSR to change with wavelength. In addition, higher finesse cavities have a narrower passband (assuming constant FSR). The narrower passband combined with FSR walk-off yields greater spectral attenuation on

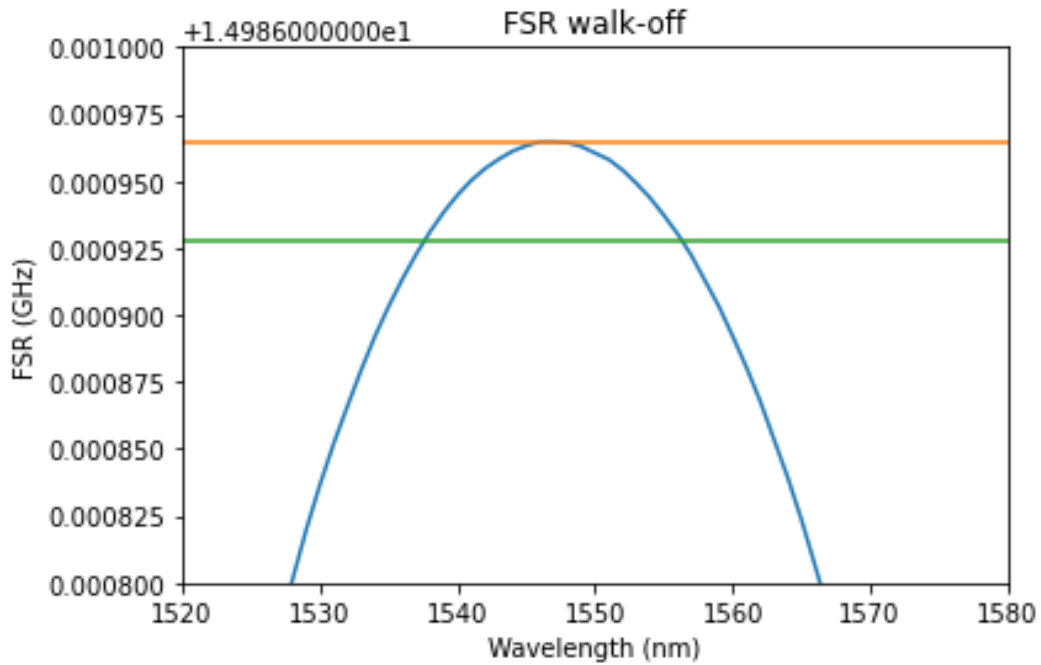


Figure 3.3: Theoretical Fabry-Perot etalon free-spectral range with respect to wavelength using Thorlabs crystalline mirrors assuming a cavity with designed FSR=14.986 GHz and Finesse=200,000.

the edges of a perfect comb spectrum. This sets an upper limit on the total optical bandwidth of a comb source that can pass through an etalon. We conclude that high finesse etalons need to address the dispersive mirror problem if they are to be used for filtering broad bandwidth optical comb sources. Otherwise, they would be unable filter wide spanning comb sources. This means that our 100k finesse etalon is incapable of filtering enough comb lines for our purposes. For us to obtain large spanning filtered comb sources, we would need to build an external lower finesse etalon that can filter broader bandwidth comb sources.

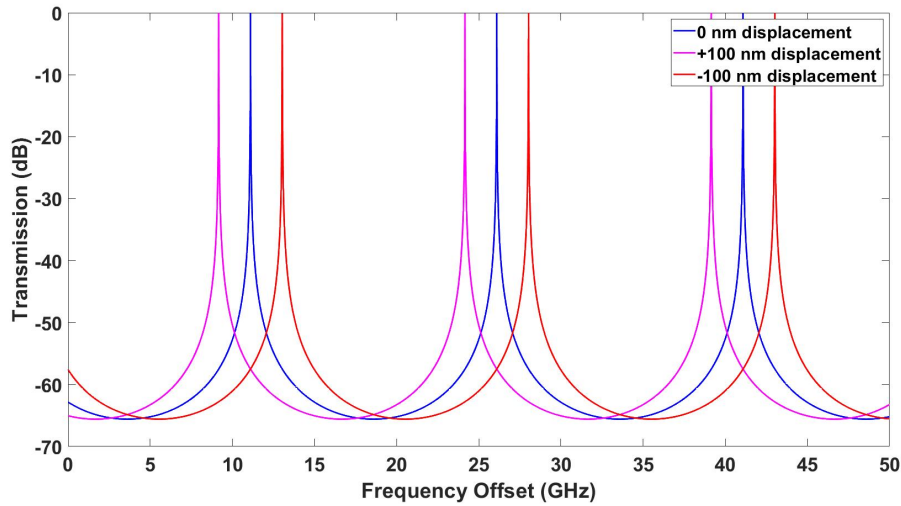


Figure 3.4: Theoretical transmission of a tunable etalon with FSR=14.9896229 GHz. In blue, the etalon resonances with no mirror translation. In red, the etalon resonances when the front mirror has translated backward by 100 nm. In magenta, the etalon resonances when the front mirror has translated forward by 100 nm.

Tunable etalon background

In the previous sections, we have discussed ultra-stable etalons using spacers. The purpose of the spacer is to provide for extremely high stability so that environmental disturbances cannot misalign the cavity. We have observed in the lab that higher finesse etalons require extreme stability for operation. We have also found that ultra-high finesse etalons would not suit our purposes for filtering large optical bandwidths (~ 4.4 THz). Here, we will discuss the operating principle of a tunable etalon. In Fig. 3.4, we plot the transmission function of an etalon with the following properties in blue. FSR: 14.9896229 GHz (10 mm length), mirror reflectivity: 99.9%, and flat curved mirror configuration.

In Fig. 3.4, we also plot the transmission function of an etalon where the cavity length has increased

by 100 nm (magenta) and decreased by 100 nm (red). As a result, the FSR has changed by 149.898 kHz (blue and magenta curves) and the FSR has changed by 149.895 kHz (blue and red curves). At the same time, all of the resonances have shifted 1.934 GHz! The drastic difference in the shifting of all of the resonances compared to the spacing between the resonances gives the tunable etalon significant flexibility in filtering arbitrary comb sources. Although a travel of 100 nm is small, commercial piezos can be purchased with the ability of expanding and contracting with far better precision. In addition to the flexibility in tuning the optical resonances, we are also able to construct etalons in-house with commercial components.

Fig. 3.5 shows a schematic of a tunable etalon employing a flat-curved configuration built in house. Fig. 3.6 shows the CAD diagram of the metal block. It is important to note that the mirrors used for all of the tunable etalons in this work are output coupler mirrors. This means that the front face of the mirror is a DBR stack while the back face is anti-reflection (AR) coated to reduce other parasitic etalon effects. The tunable etalon is constructed by first starting with a heavy metallic block with a bore hole and an indent on the front face. The front face of the block also features 4 tapped holes for screwing in Thorlabs cage assembly rods. The rods are used to hold a KC1T mount. We chose to use brass for this block but have also used steel. A ring piezo (Thorlabs PA44M3KW) is glued to the indent of the block. The AR coated side of the mirror was then glued to the ring piezo. The KC1T mount is used to hold the curved mirror of the cavity.

To reduce environmental perturbations on the tunable etalon, we have placed the cavity on an optical breadboard inside of a box lined with vibration dampening foam. The metallic block sits on top of a few sheets of sorbothane rubber and is clamped to the bread board with sorbothane rubber. The box housing the cavity is then placed on top of sorbothane spacers to reduce vibrations from the table to the box. All of the sorbothane pads and spacers were purchased on Thorlabs. These efforts significantly reduce the environmental perturbations on the optical cavity.

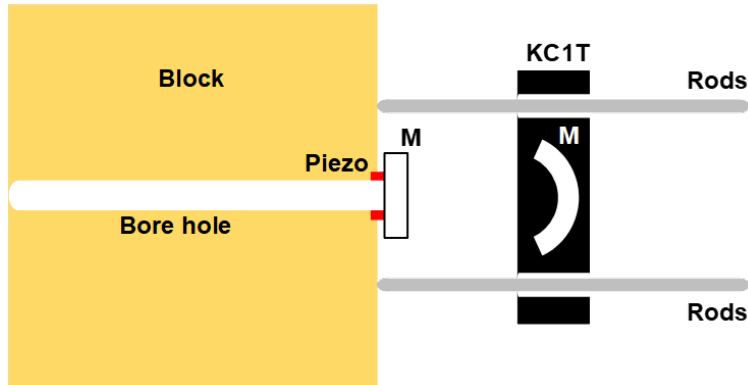


Figure 3.5: Schematic of a tunable etalon employing a flat-curved mirror configuration and a brass block as an anchor. M: mirror, KC1T: Thorlabs 30 mm cage compatible mount.

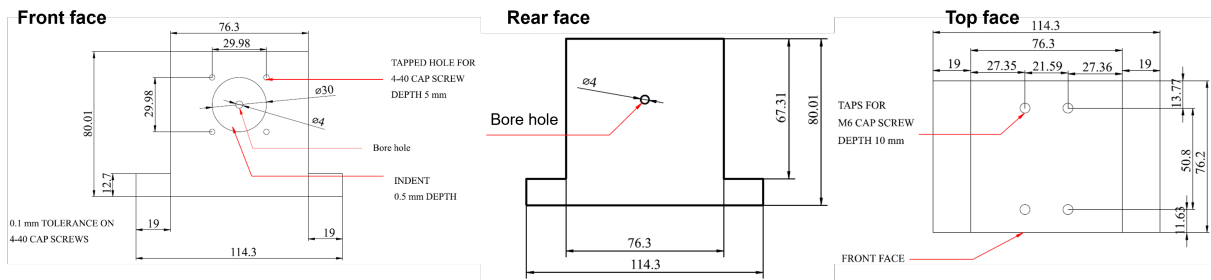


Figure 3.6: Front, rear, and top view of the CAD file of the metallic block used as an anchor for the tunable etalon.

Construction of a tunable etalon (3k finesse)

In the previous sections, we have discussed using optical cavities to perform optical filtering of noise in between comb lines. At first, we started with a haphazardly built tunable optical cavity and found that poor build quality resulted in an increase in phase noise for low frequency offsets. In addition, the haphazardly built tunable optical cavity featured high insertion loss and low stability. This motivated us to find a way to fully utilize the 100k finesse etalon for optical filtering.

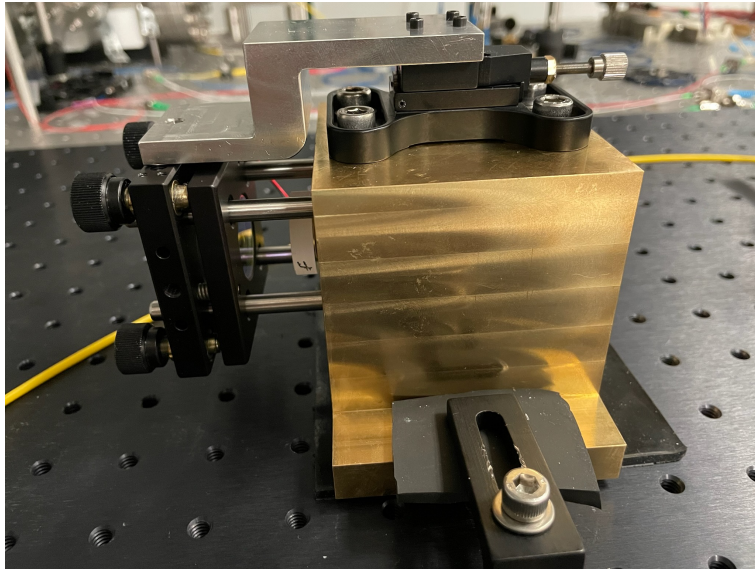


Figure 3.7: Photograph of the newly constructed $\sim 3k$ finesse tunable etalon employing flat-curved mirror configuration and mirror reflectivities of 99.97% and FSR ~ 10.5 GHz.

Unfortunately, several issues halted our progress using this approach. First, we have observed a degraded insertion loss over time (from < 1 dB to < 6 dB) that we have yet to understand. We also had difficulty in consistently getting the OEO EOM comb source in the previous section to run (we are still unsure why the comb source is inconsistent). In addition to the increased insertion loss, high finesse optical cavities suffer from the FSR walk-off effect. The FSR walk-off effect results in a limited usable optical bandwidth associated with the etalon. As the finesse of the optical cavity increases, the passband of the etalon narrows at the cost of a reduction in the total usable optical bandwidth of a comb source. The optical cavity doesn't support enough bandwidth to generate sufficiently short pulses. To remedy this, we have carefully constructed a tunable optical cavity using lower reflectivity mirrors using the design shown in Fig. 3.5 & Fig. 3.6. A photo of constructed cavity is shown in Fig. 3.7.

Fig. 3.7 shows a picture of the newly constructed tunable optical cavity. The cavity uses a brass

block as an anchor to reduce vibrations that can couple into the cavity. Brass was chosen as it has a higher density compared to steel, allowing for improved vibrational dampening. An electrically controlled piezo is glued to the brass block and the front mirror is glued to the piezo. The piezo allows the front mirror to be electrically tuned so that the cavity can track fluctuations in the comb source. A translation stage is bolted to the top of the brass block and bolted to the back mirror for ease of alignment. The optical cavity was then placed inside a thermally and acoustically isolated box to further reduce environmental fluctuations. In practice, the translation stage was not used due to the coarse tuning. Instead, angle tuning the back mirror was employed for adjusting the cavity spacing.

In addition, we used mirrors with a reflectivity of 99.92% for the optical cavity compared to the 99.9999% reflectivity mirrors. This ensured that the passband FWHM was wide enough to let a broader comb source through. We calculated a theoretical finesse of ~ 3300 using an $FSR \sim 10.5$ GHz and a passband $\Delta\nu_{FWHM} \sim 3$ MHz. We aligned the optical cavity by first aligning the input fiber launcher with the front mirror and maximizing the coupling of the back reflected light in the launcher. Then, we inserted the back mirror and sent ASE through the cavity. By measuring the throughput light on an IR camera and adjusting the back mirror, we were able to ensure the optical cavity was aligned to the fundamental TEM₀₀ spot. To test the stability of the optical cavity, we employed PDH locking of the optical cavity on our low noise CW laser from OEwaves. We observed the error signal to be stable enough to track the fluctuations of the OEwaves laser when it was free-running. To match the repetition rate of our comb source to the FSR of the etalon, we sent 100 mW of ASE power into the etalon and measured the throughput on a high speed photodetector. The resulting photocurrent was amplified by an RF low noise amplifier (LNA) and measured on an RFSA. We adjusted the optical cavity until the peak of the measured ASE spectrum aligned with the OEO signal. The peak of the ASE spectrum reveals the FSR of the cavity. To ensure the etalon can filter the OEO EOM comb, both f_0 & f_{rep} of the comb must match the etalon.

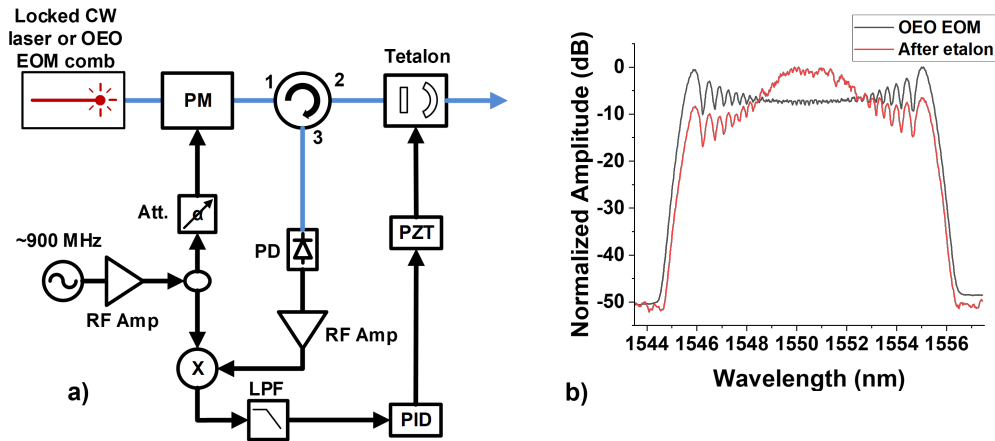


Figure 3.8: a) Schematic for testing the performance of the tunable etalon. PM: phase modulator, Tetalon: Tunable etalon, Att: RF attenuator, PD: photodiode, PZT: High voltage piezo driver, RF Amp: RF amplifier, RF Amp: RF amplifier, LPF: Low pass filter, PID: proportional-integral-derivative controller. b) Optical spectrum of the OEO EOM comb before passing through the tunable etalon (black) and after locking the tunable etalon to the OEO EOM comb.

We tested the tunable etalon insertion loss by employing Pound-Drever-Hall locking on a CW laser and measuring the throughput loss. The schematic can be seen in Fig. 3.8a when using a CW laser instead of the OEO EOM comb as the source. Similar to the PDH locking schematic in the previous chapter, a phase modulator for impressing anti-phase symmetric sidebands is used. An optical circulator is used to launcher the fiber light into the optical cavity and receive the back reflected light from the cavity. The synthesizer signal used to drive the phase modulator is also used to drive the LO port of a mixer while the back reflected light is detected, amplified, and fed into the RF port of a mixer. The IF signal is then low pass filtered and then sent into a PID controller. The correction signal is then fed into a high-voltage piezo controller which is used to tune the optical cavity. It is important to note that the synthesizer signal is at 900 MHz (as opposed to 300 MHz for the 100k finesse etalon) to ensure the phase modulated sidebands are maximally suppressed at the output of the etalon. We also included an RF amplifier after the synthesizer to amplify the signal to drive the mixer. To ensure that only a small amount of power is taken away for the phase

modulation process, we also attenuated the RF signal before entering the phase modulator. This ensures that we do not generate additional sidebands through phase modulation.

The insertion loss was measured to be ~ 4 dB, this is most likely due to the mode mismatch between the mode size of the etalon and the mode size from our fiber launchers. Unfortunately, we did not have enough time to purchase a new set of launchers with the correct mode size and were subject to availability of components in the lab. This loss can be reduced by improving the mode-matching between the etalon and the fiber launcher mode. We also tried to pass the OEO EOM comb to test the locking. The OEO EOM comb used was that in Fig. 2.20. Unfortunately, in addition to the high insertion loss (when using CW light), we also observed significant spectral distortion (when using the OEO EOM comb). The spectral distortion can be seen in Fig. 3.8b. Fig. 3.8a shows the schematic for testing the tunable etalon while Fig. 3.8b shows the optical spectrum before and after the tunable etalon. The spectral distortion appears to pass comb lines in the center but exhibits greater attenuation on the edges of the optical spectrum. Since our cavity finesse is only ~ 3300 , we believe that FSR walk-off is unlikely. To better understand these effects, we constructed an even lower finesse etalon.

Construction of a tunable etalon (600 finesse)

In the previous section, we constructed a tunable etalon with a finesse of $\sim 3k$. Unfortunately, we could not get the tunable etalon to work for us due to reasons we have yet to explain. To reduce the difficulty in matching all of the EOM comb lines to the tunable etalon resonances, we opted to reduce the finesse of the optical cavity. The reduction in finesse of the optical cavity (while keeping the FSR constant) results in a wider passband, allowing for additional comb lines with lower spectral attenuation to pass through.

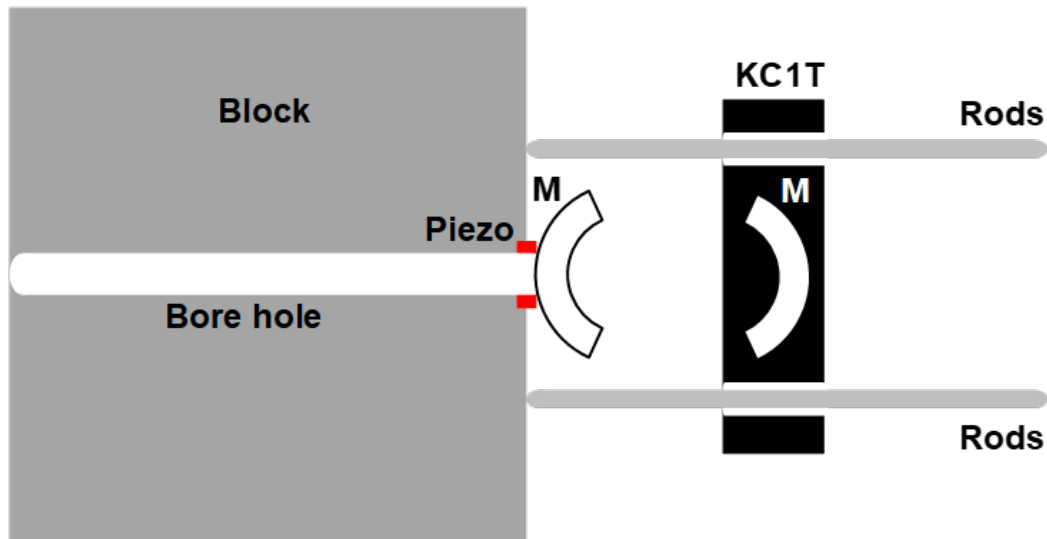


Figure 3.9: Schematic of a ~ 600 finesse tunable etalon employing a curved-curved mirror configuration anchored by a steel block. M: mirror, KC1T: thorlabs 30 mm cage compatible mount.

The lower finesse cavity uses two 99.5% curved output coupler mirrors with an ROC of 1 m. The estimated mode diameter at the waist is $407.6 \mu\text{m}$ and a FWHM of 16.9 MHz. The etalon uses a steel block as an anchor to dampen the vibrations to the cavity. One end of the block is glued to a piezo chip with a stroke free displacement up to $3.3 \mu\text{m}$. This cavity features a similar design to Fig. 3.5a with a curved mirror as the front mirror. A schematic diagram of this cavity can be seen in Fig. 3.9.

We again measured the throughput ASE on a high speed photodetector which was then amplified by an LNA and displayed on an RFSA 3.10. The FWHM of the measured curve is 49 MHz which is on the same order as the calculated FWHM of 16.9 MHz. It is important to note that the photodetected ASE does not give the exact FWHM value. However, it can still be a useful tool for roughly determining the FSR of the cavity.

We again measured the insertion loss of a CW laser through the etalon by employing PDH locking.

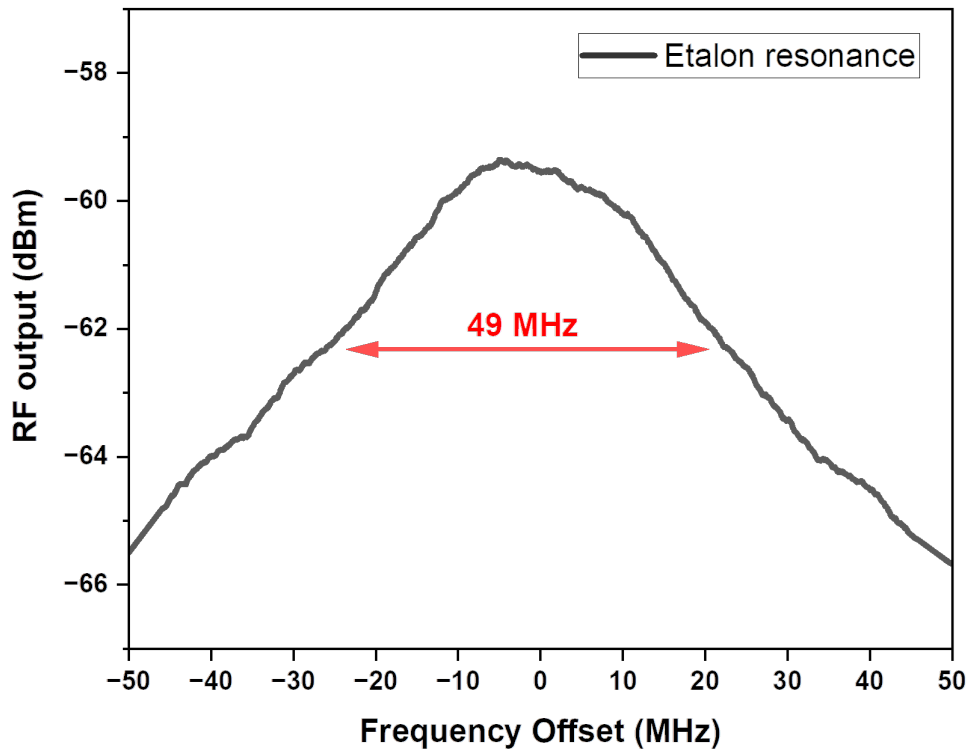


Figure 3.10: Photodetected ASE beat note of the ~ 600 finesse etalon.

This time, our insertion loss was less than 2 dB. This is a result of improved mode-matching to the cavity with a different set of fiber launchers. Our launchers feature a focused spot size of $\sim 420 \mu m$, which is close to the estimated mode diameter at the waist of the new cavity. We employed the same process of adjusting the cavity length of the cavity and measuring the frequency at which the peak of the ASE curve landed. By adjusting the peak frequency of Fig. 3.10 to match the frequency of the OEO, we should theoretically be able to match the cavity with our comb source. Unfortunately, we have found that this process of viewing the ASE curve on the RFSA provides insufficient resolution. We again measured significant spectral distortion when trying to lock our the tunable etalon to our comb source. Although the reduction in finesse allowed for lower loss

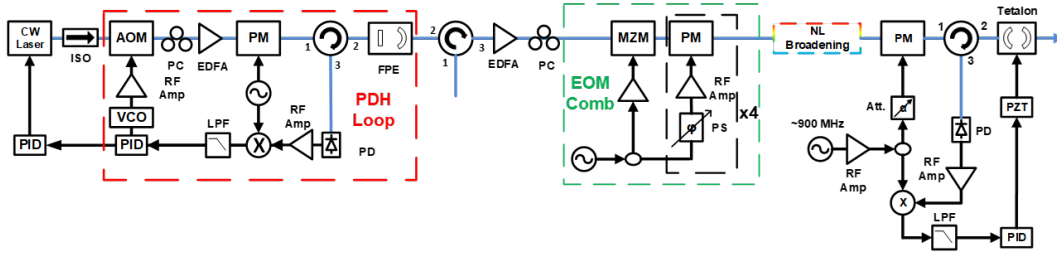


Figure 3.11: Schematic for measuring the FSR of ~ 600 finesse tunable etalon using an EOM comb with spectral broadening. AOM: acousto-optic modulator, ISO: fiber pigtailed isolator, PC: polarization controller, EDFA: Erbium doped fiber amplifier, PM: phase modulator, FPE: 100k finesse Fabry-Perot etalon, RF Amp: RF amplifier, PD: photodiode, LPF: low pass filter, PID: proportional-integral-derivative controller, VCO: voltage controlled oscillator, MZM: intensity modulator, RF synth: RF synthesizer, Att: RF attenuator, PZT: high voltage piezo controller.

and less spectral distortion, we cannot tolerate spectral distortion only 1 THz of optical bandwidth.

To solve this issue, we developed a new method to measure the FSR of our tunable etalon. A schematic diagram of the setup is shown in Fig. 3.11. The setup uses an EOM comb driven by an RF synthesizer and a few optional nonlinear loop mirrors. The nonlinear loop mirrors will be further discussed in the next chapter. It is sufficient to know that nonlinear loop mirrors are a method for generating additional comb lines and are optional.

The procedure for our technique using Fig. 3.11 is as follows. First, we lock our CW laser to our 100k finesse etalon. Since we are trying to filter our OEO EOM comb with an external etalon, we must match both f_0 & f_{rep} of the tunable etalon to the OEO EOM comb. By locking the CW laser to our 100k finesse etalon (which is used for the OEO), we are locking f_0 in place. Having light pass through the etalon when f_0 is locked implies that the tunable etalon needs only to match f_{rep} . Second, we drive our EOM comb phase modulators with an RF signal that is close to the FSR of our tunable etalon. The phase of the RF signal driving each modulator is adjusted to ensure maximum comb generation. Third, we attempt to lock the generated EOM comb using the tunable

etalon. Naturally, the FSR of the tunable etalon and f_{rep} will have a slight mismatch, hence the necessity for this technique. This can be observed on the PDH error signal when trying to lock the tunable etalon to the EOM comb. When the FSR of the etalon is sufficiently detuned from f_{rep} of the EOM comb, the error signal will be smaller in amplitude and will be slanted in the shape. This is due to each combline of the EOM comb providing a PDH error signal with different phases which serve to alter the shape. Fourth, after locking the etalon to the EOM comb, we adjust the RF drive frequency for the EOM comb until all of the comblines pass through the etalon with no attenuation.

By measuring the throughput light of the etalon on an OSA, we can observe whether there is a detuning between the FSR and f_{rep} . Once the optical spectrum distortion is minimized and the output power is maximized, the FSR value is the corresponding RF drive frequency. The advantage of this technique over previous etalon FSR measurement techniques [59] & [60] is that we can also measure the throughput optical spectra (which tells us about the dispersion of the optical cavity). We use additional spectral broadening after the EOM comb to give additional digits of precision in our measurement of the etalon FSR and to ensure the etalon can filter enough bandwidth.

Once the FSR of the tunable etalon has been measured, we can now adjust the back mirror of the optical cavity or the drive voltage on the piezo to match f_0 & f_{rep} of the etalon to our OEO EOM comb. This process is iterative and may take several adjustments on the back mirror to match the degrees of freedom. Unfortunately, we were unable to match both degrees of freedom (with sufficient precision) by simply adjusting the etalon. We were adjusting the back mirror by hand with limited success. We observed that the closest we could match the FSR and f_{rep} was within ~ 200 kHz. Each time we adjusted the cavity, the measured FSR would be ~ 200 kHz. Future endeavors of aligning a tunable etalon to a comb source should consider using a piezo-tuned mirror for better precision in angle tuning the back mirror.

Since we would like >4.4 THz of filtered optical bandwidth, we would need the detuning of the FSR and f_{rep} to be less than $\frac{\Delta v_{FWHM}}{N}$, where N is the number of comb lines. For our purposes, this value comes out to less than 50 kHz. To improve the matching of f_0 & f_{rep} , we shifted the CW laser and locked it to a different resonance on the starting 100k finesse etalon. This change sufficiently in f_0 of the EOM comb allowed us to adjust the tunable etalon FSR and f_0 to match the OEO EOM comb.

After matching both f_0 & f_{rep} of the etalon to the broadened EOM comb, we measured the insertion loss and the optical spectrum. The insertion loss was still 2 dB and no spectral distortion could be observed. To be sure the tunable etalon matches our OEO EOM comb, we sent the OEO EOM comb through the etalon. We again measured ~ 2 dB loss and no spectral distortion.

In this chapter we solved our broadband comb filtering problem. We started with trying to use our 100k finesse etalon and ran into issues due to cavity dispersion. We constructed a ~ 3 k finesse etalon and ~ 600 finesse etalon to externally filter our comb source. In addition, we came up with a new technique to match our etalon to our comb source and verified broadband operation. Unfortunately, our EOM comb bandwidth is still lacking. Our next steps are to improve the pulse quality, shorten our pulses, and increase their output power.

CHAPTER 4: HIGH CONTRAST NONLINEAR PULSE COMPRESSION

EOM combs present numerous challenges for producing coherent octave spanning supercontinuum generation. As previously shown, EOM combs exhibit a notorious temporal pedestal as a result of uncompensated higher orders of dispersion. EOM combs also produce relatively long pulse durations due to the limited number of generated comb lines. Finally, EOM combs exhibit significant phase noise multiplication compared to other comb sources. Additionally, high repetition rate (GHz) comb sources have low pulse energies. One approach to generating short pulses with EOM combs is to simply cascade as many phase modulators as possible. However, this approach is extremely expensive due to the cost of components (modulator, RF amplifier, RF switch, etc.). To generate 100 fs pulses with an EOM comb at a repetition rate of 10 GHz, one would need to use 35 phase modulators! Although the number of modulators needed at higher repetition rates decreases (due to the total larger optical bandwidth generated), several modulators are still needed. In addition to the high cost, additional phase modulators degrade the pulse contrast. This is because the higher order dispersion terms grow with the increasing modulation index without being compensated. If the phase modulators were driven by pure quadratic temporal phase (as opposed to a sinusoid), the resulting chirp would be linear. Instead, a cost-effective approach would be to use a few modulators, amplify the pulse train, then spectrally broaden the EOM comb with highly nonlinear fiber. Unfortunately, SPM is known also to degrade pulse quality. In this chapter, we will discuss SPM and a new method our group has developed for producing ultrashort pulses with high pulse contrast.

Self-Phase Modulation

Self phase modulation is a nonlinear effect in which the index of refraction of the material changes in proportion to the intensity of light. This change in refractive index modifies the phase of a light pulse propagating through the medium. This can be seen in Eq. 4.1 where n_2 is the nonlinear index of the material and I is the light intensity in the medium.

$$\Delta n = n_2 I \quad (4.1)$$

Typically, only pulses of light can produce high enough intensities for measurable phase changes. The change in phase gives rise to a chirp that is proportional to the derivative of the light pulse with respect to time. In general, the result is a pulse with linear up chirp in the centroid and anti-symmetric lumps on the edges of the pulse. The linear chirp in the centroid is easily compressible but the lumps (or wings) are difficult to compress. This can be seen in Fig. 4.1 where the intensity of the input pulse is shown on top and the instantaneous frequency is shown below. Compensating for the linear chirp results in pulse shortening at the center while the edges of the pulse exhibit temporal sidelobes.

For coherent octave spanning supercontinuum generation in fiber to occur, sub-100 fs pulse durations with low pedestal energy are required. For comb sources that produce relatively long pulses (> 400 fs), this is a serious issue. For pulses shorter than 400 fs, nonlinear compression inside fiber amplifiers can shorten pulse durations to under 100 fs. Unfortunately, our pulses are barely under 1 ps in duration and already have a significant pedestal. To reach the point where a fiber amplifier could nonlinearly compress our pulse to 100 fs requires something more sophisticated.

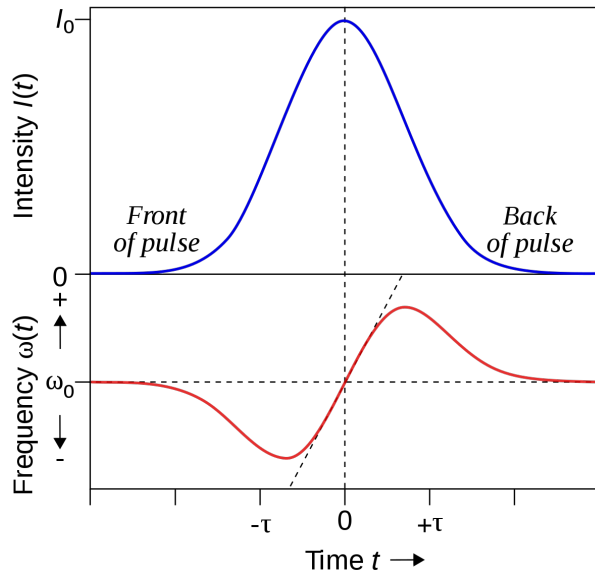


Figure 4.1: Conceptual diagram of self phase modulation. Top: input intensity profile of an optical pulse in nonlinear medium. Bottom: instantaneous frequency of pulse after undergoing SPM.

Self phase modulation in fiber

Previous work in optical pulse compression in fiber [61] has produced various pulse compression techniques. These techniques rely on the dispersion and nonlinearity of the fiber. Due to the telecom industry, significant work has been dedicated towards developing fibers with various dispersion and nonlinear coefficients. Surprisingly, the nonlinear coefficient alone does not determine the pulse dynamics in the fiber. The dispersion characteristics of the fiber dictate the pulse dynamics of the fiber. The nonlinear coefficient dictates the threshold power for nonlinear effects while the attenuation dictates the length at which nonlinear effects cease. Although silica has a small nonlinear index (n_2), the long lengths of fiber increase the nonlinear interaction length. As previously mentioned, SPM generates additional frequency components with a chirp that is proportional to the derivative of the pulse shape. There are two vastly different set of dynamics for

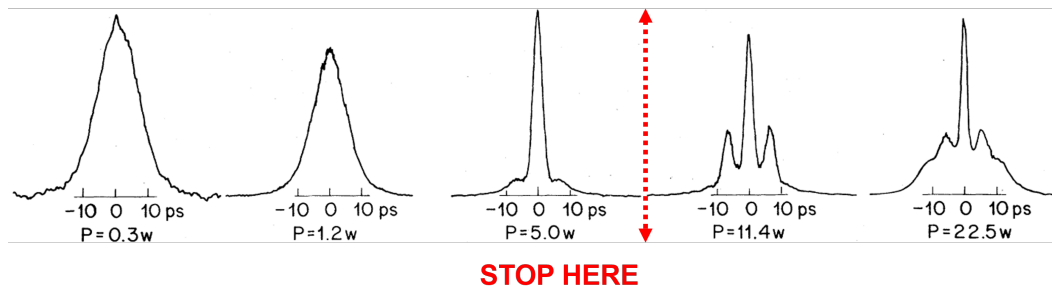


Figure 4.2: Intensity autocorrelation traces showing soliton compression in single mode fiber.

pulses in fiber (anomalous or normal dispersion). When the fiber exhibits anomalous dispersion, solitons can be formed. A soliton is pulse that does not change with propagation. It is formed by the balance of dispersion and nonlinearity. The linear chirp induced by SPM has the opposite slope compared to anomalous dispersion. When the power is increased, the nonlinear phase increases. As a result, the pulse shortens and increases the peak power of the pulse. The increase in peak power induces even more SPM which generates even more frequency components. The additional SPM because of the heightened peak power is further compressed by the anomalous dispersion. The result is a pulse spectrum that far exceeds the input pulse spectrum and a pulse that is significantly shorter than the input pulse. Unfortunately, the increased SPM produces a significant pulse pedestal riding below the main lobe of the pulse and pulse splitting. This effect can be seen in Fig. 4.2 which was adapted from [62]. In [62], a 100 MHz repetition rate mode-locked laser centered at 1550 nm emitting 7.2 ps pulses was amplified and then sent through a length of single mode fiber with various average powers. The measured intensity autocorrelation are shown in Fig. 4.2. At first, the pulse slightly narrows with increasing power and then suddenly begins to significantly compress. After 5.0 W, the output pulse begins to exhibit pulse splitting which ends up becoming a pulse pedestal. The red line added in Fig. 4.2 shows at which point soliton compression has roughly achieved maximal pulse compression. This process also leads to the generation of higher

order solitons. Additional background on solitons and higher order solitons can be found in [63]. A modification of soliton compression is known as adiabatic soliton compression. Instead of trying to achieve significant pulse compression along a single segment of anomalous dispersion fiber, various segments of fiber with different dispersion parameters are spliced together. The first segment is used to achieve maximal pulse compression with as little temporal sidelobe generation as possible. This typically occurs before the drawn red line in Fig. 4.2. A second segment with a smaller dispersion parameter compared to the first segment is used to restart the soliton compression process. This process of stopping the soliton compression in a segment and restarting soliton compression in another segment is the essence of adiabatic soliton compression. The main idea is to ensure that each segment of fiber does a small amount of nonlinear pulse compression, but never enough to generate a significant pedestal. In this way, the nonlinear pulse compression process restarts multiple times. A less achievable method for adiabatic soliton compression is to use dispersion decreasing fiber (fiber that has its dispersion parameter decrease along its length). Unfortunately, dispersion decreasing fibers are not a commercial item and cannot be easily obtained.

Unlike the anomalous dispersion giving rise to solitons, normal dispersion fiber gives rise to similaritons (or parabolic pulses) [64]. As previously mentioned, SPM generates a linear chirp at the center of the pulse with anti-phase symmetric lumps at the edges of most pulses. The linear chirp being compressible by anomalous dispersion entails that normal dispersion would stretch the pulse. The combined action of SPM and normal dispersion act to reshape the pulse to asymptotically approach a parabolic intensity profile. This can be seen in Fig. 4.3. In fig. 4.3, a simulation is performed where a Gaussian pulse is nonlinearly propagated through a length of normal dispersion fiber. As the Gaussian pulse propagates and generates SPM, the pulse stretches in time. By the middle of the plot, the pulse no longer resembles a Gaussian pulse but a parabola. Eventually, parabolic propagation ends and the pulse exhibits optical wave breaking. Optical wave breaking occurs when the trailing edge and leading edge of the next pulse overlap and interfere [65]. This

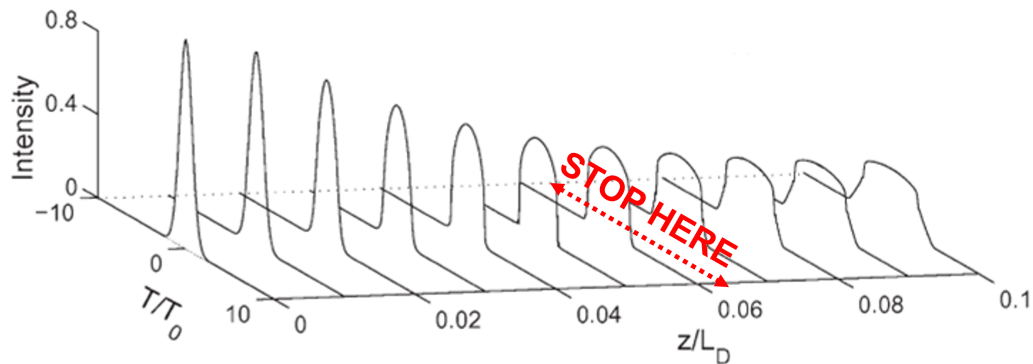


Figure 4.3: Simulated parabolic pulse propagation by nonlinearly propagating a Gaussian pulse in a normal dispersion fiber.

distorts the optical spectrum and produces sidelobes. In the time domain, the pulse no longer resembles a parabola. Unfortunately, the interference of the two pulses does not produce linear chirp that is easily compressible. The red line on the plot delineates parabolic propagation and optical wave breaking. Additional information on parabolic pulse propagation can be found in [63]. Unlike soliton compression where the pulse continuously compresses and acquires more SPM, similariton propagation continuously stretches the pulse along propagation. Since the pulse is stretching while propagating, the peak power decreases with propagation. The decrease in peak power reduces the amount of SPM induced by the pulse. In addition to the reduction in accumulated nonlinear phase, since the pulse approaches a parabola, SPM instead produces nearly perfect linear chirp (with no anti-symmetric lumps). The linear chirp is easily achieved with the proper length SMF28 fiber. In addition to the chirped pulse, the resulting compressed pulse has a much smaller pulse pedestal compared to soliton compression. For nonlinear compression using parabolic pulse propagation, a pulse is first launched into the normal dispersion fiber and reshaped into a parabola. The process is stopped right before optical wave breaking (where the red line is drawn on Fig. 4.3) occurs so that the output pulse resembles a parabola with highly linear chirp.

The pulse is then compressed using anomalous dispersion fiber and then sent back into another segment of normal dispersion fiber. This process is repeated until pulses with the desired duration are obtained.

Regardless of soliton compression (anomalous dispersion fiber) or similariton propagation (normal dispersion fiber), these techniques will always generate an additional pulse pedestal. Hence, the necessity of starting with a clean optical pulse. Unfortunately, our pulses are roughly 1 ps in duration with a significant pedestal, nonlinearly broadening our spectrum through SPM would further degrade our pulse contrast before even reaching the amplifier!

We have experimentally measured nonlinear pulse propagation in three different spools of highly nonlinear fiber (HNLF) with differing dispersion profiles centered at 1550 nm in Fig. 4.4, 4.5, & 4.6.

The setup in Fig. 4.4a starts with a CW laser PDH locked to our 100k finesse Fabry-Perot etalon. The CW laser is then used to generate an EOM comb using two phase modulators and one intensity modulator. The EOM comb is amplified by an SOA, compressed using a Finisar waveshaper (applying only linear chirp), and amplified again in a .5 W EDFA. The optical spectrum and compressed intensity autocorrelation trace are shown in Fig. 4.4b & c. The amplified and compressed EOM comb is then sent through a spool of 100 m of anomalous dispersion HNLF with 1 m of single mode fiber spliced to each end. The HNLF has a dispersion parameter of $1.16 \frac{ps}{nm*km}$ at 1550 nm and a nonlinear coefficient of $11.6 \frac{1}{W*km}$. Fig. 4.4d & e show the optical spectrum and intensity autocorrelation trace after the HNLF when the output power of the EDFA was set to 100 mW. Fig. 4.4f & g show the optical spectrum and intensity autocorrelation trace after the HNLF when the output power of the EDFA was set to 300 mW.

We observe the EOM comb sidelobes to persist in the autocorrelation traces after the HNLF. We observe a pulse compression factor of over 2x when the EDFA was set to 100 mW in Fig. 4.4e

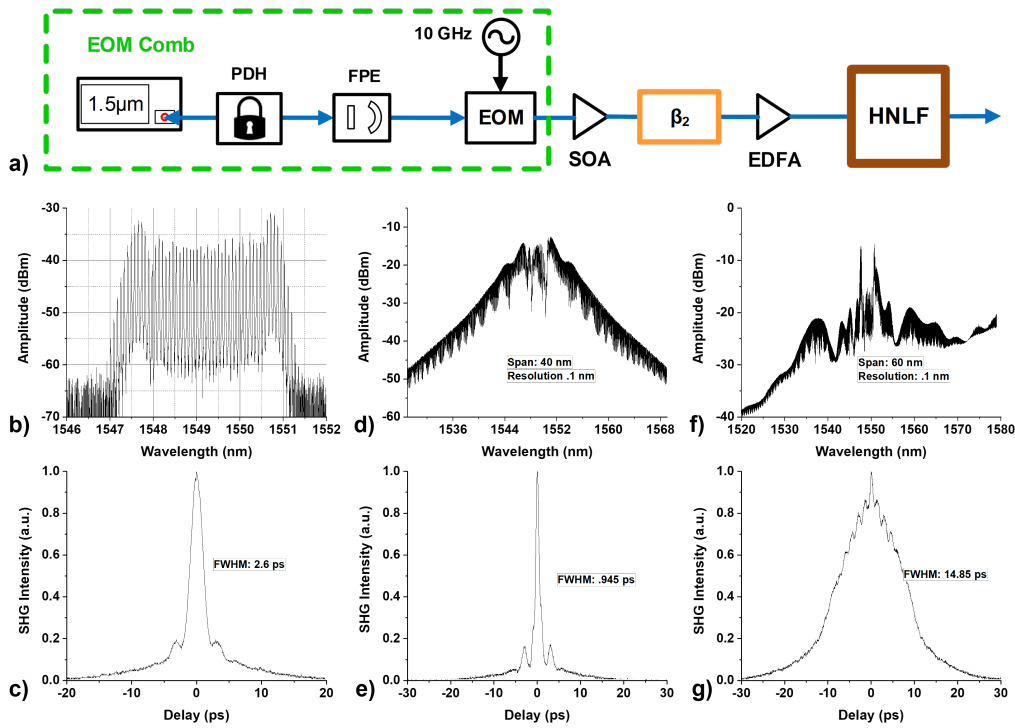


Figure 4.4: Experimental work of spectral broadening an EOM comb (consisting of two phase modulators and one intensity modulator driven by a common RF synthesizer at 10 GHz) using 100 m of anomalous dispersion HNLF from OFS. a) Schematic representation of spectrally broadening an EOM comb using anomalous dispersion HNLF. PDH: Pound-Drever-Hall locking, FPE: Fabry-Perot etalon, EOM: cascade of electro-optic modulators, SOA: semiconductor optical amplifier, β_2 : linear chirp for compressing EOM comb pulses, EDFA: erbium doped fiber amplifier, HNLF: anomalous dispersion HNLF. b) Optical spectrum of EOM comb before broadening, c) compressed intensity autocorrelation of EOM comb, d) optical spectrum of EOM comb after amplification to 100 mW and spectral broadening in 100 m of HNLF, e) intensity autocorrelation of spectrally broadened EOM comb with average power 100 mW, f) optical spectrum of EOM comb after amplification to 300 mW and spectrally broadened by HNLF, g) intensity autocorrelation of spectrally broadened EOM comb with average power 300 mW.

while the optical spectrum exhibits typical SPM spectral broadening in Fig. 4.4d. We also observe significant spectral oscillations and pulse broadening when the EDFA power was set to 300 mW in Fig. 4.4f & g. The optical spectrum no longer resembles typical SPM on the longer wavelengths. We attribute this to the aforementioned soliton compression effect where the pulse continually

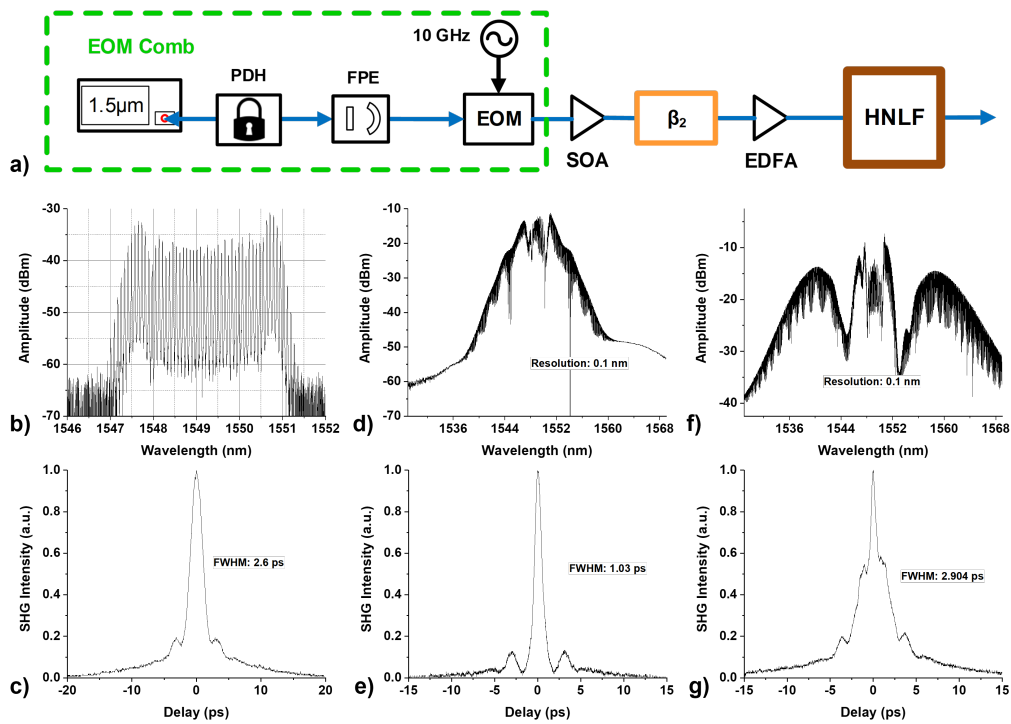


Figure 4.5: Experimental work of spectral broadening an EOM comb (consisting of two phase modulators and one intensity modulator driven by a common RF synthesizer at 10 GHz) using 100 m of zero dispersion HNLF from OFS. a) Schematic representation of spectrally broadening an EOM comb using zero dispersion HNLF. PDH: Pound-Drever-Hall locking, FPE: Fabry-Perot etalon, EOM: cascade of electro-optic modulators, SOA: semiconductor optical amplifier, β_2 : linear chirp for compressing EOM comb pulses, EDFA: erbium doped fiber amplifier, HNLF: zero dispersion HNLF. b) Optical spectrum of EOM comb before broadening, c) compressed intensity autocorrelation of EOM comb, d) optical spectrum of EOM comb after amplification to 100 mW and spectral broadening in 100 m of HNLF, e) intensity autocorrelation of spectrally broadened EOM comb with average power 100 mW, f) optical spectrum of EOM comb after amplification to 300 mW and spectrally broadened by HNLF, g) intensity autocorrelation of spectrally broadened EOM comb with average power 300 mW.

acquires additional nonlinear phase which distorts the optical spectrum and pulse profile. This can also be seen in Fig. 4.4g where although the pulse is clearly stretched, there are several spikes around the pulse which are typically indicative of significant higher order chirp.

The setup in Fig. 4.5a starts with a CW laser PDH locked to our 100k finesse Fabry-Perot etalon.

The CW laser is then used to generate an EOM comb using two phase modulators and one intensity modulator. The EOM comb is amplified by an SOA, compressed using a Finisar waveshaper (applying only linear chirp), and amplified again in a .5 W EDFA. The optical spectrum and compressed intensity autocorrelation trace are shown in Fig. 4.5b & c. The amplified and compressed EOM comb is then sent through a spool of 100 m of zero dispersion HNLF with 1 m of single mode fiber spliced to each end. The HNLF has a dispersion parameter of $0.00 \frac{ps}{nm*km}$ at 1550 nm and a nonlinear coefficient of $11.3 \frac{1}{W*km}$. Fig. 4.5d & e show the optical spectrum and intensity autocorrelation trace after the HNLF when the output power of the EDFA was set to 100 mW. Fig. 4.5f & g show the optical spectrum and intensity autocorrelation trace after the HNLF when the output power of the EDFA was set to 300 mW.

We again observe the EOM comb sidelobes to persist in the autocorrelation traces after the HNLF. We again observe a pulse compression factor of over 2x when the EDFA was set to 100 mW in Fig. 4.5e while the optical spectrum exhibits typical SPM spectral broadening in Fig. 4.5d. Unlike Fig. 4.4f & g, Fig. 4.5f & g still exhibits typical SPM broadening with significantly higher depth of modulation in the optical spectrum. We attribute this effect to the dispersion parameter of this HNLF being 0 where dispersion is not capable of stretching or compressing the pulse. In a sense, we're observing pure SPM in fiber without shaping due to dispersion. In Fig. 4.5g, we observe the pulse is stretched with fewer spikes on the intensity autocorrelation. We note that the spikes near ± 5 ps delay are due to the EOM comb while the spikes closer to the mainlobe are due to SPM.

The setup in Fig. 4.6a starts with a CW laser PDH locked to our 100k finesse Fabry-Perot etalon. The CW laser is then used to generate an EOM comb using two phase modulators and one intensity modulator. The EOM comb is amplified by an SOA, compressed using a Finisar waveshaper (applying only linear chirp), and amplified again in a .5 W EDFA. The optical spectrum and compressed intensity autocorrelation trace are shown in Fig. 4.6b & c. The amplified and compressed EOM comb is then sent through a spool of 100 m of normal dispersion HNLF with 1 m of single

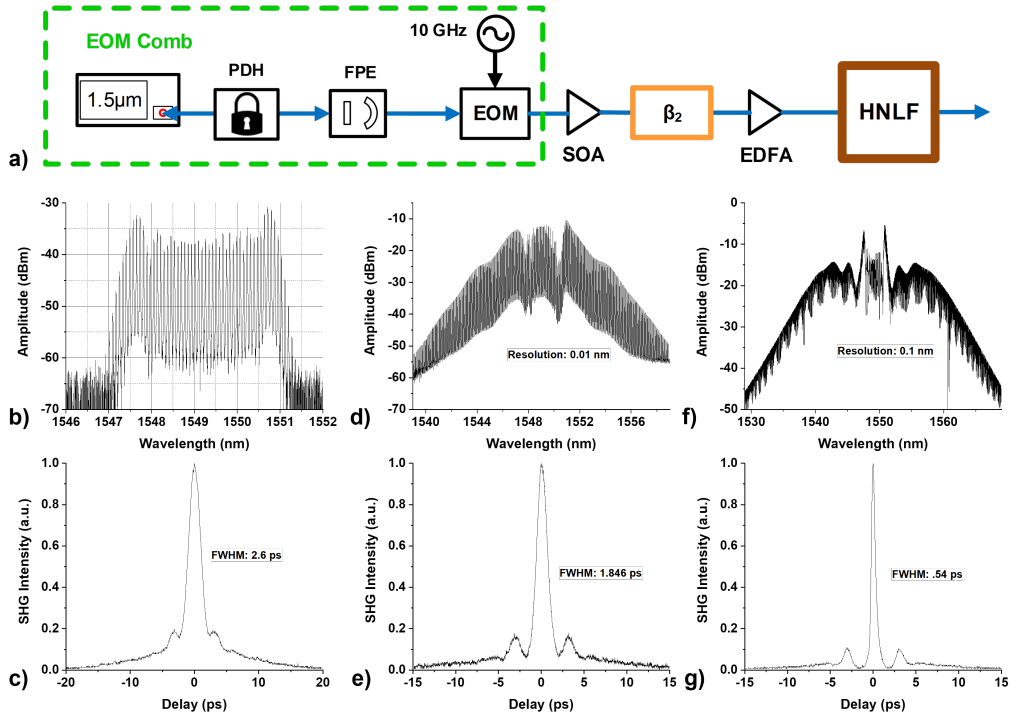


Figure 4.6: Experimental work of spectral broadening an EOM comb (consisting of two phase modulators and one intensity modulator driven by a common RF synthesizer at 10 GHz) using 100 m of normal dispersion HNLF from OFS. a) Schematic representation of spectrally broadening an EOM comb using normal dispersion HNLF. PDH: Pound-Drever-Hall locking, FPE: Fabry-Perot etalon, EOM: cascade of electro-optic modulators, SOA: semiconductor optical amplifier, β_2 : linear chirp for compressing EOM comb pulses, EDFA: erbium doped fiber amplifier, HNLF: normal dispersion HNLF. b) Optical spectrum of EOM comb before broadening, c) compressed intensity autocorrelation of EOM comb, d) optical spectrum of EOM comb after amplification to 100 mW and spectral broadening in 100 m of HNLF, e) intensity autocorrelation of spectrally broadened EOM comb with average power 100 mW, f) optical spectrum of EOM comb after amplification to 300 mW and spectrally broadened by HNLF, g) intensity autocorrelation of spectrally broadened EOM comb with average power 300 mW.

mode fiber spliced to each end. The HNLF has a dispersion parameter of $-0.72 \frac{ps}{nm*km}$ at 1550 nm and a nonlinear coefficient of $11.8 \frac{1}{W*km}$. Fig. 4.6d & e show the optical spectrum and intensity autocorrelation trace after the HNLF when the output power of the EDFA was set to 100 mW. Fig. 4.6f & g show the optical spectrum and intensity autocorrelation trace after the HNLF when the

output power of the EDFA was set to 300 mW.

We still observe the EOM comb sidelobes to persist in the autocorrelation traces after the HNLf. This time, we observe a much smaller pulse compression factor when the EDFA was set to 100 mW in Fig. 4.6e while the optical spectrum exhibits typical SPM spectral broadening in Fig. 4.6d. Unlike Fig. 4.4f & g, Fig. 4.6f & g still exhibits typical SPM broadening with a little higher depth of modulation in the optical spectrum. We attribute this effect to the dispersion of this HNLf being normal dispersion. Since the pulse is instead being stretched while propagating in the HNLf, the accumulated nonlinear phase due to SPM is significantly reduced. In Fig. 4.5g, we observe the pulse is extremely short compared to the input. The pulse compression that is occurring after the HNLf is due to the anomalous dispersion 1 m long SMF fiber spliced pigtail.

Having shown nonlinear spectral broadening in three different spools of HNLf, we observe that the EOM comb sidelobes do not disappear. Although the central lobe of the EOM comb can be significantly compressed, the original sidelobes still remain. In addition, the main lobe can generate a new set of sidelobes due to the SPM chirp being nonlinear. Unfortunately, the temporal pedestal (now caused by SPM and the original EOM comb sidelobes) can also be amplified by an amplifier.

Linear Pulse Shaping

As previously mentioned, the EOM comb sidelobes are a result of uncompensated higher order dispersion due to the sinusoidal modulation. Propagating the amplified and mostly compressed EOM comb pulses through a section of HNLf can significantly compress the main lobe of the EOM comb in exchange for adding a new set of sidelobes. One way to simultaneously remove both the temporal pedestal native to EOM combs and the SPM nonlinear chirp is to use a linear

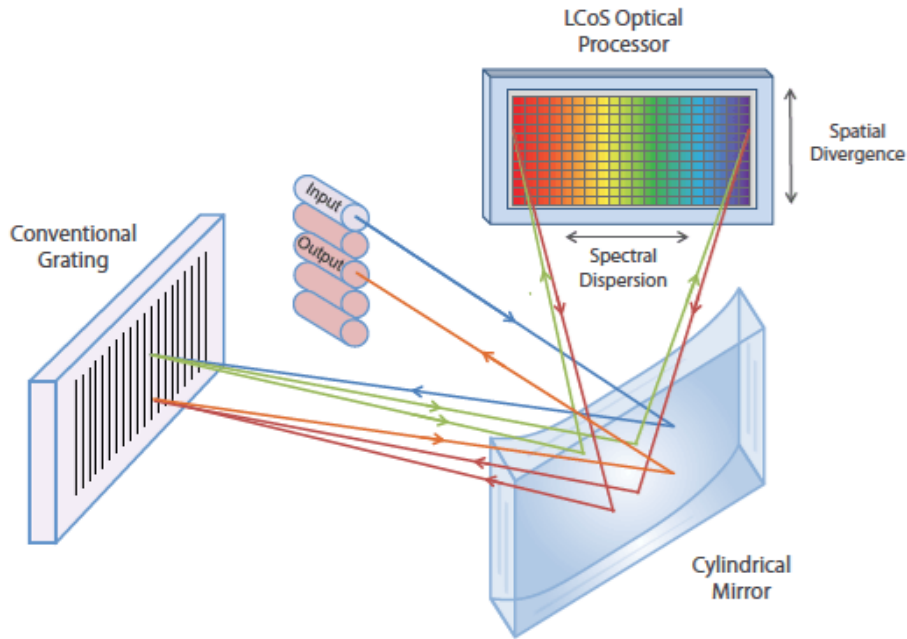


Figure 4.7: Schematic of a commercially available grating based pulse shaper from Finisar (now Coherent).

pulse shaper. This approach uses a spatial light modulator (SLM) based grating pulse shaper (wavershaper). A schematic of a commercial grating based pulse shaper sold by Finisar (now Coherent) is shown in Fig. 4.7. The wavershaper works by using a grating to separate the pulse spectral components and then sending each spectral component through an SLM. By applying a specific voltage on the SLM pixels, the individual phase components of the pulse can be changed. This allows for full amplitude and phase control of each spectral component, allowing for arbitrary amplitude and phase masks to be generated. An approach for removing the EOM comb sidelobes, SPM sidelobes, and undoing amplifier distortions was done in [17]. Fig. 4.8 shows their schematic and Fig. 4.9 shows their data adapted from [17].

Fig. 4.8 shows the schematic for obtaining high contrast ultrashort pulses from an EOM comb as done in [17]. The system starts with a CW laser PDH locked to an ultra-high finesse cavity. The

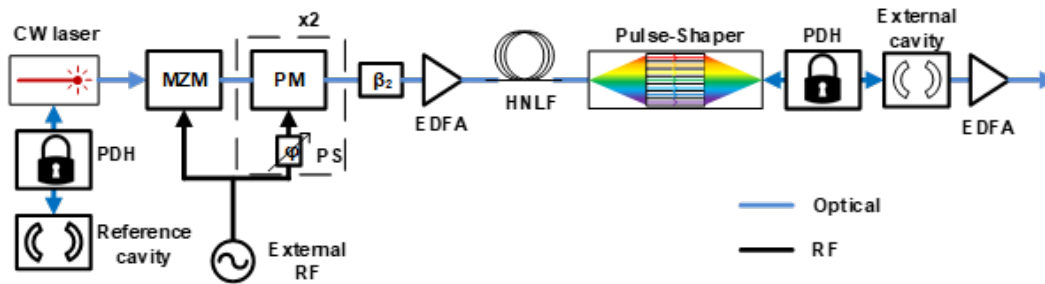


Figure 4.8: Schematic representation of an EOM comb spectrally broadened by HNLF, reshaped using a linear pulse shaper, and then amplified again. MZM: intensity modulator, PM: phase modulator, PDH: Pound-Drever-Hall lock, β_2 : linear chirp for compressing EOM comb, EDFA: erbium doped fiber amplifier, HNLF: 100 m of highly nonlinear fiber, pulse-shaper: grating based pulse shaper.

stabilized laser is then sent through two phase modulators and one intensity modulator driven at 33 GHz to generate an EOM comb. The optical spectrum of the 33 GHz EOM comb is shown in Fig. 4.8a. The 33 GHz EOM comb is then mostly compressed using linear chirp and then amplified up to .5 W in an EDFA. The amplified pulses are then sent through 100 m of HNLF for nonlinear spectral broadening. The resulting optical spectrum and intensity autocorrelation are shown in Fig. 4.9b & c in green. The broadened EOM comb is then sent through a pulse shaper to adjust the amplitude and phase of each comb line. In Fig. 4.9b & c (in black) shows how the pulse pedestal can be suppressed by flattening the optical spectrum in 5 nm increments. From Fig. 4.9c, we observe the pulse pedestal to significantly decrease after spectral flattening was applied. Fig. 4.9d & e shows the optical spectrum and intensity autocorrelation respectively after complete spectral flattening. The spectrum no longer exhibits the same oscillations at the top. The resulting autocorrelation also shows a pedestal free output pulse. Fig. 4.9d & e are taken after the final amplifier in the system which shows that linear shaping can also be used to suppress distortions due to the amplifier as well as gain narrowing.

Although this approach has been shown to suppress the pulse pedestal due to the EOM comb

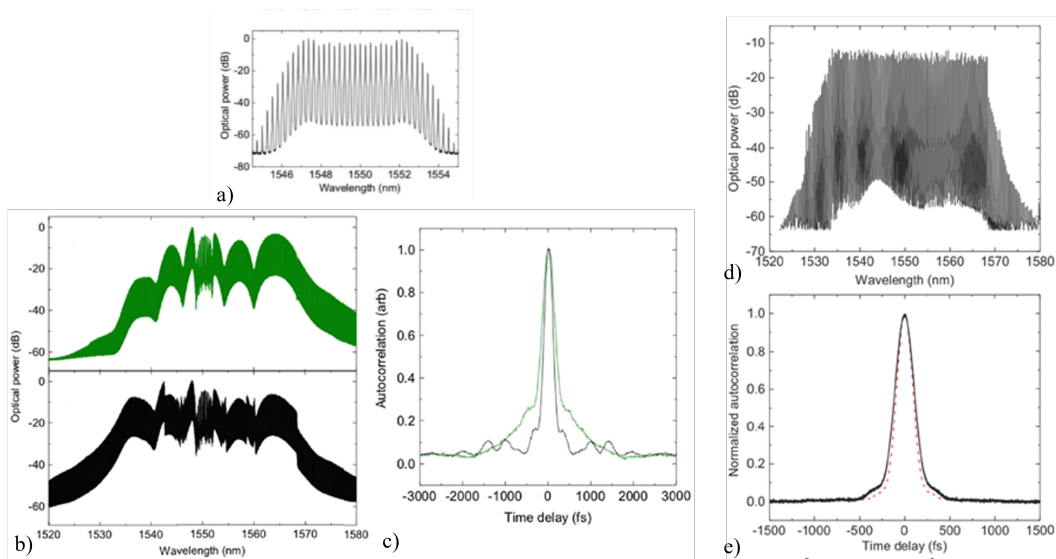


Figure 4.9: Associated data of an EOM comb spectrally broadened and shaped using pulse shaper. a) Optical spectrum of the 33 GHz EOM comb using 2 phase modulators and 1 intensity modulator, b) optical spectrum of EOM comb after amplification to .5 W and subsequent nonlinear spectral broadening in 100 m of HNLf before shaping (green) and after spectral flattening in 5 nm increments (black), c) intensity autocorrelation trace of spectrally broadened EOM without shaping (green) and with shaping in 5 nm increments (black), d) optical spectrum of spectrally broadened EOM after full line by line shaping, e) intensity autocorrelation of spectrally broadened EOM comb after full line by line shaping (black) and transform limited autocorrelation (red).

and SPM, this approach has many issues. The use of a waveshaper is expensive, lossy (5 dB insertion loss before any spectral shaping!), limited operating wavelength range, and cannot handle high power. Finally, the output pulses were still not short enough for supercontinuum generation. To generate an octave, a specially prepared fiber using two different dispersion profiles (limited information was presented regarding the fibers for supercontinuum generation) was used (chapter 6 will discuss supercontinuum generation). We seek an alternative solution that does not provide high losses and can be easily implemented.

Saturable Absorption

The issue discussed in the previous section is that a nonlinear pulse compressor is needed to shorten EOM comb pulses. SPM can aid in producing ultrashort pulses but also degrades the pulse contrast. Using a waveshaper, the degradation in pulse contrast by SPM can be mitigated at the cost of power, complexity, and money. A device that can simultaneously shorten a pulse and eliminate pulse pedestals is needed.

A saturable absorber is a device that exhibits a nonlinear phenomenon in which weak portions of an optical pulse experience additional loss compared to strong portions of an optical pulse. This gives rise to a nonlinear temporal filter function that can simultaneously remove temporal sidelobes and be used for pulse compression. There are two types of saturable absorbers (fast and slow). Fast saturable absorbers (artificial saturable absorbers) typically have recovery times on the order of fs while slow saturable absorbers (material based saturable absorbers) have recovery times on the order of ns-ps.

The important characteristics of a saturable absorber are: modulation depth, relaxation time, saturation fluence, and non-saturable loss. The modulation depth details the attenuation of low intensity light compared to high intensity light. The relaxation time details the time it takes for the saturable absorption effect to recover. The saturation fluence gives the required energy to bleach the saturable absorber. The non-saturable loss details the loss of the saturable absorber even when it is bleached. Unfortunately, material based saturable absorbers do not have sufficient modulation depth and bandwidth to suppress the EOM comb sidelobes. We need a saturable absorber that can deliver modulation depths of at least 90%, low saturation fluence, and low non-saturable loss. The slow saturable absorber would also be unable to suppress both sidelobes of the EOM comb. Instead, it would only be able to eat the front sidelobe of the pulse and would still be recovering while the trailing sidelobe would pass through. Artificial saturable absorbers have the desired re-

covery time for suppressing the sidelobes. However, not all artificial saturable absorbers can be externally implemented with the desired modulation depth.

Nonlinear Loop Mirrors

As previously mentioned, artificial saturable absorbers exhibit extremely fast recovery times (\sim fs) (owing to the ultrafast kerr effect, recoverytime \sim 13 fs) and can have much higher modulation depths. Unlike material based saturable absorbers, they have a wide range of operating wavelengths and come in a wide variety. Typically, artificial saturable absorbers have a high saturation fluence. This becomes an issue for high repetition rate comb sources due to the significantly lowered pulse energies. Unlike other artificial saturable absorbers, a nonlinear loop mirror (NLM) can be made with a low saturation fluence.

NLMs come in two variants, the nonlinear optical loop mirror (NOLM) [66] and the nonlinear amplifying loop mirror (NALM) [67]. The construction of a NLM is that of a sagnac interferometer where the symmetry is broken using the nonlinear phase shift acquired due to SPM. The NOLM imbalances the interferometer using a difference in power whereas the NALM imbalances the interferometer using a gain section. The benefit to using a NLM is that it can be easily incorporated into any setup, exhibits a high modulation depth [68], and are cost-effective. Despite most artificial saturable absorbers having high saturation fluence, the saturation fluence of a NLM can be lowered by simply using longer lengths of fiber. The NALM can also provide gain to a pulse train, allowing it to simultaneously amplify and improve the pulse contrast. A diagram to explain the operation of a NLM is shown in Fig. 4.10.

The switching behavior of the NLM can be analyzed using a scattering matrix approach [69]. The

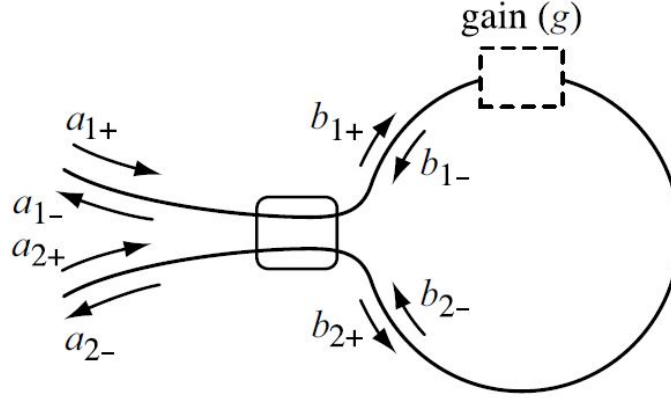


Figure 4.10: Simplified diagram of a nonlinear amplifying loop mirror.

resulting output normalized to the input power and gain for a NALM is shown in Eq. 4.2 and 4.3.

$$\left| \frac{a_{1-}}{a_{1+}} \right|^2 \exp(-2g) = 4\alpha(1-\alpha) \cos^2\left(\frac{\Delta\phi}{2}\right) \quad (4.2)$$

$$\left| \frac{a_{2-}}{a_{1+}} \right|^2 \exp(-2g) = 1 - 4\alpha(1-\alpha) \cos^2\left(\frac{\Delta\phi}{2}\right) \quad (4.3)$$

Where, $\Delta\phi = \phi_{12} - \phi_{21}$, is the phase difference between the clockwise and counter-clockwise paths. For a NOLM, the gain is set to 0 and $\Delta\phi = (1 - 2\alpha)\gamma|a_{1+}|^2L$. It is important to note that the nonlinear phase shift that gives rise to the switching behavior is dependent on the product of the peak power, nonlinear fiber coefficient, and length of fiber. It is also important to note that a NOLM typically does not work with a 50/50 coupler because there would be no difference in phase to provide the switching behavior. The exception to this would be to imbalance the acquired phase shift by means inside the loop [70].

Experimental efforts on using a 40/60 NOLM and a 50/50 NALM can be seen in Figs. 4.11 [71] and 4.12. It is important to note that the NOLM is a passive device and therefore needs prior amplification before working as intended. A NALM typically does not require prior amplification

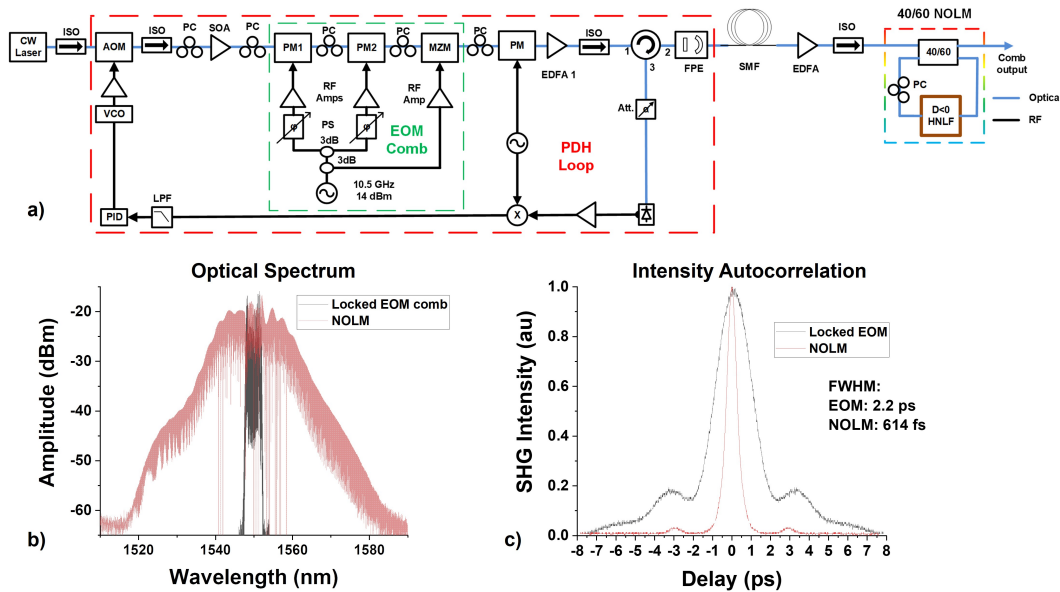


Figure 4.11: Experimental work of nonlinear pulse compression using a 40/60 NOLM on an EOM comb (with 2 phase modulators driven by an external RF synthesizer at 10.5 GHz) locked and filtered by our 100k finesse etalon. a) AOM: acousto-optic modulator, ISO: fiber pigtailed isolator, PC: polarization controller, SOA: semiconductor optical amplifier, PM: phase modulator, MZM: intensity modulator, EDFA: Erbium doped fiber amplifier, FPE: 100k finesse Fabry-Perot etalon, SMF: 540 m of standard single mode fiber, VCO: voltage controlled oscillator, RF Amps: RF amplifiers, PS: RF phase shifter, Att: optical attenuator, LPF: low pass filter, PID: proportional-integral-derivative controller, 40/60: 40/60 fiber optic coupler, D<0 HNLF: 100 m of normal dispersion HNLF with low loss splices SMF28 pigtailed, b) Optical spectrum of EOM comb (black) and NOLM output (red), c) Intensity autocorrelation of EOM comb (black) and NOLM output (red).

unless the input power is too low to saturate the gain medium.

Fig. 4.11a shows our experimental results using a 40/60 NOLM. The system starts with a CW laser passing through an AOM, SOA, and comb generating modulators. The entire EOM comb is then locked to our 100k finesse etalon (~ 1.5 GHz FSR, ~ 15 kHz FWHM). Since the EOM comb is generated before the etalon, both f_0 & f_{rep} are locked to the etalon. The EOM comb is driven by an external RF synthesizer at ~ 10.5 GHz which is $7 \times$ FSR. The EOM comb is then compressed using

540 m of SMF28 fiber and amplified up to .6 W in an EDFA. The amplified and compressed EOM comb is then sent into a 40/60 NOLM. The input to the NOLM has a fiberized isolator to prevent the back reflected light from coupling into the EDFA. The NOLM consists of a 40/60 coupler, in-line fiber polarization controller, and 100 m of normal dispersion HNLFF ($D = -.7 ps/nm/km$) for nonlinear phase accumulation. The HNLFF is the main source of nonlinear phase accumulation from the pulse due to the long length of fiber and high nonlinear coefficient ($10.7 W^{-1}km^{-1}$). In addition, the HNLFF has SMF28 pigtailed splices to each end of the 100 m HNLFF for efficient coupling. The optical spectrum and intensity autocorrelation of the pulses before (black) the NOLM and after (red) are shown in Fig. 4.11b & c respectively. The red vertical lines that drop to the bottom of the plot shown in Fig. 4.11b are an artifact of the OSA and are not part of the spectrum. From the optical spectrum in Fig. 4.11b, we observe significantly less ripple at the top compared to a purely SPM broadened EOM comb. We also observe less abrupt transitions on the edges of the spectrum compared to the EOM comb spectrum. The intensity autocorrelation in Fig. 4.11c shows a dramatic reduction of power in the pulse pedestal after the NOLM. We also observe a significant amount of pulse shortening after passing through the NOLM. Despite the significant improvement in the pulse contrast and duration, they pulses are still not short enough and still exhibit some temporal ringing. This is because a 40/60 NOLM still has a finite extinction ratio that cannot fully suppress the pedestal. To fully suppress the temporal pedestal in a pulse, a 50/50 coupler must be used. However, a 50/50 coupler in a NOLM does not work unless special precautions are made to imbalance the nonlinear phase shift. Another alternative is to replace the 40/60 NOLM with a 50/50 NALM for better switching contrast.

Fig. 4.12 shows our experimental data using a 50/50 NALM for nonlinear pulse shaping. Fig. 4.12a shows the schematic of our system. The system starts with a CW laser followed by an AOM, a cascade of 4 phase modulators and one intensity modulator for EOM comb generation. The phase modulator after the intensity modulator is used for PDH locking and the amplifiers

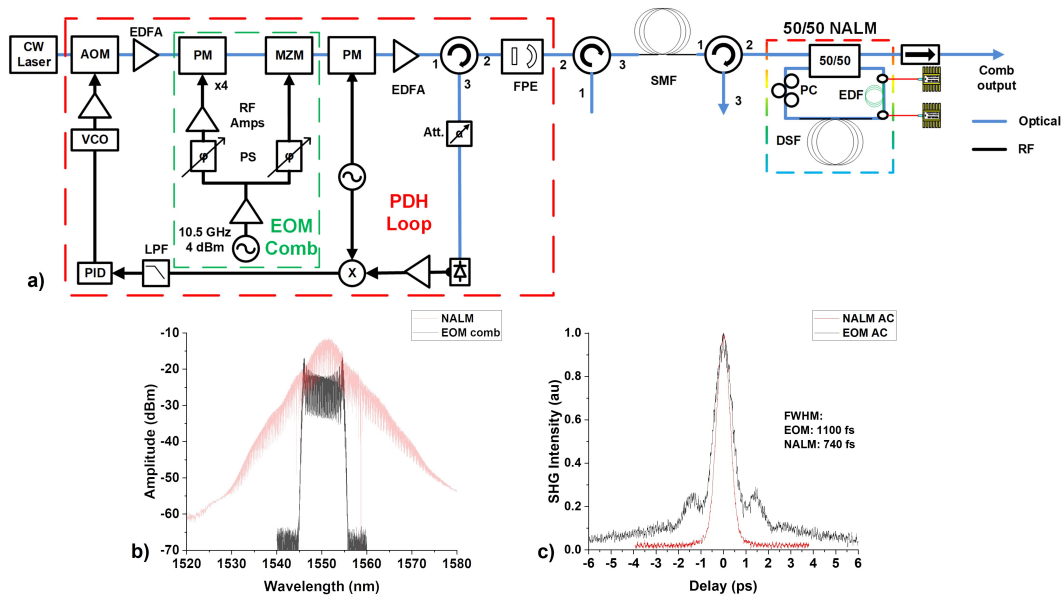


Figure 4.12: Experimental work of nonlinear pulse compression using a 50/50 NALM on an EOM comb (with 4 phase modulators driven by an external RF synthesizer at 10.5 GHz) locked and filtered by our 100k finesse etalon. a) AOM: acousto-optic modulator, ISO: fiber pigtailed isolator, PC: polarization controller, PM: phase modulator, MZM: intensity modulator, EDFA: Erbium doped fiber amplifier, FPE: 100k finesse Fabry-Perot etalon, SMF: 250 m of standard single mode fiber, VCO: voltage controlled oscillator, RF Amps: RF amplifiers, PS: RF phase shifter, Att: optical attenuator, LPF: low pass filter, PID: proportional-integral-derivative controller, 50/50: 50/50 fiber optic coupler, DSF: 110 m of dispersion shifted fiber, EDF: 12 m of M12-980-125 Erbium doped fiber bi-directionally pumped by two 1 W 976 nm laser diodes, b) Optical spectrum of EOM comb (black) and NALM output (red), c) Intensity autocorrelation of EOM comb (black) and NALM output (red).

before the etalon are to compensate for losses. The EOM comb is driven by an RF synthesizer at ~ 10.5 GHz which is again 7x the FSR of the 100k finesse etalon we used. Again, since the EOM comb is locked to the etalon, both f_0 and f_{rep} of the EOM comb are locked and filtered by the etalon. It is also important to note that 4 phase modulators were used instead of 2 as shown in Fig. 4.11a. This entails that the EOM comb bandwidth is wider and leads to shorter pulses when compressed. The EOM comb is then compressed by propagating through 250 m of SMF28 fiber before entering the 50/50 NALM. A circulator is placed at the input of the NALM to ensure the

back reflected light does not go back into the preceding parts of the system. In addition, an isolator is placed at the output of the NALM to ensure back reflections are not coupled into the NALM from other sources. The NALM uses 110 m of dispersion shifted fiber (DSF) with a dispersion parameter of $-0.8 \frac{ps}{nm*km}$ and a MFD of $8.6 \mu m$ for nonlinear phase accumulation. We employed 12 m of M12-980-125 erbium doped fiber (EDF) bi-directionally pumped by two 1 W 976 nm laser diodes for the gain section and an inline fiber polarization controller. The DSF has a much smaller nonlinear coefficient ($\sim 3 \frac{ps}{nm*km}$) owing to its larger MFD. Since our starting EOM comb uses 4 phase modulators instead of 2, the starting EOM comb here has a shorter pulse duration than in Fig. 4.11. Shorter pulses entails higher peak power, which means more nonlinear phase shift with the same average power. Fig. 4.12b & c shows the measured optical spectrum and intensity autocorrelation before the NALM (in black) and after the NALM (in red). In Fig. 4.12b, we observe significantly less spectral broadening compared to the NOLM case but no oscillations on the top of the spectrum appear. This explains the measured intensity autocorrelation in Fig. 4.12c where we observe the pulse pedestal to be completely suppressed. Again, the pulses are still not short enough after the NALM but we find that the pulse pedestal can be completely suppressed by a 50/50 NALM.

From Fig. 4.11 and 4.12, we have experimentally measured the output spectrum & pulse profile after propagating through a 40/60 NOLM and a 50/50 NALM. Individually, the NOLM and NALM are incapable of providing the necessary pulse parameters needed. The NOLM is incapable of completely suppressing the sidelobes while the NALM's pulse shortening capacity is limited. However, by combining multiple NLMs, it is possible to achieve both high contrast and ultrashort pulse durations. Fig. 4.13 shows how both a 40/60 NOLM and a 50/50 NALM can be used to produce high contrast and ultrashort pulses.

Fig. 4.13a our experimental results of combining a NOLM and a NALM for producing ultrashort high contrast pulses. The output of Fig. 4.11 is then pulse-picked by a factor of 64. Pulse-picking

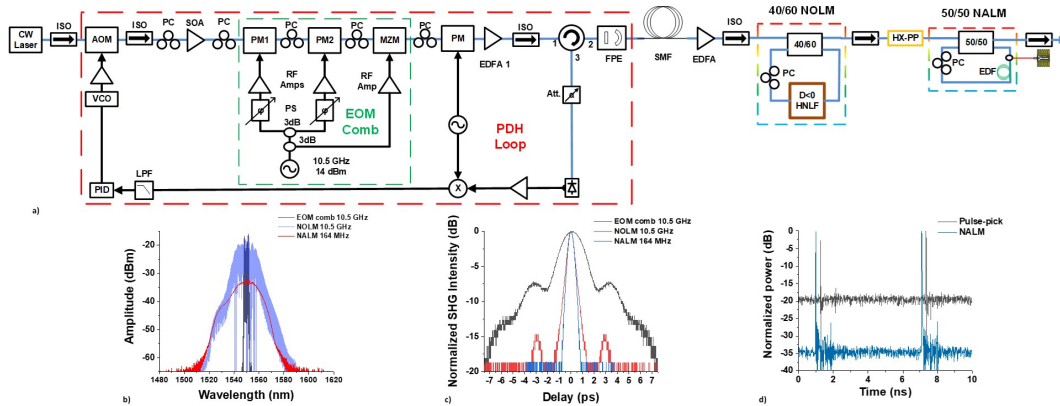


Figure 4.13: Experimental work of nonlinear pulse compression by cascading a 40/60 NOLM and a 50/50 NALM on an EOM comb (with 2 phase modulators driven by an external RF synthesizer at 10.5 GHz) locked and filtered by our 100k finesse etalon. a) Schematic diagram using an EOM comb followed by a 40/60 NOLM and a 50/50 NALM. AOM: acousto-optic modulator, SOA: semiconductor optical amplifier, ISO: fiber pigtailed isolator, PC: polarization controller, PM: phase modulator, MZM: intensity modulator, EDFA: Erbium doped fiber amplifier, FPE: 100k finesse Fabry-Perot etalon, SMF: 540 m of standard single mode fiber, VCO: voltage controlled oscillator, RF Amps: RF amplifiers, PS: RF phase shifter, Att: optical attenuator, LPF: low pass filter, PID: proportional-integral-derivative controller, 40/60: 40/60 fiber optic coupler, D<0 HNLF: 100 m of normal dispersion HNLF with low loss splices to SMF28 pigtails, HX-PP: high extinction electro-optic pulse-picker, 50/50: 50/50 fiber optic coupler, EDF: 2.6 m of Er40-4/125 erbium doped fiber pumped by a 1 W 976 nm laser diode, b) Optical spectrum of EOM comb (dark blue), after NOLM (light blue), after NALM (red), c) Intensity autocorrelation of EOM comb (dark blue), after NOLM (light blue), and after NALM (red), d) sampling scope trace after pulse-picking (black) and after NALM (blue).

reduces the repetition rate of the pulse train from ~ 10.5 GHz to ~ 164 MHz (pulse-picking will be discussed in detail in the next chapter). It is important to note that pulse-picking not only reduces the repetition rate but also the average power in the pulse train by the same factor. The benefit is that lower repetition rate pulses (assuming same average power) have higher pulse energies which leads to higher nonlinearity. This means that less fiber is needed for the same amount of nonlinear phase shift. The pulse-picked pulse train is then sent into a 50/50 NALM with fiber isolators at the input and output. This NALM consists of a 50/50 coupler, fiber polarization controller, 1 m of

SMF28, and 1 m of Liekki Er110-4/125 EDF pumped by a 1 W 976 nm laser diode. The optical spectrum and intensity autocorrelation traces after each step are shown in fig. 4.13b, c respectively. The HX-PP is used to downsample the repetition rate by a factor of 64 (from 10.5 GHz to \sim 160 MHz). By downsampling the repetition rate, higher peak powers with the same average power can be obtained. However, the suppression of the adjacent pulses (extinction ratio of the pulse-picker) is determined by several factors and is limited by the electronics. A saturable absorber can also be used to enhance the extinction ratio of the pulse-picking process (shown in fig. 4.13d). From fig. 4.13b, the optical spectrum exhibits a smoother profile at the top while the autocorrelation trace in fig. 4.13c shows a complete removal of the sidelobes after the NALM. In fig. 4.13d, the extinction ratio of the pulse-picked EOM comb is shown to improve by \sim 15 dB. As a result, it is possible to simultaneously obtain ultrashort pulses with high pulse contrast.

An issue that has not been clearly mentioned is that long lengths of non-polarization maintaining optical fiber exhibit random polarization fluctuations. It has been shown by placing a polarization controller inside a non polarization maintaining (PM) NLM and adjusting the polarization, the switching state can be changed. Although the polarization controller can make it easier for a NLM to be operated in switching mode, it also reveals an issue related to NLMs using long lengths of non-polarization maintaining fiber. The same random polarization fluctuations in non-PM fibers can cause the switching state to randomly change. The random fluctuations in the switching state are also accompanied by changes in the output power. Considering modulators typically use a micro polarizer that can handle limited power in the orthogonal polarization, this issue makes a non-PM NLM difficult to work with over long periods of time. An alternative to this issue is shown in Fig. 4.14.

Fig. 4.14 shows our experimental results in using a NALM with shorter fiber lengths. The schematic, shown in Fig. 4.14a starts with the same EOM comb locked to the 100k finesse etalon as shown in Fig. 4.12. Again, since the EOM comb is locked to the etalon, both f_0 & f_{rep} are locked

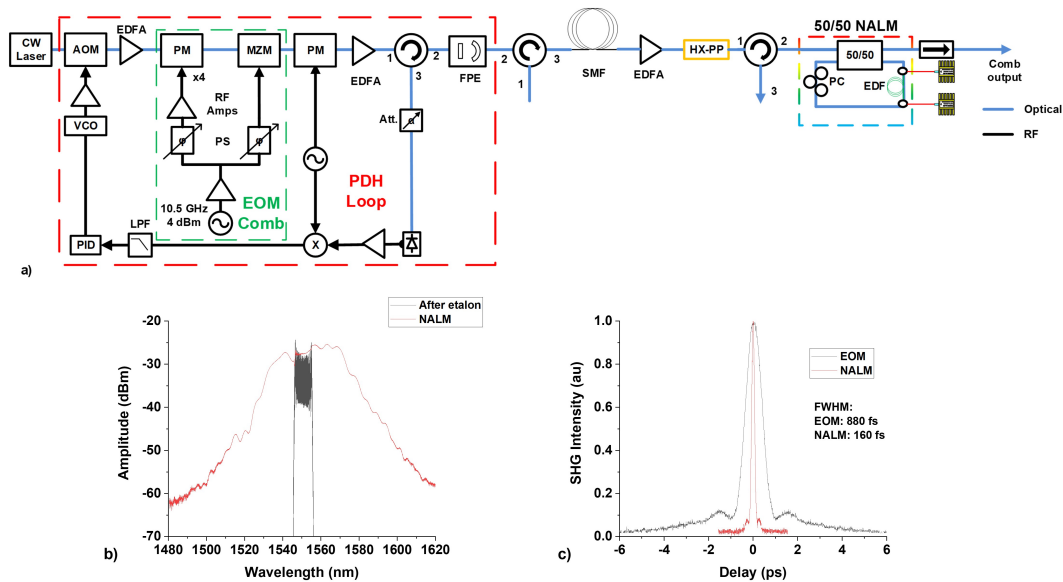


Figure 4.14: Experimental work of nonlinear pulse compression by using a short length 50/50 NALM on an EOM comb (with 4 phase modulators driven by an external RF synthesizer at 10.5 GHz) locked and filtered by our 100k finesse etalon. a) Schematic diagram of an EOM comb followed by a short length 50/50 NALM. AOM: acousto-optic modulator, ISO: fiber pigtailed isolator, PC: polarization controller, PM: phase modulator, MZM: intensity modulator, EDFA: Erbium doped fiber amplifier, FPE: 100k finesse Fabry-Perot etalon, SMF: 250 m of standard single mode fiber, VCO: voltage controlled oscillator, RF Amps: RF amplifiers, PS: RF phase shifter, Att: optical attenuator, LPF: low pass filter, PID: proportional-integral-derivative controller, HX-PP: high extinction electro-optic pulse-picker, 50/50: 50/50 fiber optic coupler, EDF: 2.6 m of Er40-4/125 erbium doped fiber pumped by a 1 W 976 nm laser diode, b) Optical spectrum of EOM comb (black), after NALM (red), c) Intensity autocorrelation of EOM comb (black), and after NALM (red).

to the etalon. The EOM comb is driven by an external synthesizer at $7 \times \text{FSR}$ of the etalon. The EOM comb is then compressed using 250 m of SMF28 fiber and then amplified up to 300 mW by an EDFA. The amplified and compressed EOM comb is then sent through an electro-optic pulse-picker for downsampling the repetition rate by 64. The new repetition rate of the EOM comb after the pulse-picker is ~ 164 MHz. After the pulse-picker a 50/50 NALM is used to both improve the extinction ratio of the pulse-picker and compress the pulse. The NALM consists of 2.6 m of Liekki

Er40-4/125 EDF pumped by a 1 W 976 nm lasers diode, a fiber polarization controller, 50/50 coupler, and SMF28. The input of the NALM is spliced to a circulator to ensure the back reflected light does not affect the previous components while the output of the NALM is spliced directly to an isolator to prevent back reflections from entering the NALM. The total length of SMF28 in the NALM from all components is roughly the same length as the EDF. Fig. 4.14b & c shows the optical spectrum and intensity autocorrelation before the NALM (black) and after the NALM (red) respectively. The optical spectrum after the NALM shows significant spectral broadening compared to fig. 4.12b. We attribute this effect to the significantly higher pulse energy present in the gain fiber section of the NALM which gives rise to additional spectral broadening inside the gain fiber (which is common to both the clockwise and counterclockwise propagating pulses). This additional nonlinear phase accumulation in both directions increases the total acquired nonlinear phase which significantly decreases the pulse duration. Unfortunately, this increased nonlinear phase accumulation also leads to the addition of sidelobes around the main pulse. This effect is shown in 4.14c, where the output of the NALM still exhibits temporal sidelobes. The optical spectrum in Fig. 4.14b also exhibits spectral oscillations as opposed to the proper pulse shaped spectrum shown in Fig. 4.12b. Despite this, we are still able to obtain significantly shortened pulses with better contrast than before the NALM.

Although the NALM in Fig. 4.14 is not fully switching, the output power and polarization is stable. This is because the length of fibers used in the NALM are relatively short (under 10 m). Although non-PM fibers can provide random polarization fluctuations, short lengths of fibers (< 10 meters) do not exhibit enough random polarization fluctuations to cause an issue. This means that non-PM fibers can still be used for low noise saturable absorption given the lengths are short.

Finally, we constructed two 50/50 NALMs both using 2.6 m of Er40-4/125 pumped by a 1 W 976 nm laser diode. Our experimental work of cascading NALMs is shown in Fig. 4.15. Fig. 4.15a shows the schematic of the OEO EOM comb followed by a cascade of NALMs. The system

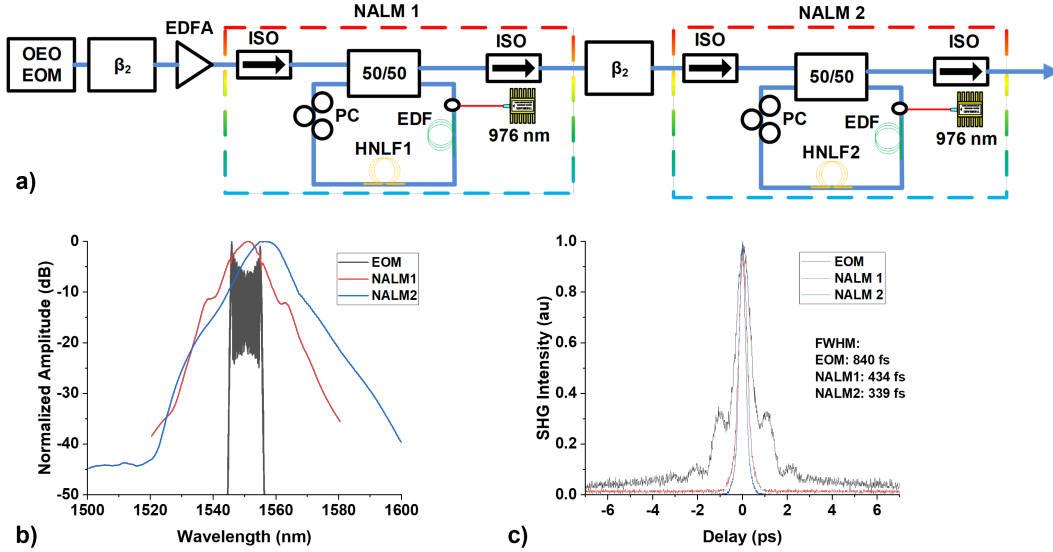


Figure 4.15: Experimental work of nonlinear pulse compression by using cascaded 50/50 NALMs on an OEO EOM comb (EOM comb is generated by 4 phase modulators and one intensity modulator driven by the OEO loop at ~ 10.5 GHz). a) Schematic diagram of OEO EOM comb followed by cascade of 50/50 NALMs. OEO EOM: OEO EOM comb employing 1 intensity modulator and 4 phase modulators (phase modulators placed after the etalon), β_2 : linear chirp from finisar waveshaper, ISO: fiber pigtailed isolator, PC: polarization controller, EDFA: Erbium doped fiber amplifier, 50/50: 50/50 fiber optic coupler, EDF: 2.6 m of Er40-4/125 erbium doped fiber pumped by a 1 W 976 nm laser diode, HNL1: 100 m of zero dispersion HNLF with low loss splices to SMF28 on each side, HNL2: 100 m of normal dispersion HNLF with low loss splices to SMF28 on each side, b) Optical spectrum of EOM comb (black), after NALM 1 (red), and after NALM 2 (blue), c) Intensity autocorrelation of EOM comb (black), after NALM 1 (red), and after NALM 2 (blue).

starts with the OEO EOM comb shown in Fig. 2.20a generating an EOM comb driven by an OEO at $7 \times \text{FSR}$ of our 100k finesse etalon. The OEO EOM comb is then compressed using a Finisar waveshaper applying $4.75 \frac{\text{ps}}{\text{nm}}$ linear chirp. We note that the waveshaper can be replaced using SMF28 without issue. We simply use the waveshaper to apply linear chirp for convenience. The compressed EOM comb is then amplified to compensate for the losses from the waveshaper and sent into the first NALM. The first NALM consists of 100 m of $D = 0 \frac{\text{ps}}{\text{nmkm}}$ HNLF (with low loss splices to SMF28 fiber pigtailed on each end), a fiber polarization controller, 50/50 coupler, and 2.6

m of Liekki Er40-4/125 EDF pumped by a 1 W 976 nm laser diode. The input and output of the NALM are directly spliced to fiber isolators to prevent back reflections from causing problems. The output of NALM 1 is then compressed using another Finisar waveshaper. The second waveshaper again only applies linear chirp, this time $-0.22 \frac{ps}{nm}$ dispersion. NALM 2 consists of a 50/50 coupler, fiber polarization controller, 2.6 m of Liekki Er40-4/125 EDF pumped by 1 W 976 nm laser diode, and 100 m of $D=-0.72 \frac{ps}{nm*km}$ HNLFF with low loss splices to SMF28 fiber pigtails on each end. Again, the input and output ports of the NALM are directly spliced to an isolator to prevent back reflections from being an issue. Although these NALMs suffer from the same polarization stability, we observed significant spectral broadening and pedestal reduction. This can be seen in the optical spectrum and intensity autocorrelation traces in Fig. 4.15b & c respectively. The optical spectrum shown in Fig. 4.15b shows the EOM comb (black), NALM 1 (red), and NALM 2 (blue) optical spectrum. After the NALM 1, we see a sech like pulse with small spectral wings. After NALM 2, we observe the optical spectrum to shift towards longer wavelengths and the bandwidth increases. The shape of the spectrum after NALM 2 is also much closer to the classic sech pulse spectrum. In Fig. 4.15c, the intensity autocorrelation after the EOM comb (black), NALM 1 (red), and NALM 2 (blue) is shown. The EOM comb exhibits high temporal sidelobes which are completely removed after NALM 1. The autocorrelation FWHM drops almost by a factor of 2. After NALM 2, the decrease in FWHM is less dramatic but we see the high pulse contrast is maintained. The change in pulse shortening can be explained by the fact that an EOM comb's time-bandwidth product is .88 while the time-bandwidth product of a sech pulse is .315. Not only is there spectral broadening taking place in the NALM, but the pulse is completely reshaped after NALM 1. After NALM 2, the pulse shape is roughly the same and therefore any pulse shortening is just through increasing the bandwidth. We observe the optical spectrum after NALM 2 to support sufficiently short pulses with no pedestal energy for coherent octave spanning supercontinuum generation. Although the transform limited pulse duration after the second NALM is $\sim 240fs$, the pulses are sufficiently short and clean such that a nonlinear fiber amplifier can further compress the pulse duration to

under 200 fs.

Although we have demonstrated an approach for generating ultrashort pulses with high contrast, the NLMs produce randomly polarized light. How does one build a reliable low noise NLM for high repetition rate sources? The only way to reduce the power necessary for switching in a NLM without using a polarization controller is to use longer lengths of fiber. But long lengths of non-PM fiber are the source of the fluctuations! There are two solutions to this predicament. One can employ the polarization insensitive nonlinear optical loop mirror [72] or use only PM fiber and PM couplers [73]. Although [73] only used a NOLM, a NALM is also possible using only PM fibers. We were unable to obtain polarization maintaining highly nonlinear fiber suitable for NALMs in time for this work. Future endeavors may involve using PM fibers and components for the NLMs.

We have experimentally demonstrated improvements in both pulse duration and pulse contrast using nonlinear loop mirrors. In Fig. 4.13, we demonstrated the ability to completely remove the pulse pedestal and reduce the pulse duration by nearly 10x. In Fig. 4.12, we demonstrated that the pulse pedestal of the EOM comb can be removed in a single stage. We also discussed how Fig. 4.13 and 4.12 are sensitive to polarization fluctuations leading to using short lengths of fiber for a NALM such as in Fig. 4.14. Although polarization fluctuations remain to be an issue for non-PM NLM, we continue to employ a non-PM NALM as in Fig. 4.15.

This chapter discussed a cost-effective and fully fiber based alternative approach to producing ultrashort pulses with high contrast. By using nonlinear loop mirrors, we have demonstrated complete suppression of the EOM comb pedestal as well as reducing the pulse duration close to the target or below 200 fs. Again, the pulse duration and the peak power are not at the target for generating coherent octave spanning supercontinuum generation. The generated pulses shown in this chapter can be amplified to reach the targeted pulse parameters. This will be the subject of the next chapter.

CHAPTER 5: ULTRASHORT PULSE AMPLIFICATION

In the previous chapter, we have demonstrated significant improvement in the pulse contrast and pulse duration of an EOM comb. Unfortunately, the pulse energies after the NLMs are still insufficient to reach our target (pulse energy > 0.2 nJ & pulse duration < 200 fs for waveguides, pulse energy > 1 nJ & pulse duration < 100 fs for fiber). In this chapter, we seek to construct an optical amplifier that can meet our needs to reach the pulse parameters.

Ultrashort pulse amplification in Erbium doped fiber amplifiers

Erbium doped fiber amplifiers (EDFA) are currently the most popular gain medium for amplifying light in the telecom band. They exhibit significantly less optical nonlinearities compared to semiconductor optical amplifiers and are capable of reaching much higher output powers. EDFAs are also capable of providing over 20 dB of gain with low noise figure. Due to the commercial popularity, EDFAs are easy to purchase. However, for nano-joule pulse energies, commercial EDFAs are not a viable option. This is due to a variety of factors ranging from the amplifier length, the types of fibers used in the EDFA, and even the pump source. For amplification of ultrashort pulses, several parameters must be considered. To low dispersion over the amplifier, short Erbium doped fiber lengths must be used. To achieve the necessary gain for a short length of gain fiber, highly doped fibers must be used. At the same time, it is helpful to select a gain fiber with normal dispersion (dispersion parameter < 0 ps/nm/km) to ensure pulse breakup due to soliton compression does not occur. As previously mentioned, nonlinear propagation in anomalous dispersion fiber leads to soliton compression while nonlinear propagation in normal dispersion fiber leads to parabolic pulse propagation. The mode field diameter (MFD) of the gain fiber is also important as a reduced MFD results in a higher nonlinear coefficient. Last but not least, one must consider the desirable

Name	Output power (mW)	EDF length (m)	Pump direction	Dispersion: (Normal or anomalous)	Peak core absorption ($\frac{dB}{m}$)	Mode field diameter (μm)
Er110	80	.8	Co-propagating	Normal	110	6.5
Er80 HD-PM	150	1.1	Co-propagating	Normal	80	6.5
Er40	210	2.6	Co-propagating	Normal	40	6.5
M12	280	5.5	Co-propagating	Normal	20	6

Figure 5.1: Measured output powers using an input of 1 mW CW at 1550 nm and a 1 W 976 nm pump laser for various Erbium doped fibers.

output power. Unlike Ytterbium, Erbium exhibits a significantly lower absorption cross section, excited state absorption, and quenching effects. These factors lead to a lower pump to output power conversion efficiency. High output powers in highly doped Erbium doped fibers necessitate significantly higher pump availability. With all of these considerations in mind, we choose to use the Liekki-Er110-4/125 and Er40-4/125 Erbium doped fibers for our home-built EDFAs. Other gain fibers from other companies (EDF80 or EDF150 from OFS) could be purchased, but their nonlinear coefficient (as a result of a smaller core size) is much larger which can complicate our design. Figure 5.1 shows a table of experimentally measured saturation powers for various Erbium doped fibers using a 1 W 976 nm pump diode.

From Fig. 5.1, we observe an increase in output power for lower peak core absorption (which implies lower doping density). At the same time, a longer length of Erbium doped fiber (with lower doping density) is used to achieve higher output powers. Fig. 5.1 also gives a first step in determining what type of fiber and length would be required for a desired output power. If even higher average powers are required, then additional pump power must be available. It is important to note that the output end of the EDF was flat cleaved and spliced to a fiberized isolator with SMF28 pigtailed. Currently, the highest power single mode laser diode centered at 980 nm

on the market can provide up to 1 W of power (976 nm laser diodes also work for pumping EDF and they exhibit the same output power as 980 nm laser diodes). For a single mode laser diode centered at 1480 nm, that power is 0.6 W. Although the power out of the 980 nm laser diodes is higher, the conversion efficiency of pumping at 1480 nm is roughly double that of pumping at 980 nm. This means that pumping at 1480 nm was a better option for achieving higher output power. Due to the increased conversion efficiency, pumping at 1480 nm produces less heat in the fiber compared to pumping at 980 nm. The increased heat load can manifest itself in the output light as a constant fluctuation in output polarization of the fiber (assuming non polarization maintaining fiber). Various pumping schemes for fiber based amplifiers are shown in Fig. 5.2. The three pump schemes shown are co-propagating pump, counter propagating pump, and bi-directionally pumped. The co-propagating pump case has the pump light traveling in the same direction as the signal light. The counter propagating pump case has the pump light traveling the opposite direction as the signal light. The bi-directionally pumped case is when the gain fiber is pumped with pump light from both ends.

Fig. 5.2 shows the different methods in which single transverse pump light can be sent into an EDF. The co-propagating pump scheme shown at the top has the pump light and signal light propagating in the same direction. The counter propagating pump scheme shown in the middle has the pump light and signal light propagating in opposite directions. The bi-directional pumping scheme shown at the bottom is a combination of the co-propagating and counter propagating schemes. It is important to note that an isolator is placed at the output to ensure the optical gain is only absorbed by the signal light. The different pump schemes have different properties and will not be discussed here. Although not recorded in Fig. 5.1, we have observed higher output powers when counter propagating the pump light with respect to the signal. However, counter propagating the pump with respect to the signal produces more ASE at the output end of the EDFA. Unfortunately, the maximum output power with these pumping schemes is still limited due to the available

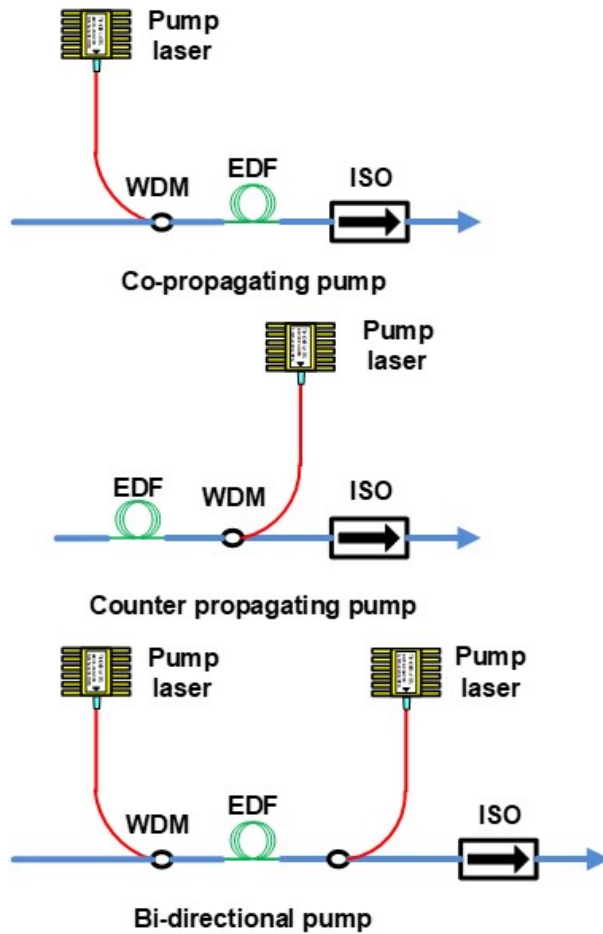


Figure 5.2: Various pump configurations in fiber. From top to bottom: co-propagating pump, counter propagating pump, and bi-directional pump.

pump powers. Fig. 5.3 shows several methods of combining several pump diodes. This allows for the output power of an EDFA to be extended even further by introducing additional single mode pumps.

The pump combining techniques in Fig. 5.3 are polarization based, spectral, and a combination of the two. Spatial pump combining is not an option for commercially available components for single mode fiber based devices. In polarization pump combining, the pump light is combined onto

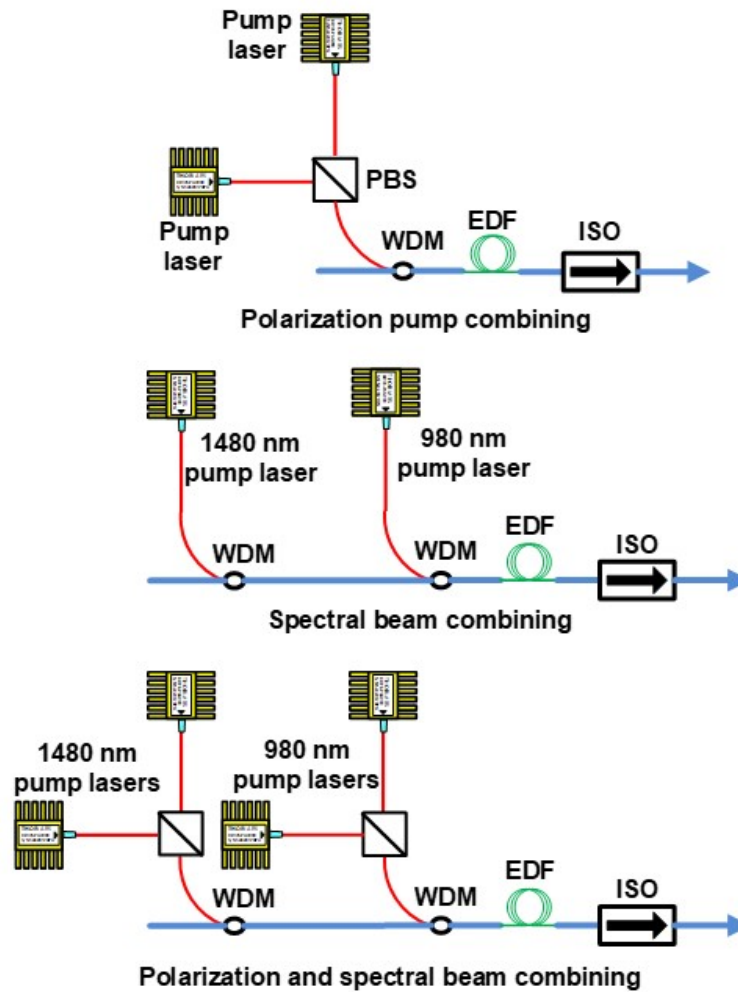


Figure 5.3: Fiber pump combining architectures. From top to bottom: Polarization beam combining, spectral beam combining, and polarization plus spectral beam combining.

a single fiber using a polarization beam splitter/combiner (PBS/PBC). In spectral pump combining, the pump light is simply combined onto a single fiber by using a 1480/1550 WDM and then a 980/1550 WDM. Reversing the order of WDMs would require custom made WDMs to ensure minimal loss of the pump light. The combination of spectral and polarization beam combining is shown at the bottom of the figure. It is critical to note that isolators on the pump sources would prevent random injection locking events on the pump laser diodes when bi-directionally

pumping the gain fiber. Unfortunately, the inclusion of isolators degrades the total available pump power. Even with polarization and spectral beam combining in a bi-directional pumping scheme, the output power of the EDFA is limited to only 1 W (assuming a conversion efficiency of 50%). It is also important to note the selection of components. Some vendors use tapered fibers for the WDMs while others may use micro-optics for the WDMs. The micro-optics based WDMs typically handle less than 1 W of optical power while the tapered fiber based components handle 5 W of optical power. At the same time, tapered fiber based components have a significantly smaller operating bandwidth than the micro-optics based components. The next section presents two alternative pump sources for obtaining even higher output powers from an EDFA.

Watt Class EDFAs

In the previous section, we discussed several methods of core pumping an Erbium doped fiber. Core pumping relies on single mode pump sources and requires the gain fiber's core to be doped with rare earth elements. However, the output power of any fiber amplifier is limited by the total available pump power. Single mode laser diodes are limited in power due to a variety of reasons which limits the available pump power.

An alternative is to use a double clad gain fiber and a multi-mode laser diode. Unlike their single mode counterparts, multi-mode diodes offer significantly higher output powers (100 W and above) which can be used to achieve even greater output powers in an optical amplifier. However, double clad Erbium doped fibers typically have a low pump absorption which necessitates a long amplifier length. In addition, most companies do not spec the dispersion parameter in double clad gain fibers. This makes selection of double clad gain fibers for pulsed operation challenging. One method to avoid the nonlinear interactions inside the amplifier (assuming a long length of fiber is unavoidable) is to employ chirped pulse amplification (CPA). A schematic of employing CPA is shown in Fig.

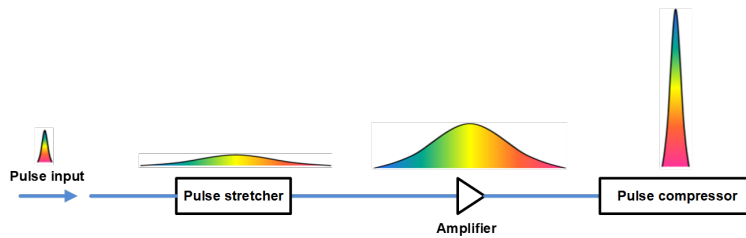


Figure 5.4: Conceptual diagram of chirped pulse amplification.

5.4.

By pre-stretching a pulsed input to a fiber amplifier, the nonlinearity of the amplifier is significantly reduced. This is because the nonlinearity is proportional to the length of the amplifier, the effective area, and the power. By pre-stretching the input, the peak power is significantly reduced. An issue with this approach is that it requires additional components such as a pulse stretcher and a pulse compressor. The pulse stretcher can be realized by using chirped fiber bragg gratings (CFBGs) or even a 4f grating compressor/stretchers. However, additional caution must be exercised when building the pulse compressor. This is because the whole point of using CPA was to avoid fiber nonlinearities in the amplifier. Re-compressing the pulse after the amplifier requires a free-space compressor or hollow core fiber (HCF) such that the nonlinearities are reduced. Since SMF28 exhibits anomalous dispersion at 1550 nm, entering the fiber with high peak power pulses would result in soliton compression (which as previously stated can result in pulse splitting or severe pulse pedestals). This option usually requires hollow core fibers and is more difficult in practice to implement. The most common option for re-compressing pulses after CPA in a fiber amplifier is to compress the pulse in free space. However, a free space compressor also has loss (whether it's from each component or from coupling back into fiber). Finally, if the compressed pulses are to SMF28 again, the length must be kept extremely short to avoid pulse splitting. The length of SMF28 that is tolerable depends on the pulse peak power after recompression and must be simulated to

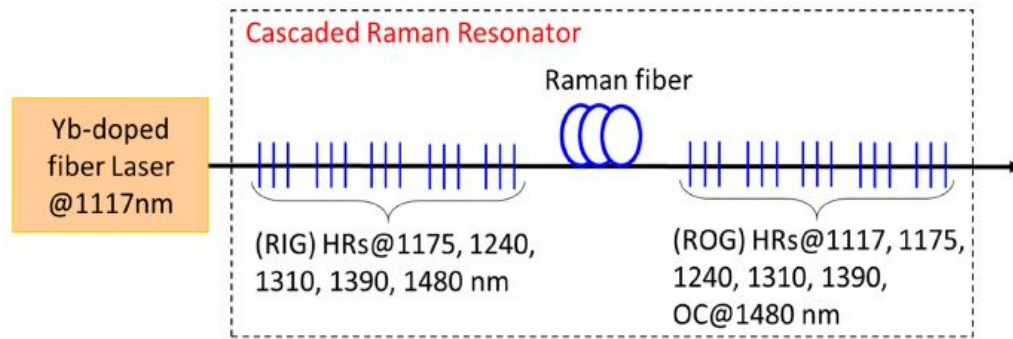


Figure 5.5: Schematic for a cascaded Raman fiber laser. RIG: Raman cavity input grating, HR: high reflector, ROG: Raman cavity output grating.

know. The main takeaway is that employing CPA for obtaining high peak power pulses in a fiber amplifier requires one to think carefully about how to re-compress the pulse after the amplifier. It also requires simulations to give an idea of how much nonlinearity will be induced after the compressor stage as the output would still need to be inside single mode fiber.

Another approach to obtaining high output powers using an EDFA would be to use a Raman fiber laser as a pump source. A schematic of a Raman fiber laser is shown in Fig. 5.5. The cascaded Raman fiber laser (RFL) shown in Fig. 5.5 starts with an Ytterbium (Yb) doped fiber laser operating at 1117 nm. Unlike other rare earth doped fiber lasers, Yb lasers have been demonstrated to produce extremely high output powers (multi-kW).

A high power Yb fiber laser can easily be built by using double clad Yb doped fiber and using multi-mode laser pump diodes at 976 nm. The high power laser centered at 1117 nm is then frequency down shifted using the Raman nonlinearity. In silica glass, the peak Raman gain is ~ 13 THz away from the pump light. The Raman resonator is formed by using fiber Bragg gratings (FBG) with high reflectivity at the specific wavelengths of the peak Raman shifted pump. This produces a cascaded effect of stimulated Raman scattering (SRS) where the initial 1117 nm pump

light is frequency converted in several steps to 1480 nm. This process has been found to be fairly efficient in generating over 100 W of single mode CW light centered at 1480 nm [74]. The RFL output at 1480 nm then becomes a high power laser that can be used to core pump an Erbium doped fiber.

We were able to acquire two Raman fiber lasers with an output centered at 1470 nm and an output power of 3 W. In theory, simply combining the RFL and the signal light into an Erbium doped fiber would be sufficient for building a high power EDFA. In practice, when the gain of an EDFA is high enough, the output end of the Erbium doped fiber needs to be angle cleaved and spliced to the output delivery fiber [22]. By angle cleaving the output end of the Erbium doped fiber, Fresnel reflections (due to the index mismatch between EDF and SMF28/free space) do not couple back into the core. Instead, the Fresnel reflection is coupled into the cladding where no gain is present.

In our experiment, we configured the EDFA in a co-propagating pump configuration using a 3 W RFL centered at 1470 nm as the pump source. We used roughly 4.5 m of Liekki Er40-4/125 as the gain fiber and cleaves of at least 8 degrees to reduce back reflections. The gain fiber used has a numerical aperture of .2 which leads to an acceptance angle of $\approx 8^\circ$. By cleaving the gain fiber at an angle greater than the acceptance angle, we expect to significantly reduce the back reflections that can take away gain from our signal. The output end of the gain fiber is spliced to a high power isolator with SMF28 leads. To protect the preceding stages of our setup, we spliced a high power isolator to the input end of the WDM.

After splicing the output end of the gain fiber to the isolator, we employed a cutback method to optimize the gain fiber length. The input end of the gain fiber was flat cleaved to expedite the optimization process. To test the output power of the home-built power amplifier shown in Fig. 5.6, we preamplified a CW laser (1550 nm) to 40 mW, then powered the pump laser. We measured an output power of 1.55 W using a free-space power meter. An optimized splice recipe for the angle

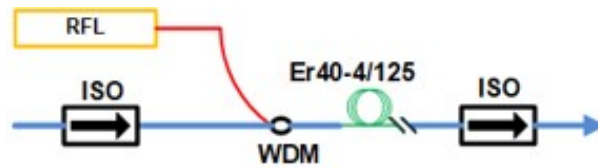


Figure 5.6: Schematic diagram for testing home-built EDFA using RFL. ISO: 5 W power handling fiber isolator, WDM: 1480/1550 wavelength division multiplexer, Er40-4/125: 4.5 m of Liekki Erbium doped fiber Er-40-4/125.

cleaved gain fiber should yield higher output powers. However, we still observe an improved conversion efficiency of at least 50% compared to other works demonstrating a conversion efficiency of 40% [22], [75].

Although we built a Watt class EDFA with a short gain fiber length, we are still unable to reach pulse energies of 1 nJ at a repetition rate of 10 GHz. To reach such pulse energies at 10 GHz, we would need 10 Watts of output power. Not only is that difficult because of the required pump power (20 W of pump required to obtain 10 W of output power), it is also difficult to find parts that can handle that much power. Our WDM for combining the pump and signal lights can only handle 5 Watts max. To avoid destroying components, we seek an alternative method to reducing the power constraints.

Gain narrowing

We discussed how to build EDFAs with an emphasis on pulsed input. An additional concern that we have yet to mention but observed is gain narrowing. Gain narrowing occurs when the input bandwidth is comparable to the gain spectrum of the amplifier. The amount of gain narrowing a pulse experiences is dependent on the amount of gain the amplifier provides. Gain narrowing

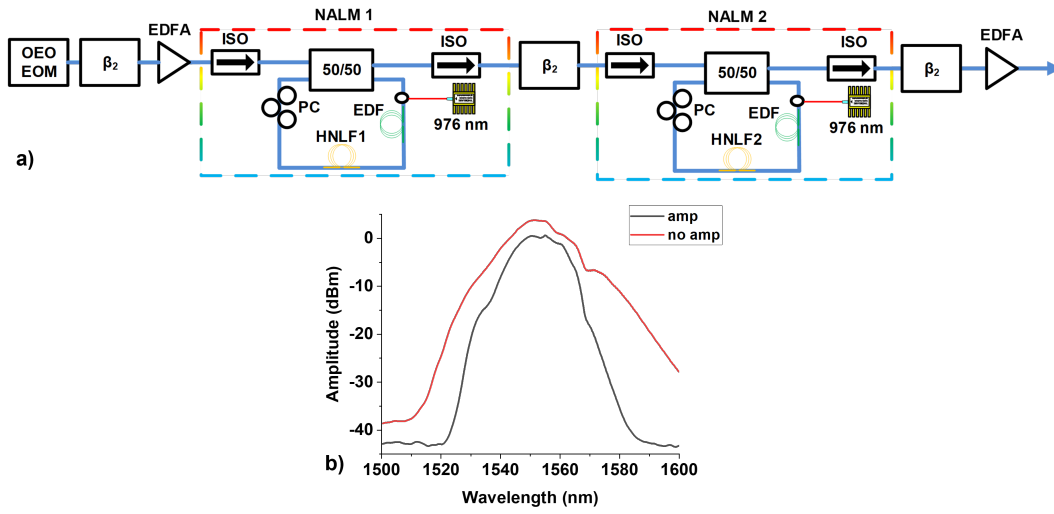


Figure 5.7: Experimental data demonstrating gain narrowing in a commercial 2 W EDFA. a) Schematic for generating broad bandwidth pulses followed by an EDFA producing gain narrowed pulses. β_2 : linear chirp from finisar waveshaper, ISO: fiber pigtailed isolator, PC: polarization controller, EDFA: Erbium doped fiber amplifier, 50/50: 50/50 fiber optic coupler, EDF: 2.6 m of Er40-4/125 erbium doped fiber pumped by a 1 W 976 nm laser diode, HNLF1: 100 m of zero dispersion HNLF with low loss splices to SMF28 on each side, HNLF2: 100 m of normal dispersion HNLF with low loss splices to SMF28 on each side. b) optical spectrum after NALM 2 (red) and after final EDFA (black).

occurs because the center of a pulse spectrum absorbs higher gain than the wings of the pulse spectrum. Previous work on self-referencing mode-locked fiber lasers was done using significantly lower repetition rates than 10 GHz. This means that to achieve the required pulse energy for supercontinuum generation, much lower average powers were required (and consequently less gain). To achieve 1 nJ pulse energies at a repetition rate of 250 MHz, only 250 mW of average power is required. To achieve 1 nJ pulse energies at a repetition rate of 10 GHz, 10 W of average power is required. This entails significantly higher gain is required for the high repetition rate case which leads to significantly more gain narrowing. Fig. 5.7 shows our experimental data showing gain narrowing in the lab. The schematic shown in Fig. 5.7a starts with the OEO EOM comb from Fig. 2.20 which is compressed with linear chirp. The OEO EOM comb is then reshaped through

a cascade of 50/50 NALMs as shown in Fig. 4.15a. The output after NALM 2 is then pre-chirped before entering a commercially built 2 W EDFA with normal dispersion gain fiber. The final EDFA uses a double clad fiber pumped by a multi-mode 976 nm laser diode. Fig. 5.7b shows the optical spectrum after NALM 2 (red) and after the 2 W EDFA (black). From Fig. 5.7b, we observe a significant reduction in the optical spectrum. Initially, the output spectrum of NALM 2 supported ~ 240 fs pulses. But the output spectrum after the EDFA barely supports sub-500 fs pulses. We will discuss our solution to the complicated amplifier design criteria in the following sections. It is important to note that previous work in self-referencing an EOM comb also encountered this issue [17]. The current solution has been to either flatten the optical spectrum or to use longer input pulses to the power amplifier.

Pulse-picking

Pulse-picking is a process in which the repetition rate of a pulse train is downsampled by an integer factor. This is done by employing a temporal gate signal that allows only 1 in every N pulses in the pulse train. The downsampling reduces the repetition rate by N and reduces the average power in the pulse train by N. By reamplifying the pulse train (after pulse-picking), significantly higher pulse energies can be obtained. This is generally the case because an optical amplifier often saturates at a particular average power due to gain saturation. Keeping in mind that pulse energy $E_p \sim P_{av}T_{rep}$, if the average power is clamped by the gain medium, the only option to increase pulse energies would be to reduce the repetition rate. In practice, pulse-picking for high repetition rates (1 GHz and above) becomes challenging. Fig. 5.8 shows a conceptual diagram of pulse-picking in the time domain.

At the top of Fig. 5.8, a pulse train with a high repetition rate is shown in blue. For the pulse-picker to generate a synchronized gate signal, it must receive an external divided down clock

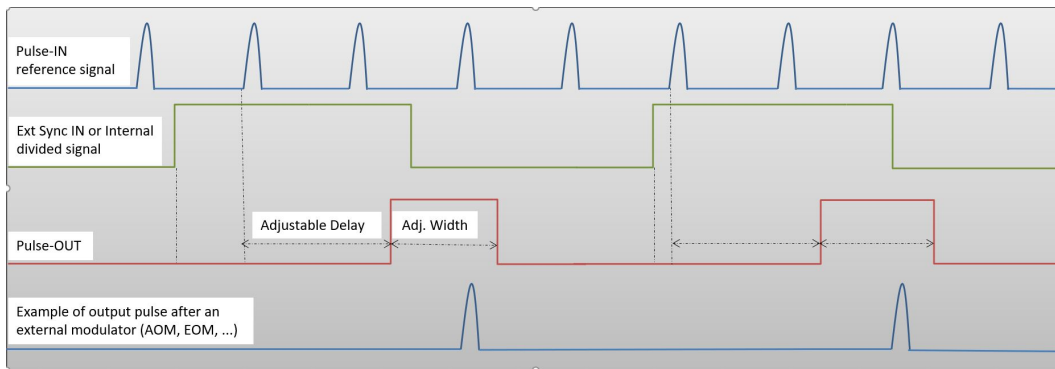


Figure 5.8: Conceptual diagram of pulse-picking in the time domain.

signal (shown in green). From the synchronized clock, the gate signal is generated (shown in red), which is used to temporally select a single pulse within the repetition rate (shown at the bottom). Theoretically, this process is simple because one needs to simply provide the input pulse train, the pulse-picker, and a synchronized divided down signal. In practice, high repetition rate sources are more difficult to pulse-pick because of the short gate signal required to effectively suppress adjacent pulses. For example, to pulse-pick a 10 GHz repetition rate pulse train to 1 GHz, the gate signal's rising and falling edges together must be shorter than 100 ps. In practice, this typically entails a gate signal with a FWHM < 50 ps. Otherwise, insufficient extinction in the pulse-picking process would occur and give rise to additional noise. In addition to the pulse generator requirements, the pulse-picker must have enough bandwidth to even respond to the electrical pulse. Unfortunately, acousto-optic modulators and SOA's have insufficient electrical bandwidth for pulse-picking repetition rates of 1 GHz and above. Our only option is to use electro-optic modulators for pulse-picking despite having a lower extinction ratio.

Pulse-pick by 64

From the previous sections, we have discussed how pulse-picking can be used to relax the requirements on an optical amplifier for providing nano-joule pulse energies with sub-100 fs pulse durations. Since our oscillator has a repetition rate of ~ 10.5 GHz, we would need 10.5 W of average power to reach 1 nJ pulse energies. From the previous sections, it is extremely difficult to obtain even 1 W of average power with single mode pump diodes. Although options for building and obtaining Watt class EDFAs are available, several Watts of output power is still beyond our capability. These issues can be alleviated by downsampling the repetition rate by larger factors. In this section, we discuss pulse-picking a 10.5 GHz pulse train down to ~ 164 MHz. By reducing the repetition rate by 64 times, the average power is reduced by 18 dB and the new repetition rate becomes $f_{rep} \sim 164$ MHz. At the same time, only 164 mW of average power is required to reach 1 nJ of pulse energy. This significantly relaxes the design requirements on EDFAs and allows us to use single mode laser diodes for pumping the EDF.

A sampling scope trace of the electrical gate signal used for pulse-picking our 10.5 GHz pulse train down to 164 MHz is shown in Fig. 5.9.

Although the gate signal in Fig. 5.9 is incapable of providing complete extinction of adjacent pulses for pulse-picking, it is still possible to employ saturable absorption to enhance the extinction ratio. This was done in Fig. 4.13 and 4.14 using a 50/50 NALM to simultaneously enhance the extinction ratio and reduce the pulse sidelobes. Ideally, the next step would be to simply amplify the pulse-picked pulse train and obtain ultrashort pulses.

Fig. 5.10a shows the schematic for an EOM comb using four phase modulators and one intensity modulator driven by a common RF synthesizer at ~ 10.5 GHz that is locked & filtered by a 100k finesse etalon. The EOM comb is first compressed using 222 m of SMF28 fiber, amplified up to

Sampling scope

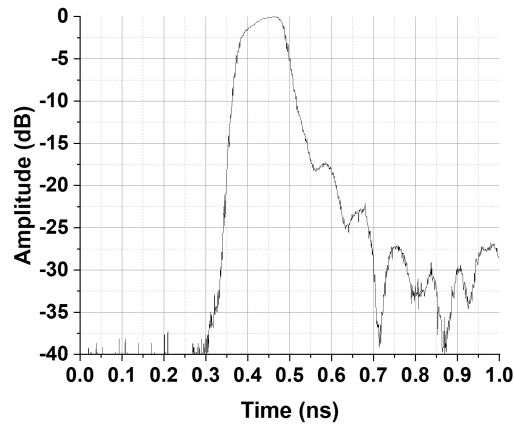


Figure 5.9: Sampling scope trace of our electrical gate signal with a repetition rate ~ 164 MHz.

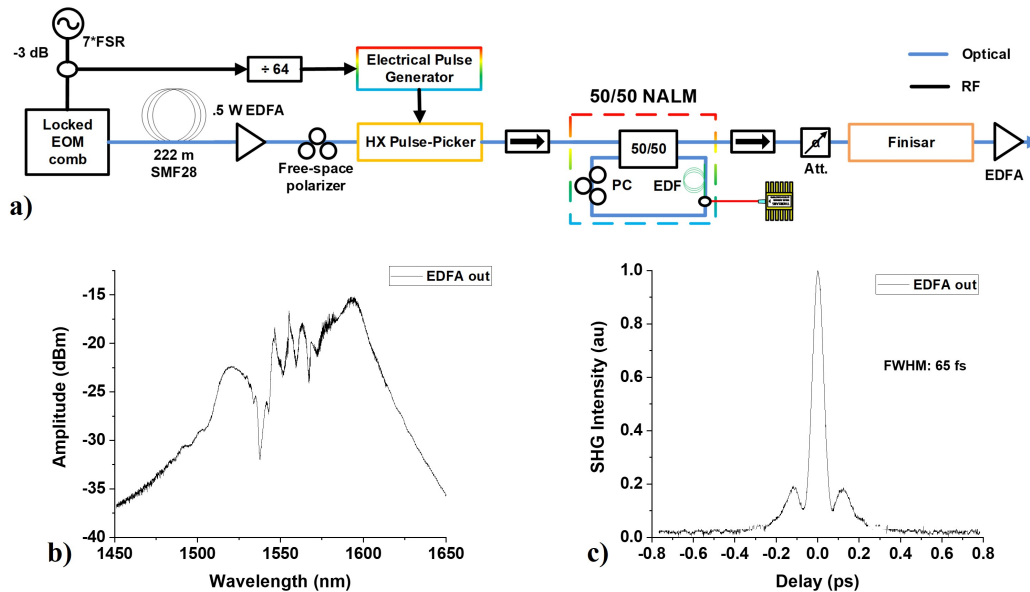


Figure 5.10: a) Experimental setup for generating ultrashort high peak power pulses seeded by an EOM comb. EDFA: erbium doped fiber amplifier, ISO: fiber isolator, HX pulse-picker: high extinction electro optic pulse-picker, $\div 64$: divide by 64 countdown trigger box, EDF: 2.6 m of Liekki Er40-4/125 Erbium doped fiber, Att: adjustable optical attenuator. b) Optical spectrum after the final EDFA. c) Intensity autocorrelation after the final EDFA.

300 mW, pulse-picked by 64, and then reshaped by a 50/50 NALM. The output of the NALM is then fed into a finisar waveshaper as a tunable dispersive delay line and then sent through a home-built EDFA using 2.6 m of Er40-4/125 EDF. Prior to the finisar waveshaper, the setup and diagnostics are exactly the same as in Fig. 4.14. The home-built EDFA amplifies the pulses up to 250 mW while 1.5 m of SMF28 fiber is used to compress the output pulses. The optical spectrum and intensity autocorrelation after the EDFA are shown in Fig. 5.10b and c. From the intensity autocorrelation, we observe a significant amount of temporal compression as the pulse duration is under 65 fs. These pulse properties are suitable for coherent octave spanning supercontinuum generation and will be explored in chapter 6.

Pulse-pick by 8

We have discussed the benefit to pulse-picking, however, it is not clear how pulse-picking can affect the coherence of supercontinuum generation. Few works in the literature give a clear answer on whether pulse-pick factor can be a decoherence mechanism for supercontinuum generation. It has been mentioned in the literature that pulse-picking does not affect the coherence of a generated continuum [76], but pulse-picking a 250 MHz repetition rate laser and a 10 GHz one are very different due to the required gate pulse duration. In this section, we combine the previous section's discussion on high power EDFAs with the OEO EOM comb.

Unfortunately, the gate signal shown in Fig. 5.9 on it's own does not provide sufficient extinction for adjacent pulses at a repetition rate of 10.5 GHz. The previous section showed that a NALM can be used to enhance the extinction. However, the inclusion of the NALM adds additional ASE after the etalon in the pulse train. The additional ASE can become a problem for generating coherent octave spanning supercontinuum generation (which is the topic of the next chapter). The pulse generator shown in Fig. 5.9 also cannot operate at higher frequencies (repetition rate bandwidth:

Sampling scope

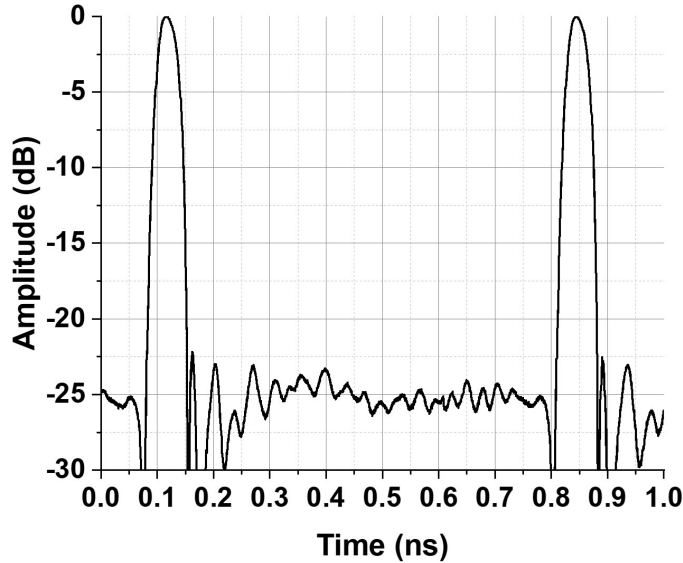


Figure 5.11: Sampling scope trace of newly acquired electrical pulse generator operating at a repetition rate of 1.3 GHz.

20 MHz - 200 MHz), meaning the pulse-pick rate is set to a maximum of 200 MHz. To remedy these issues, we purchased a new electrical pulse generator. A sampling scope trace of the output of the pulse generator operating at 1.3 GHz is shown in Fig. 5.11.

Fig. 5.11 shows a sampling scope trace of the new electrical pulse generator operating at a repetition rate of 1.3 GHz ($\sim \frac{10.5\text{GHz}}{8}$). The output of the pulse generator is attenuated by 20 dB to ensure the sampling scope is not overloaded. We observe that not only does the new pulse generator offer significantly shorter pulses, but the rising and falling edges lie within less than 100 ps. The limited extinction ratio in the sampling scope trace is due to the external attenuation which prevents observing the full dynamic range of the signal.

With the new electrical pulse generator and a tunable optical cavity, we are in a position to demon-

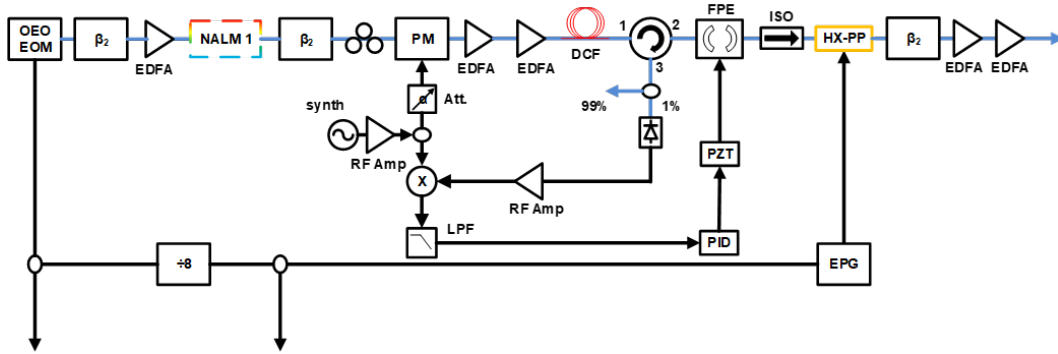


Figure 5.12: Experimental schematic for generating ultrashort high contrast pulses with pulse pick rate of 8. EDFA: erbium doped fiber amplifier, NALM 1: nonlinear amplifying loop mirror, PM: phase modulator, β_2 : linear chirp applied by Finisar waveshaper, DCF: 0.7 m dispersion compensating fiber, FPE: Tunable ~ 600 finesse etalon, ISO: fiber isolator, HX-PP: high extinction pulse-picker, Att: RF attenuator, synth: RF synthesizer operating at 900 MHz, RF Amp: RF amplifier, PD: photodiode, PZT: high voltage piezo driver, LPF: low pass filter, PID: proportional-integral-derivative controller, EPG: electrical pulse generator.

strate an even lower noise architecture for generating ultrashort high contrast pulses. This is shown in Fig. 5.12. The diagnostic traces for this architecture are shown in Fig. 5.13.

The experimental setup shown in Fig. 5.12 starts with the same OEO EOM comb from Fig. 2.20 followed by NALM 1 shown in fig. 4.15. Unlike Fig. 4.15, NALM 2 is not used. The output of NALM 1 is then fed into another finisar waveshaper providing only linear chirp. We again note that the waveshaper can be replaced with single mode fiber and was used only as a convenience. The pulses were then sent through a phase modulator for PDH locking of the tunable Fabry-Perot etalon. A fiber polarizer (not shown) is placed prior to the phase modulator to protect it from polarization fluctuations. Prior to entering the etalon, the pulses were amplified by two EDFAs. The first EDFA acts as a preamplifier while the second EDFA (double clad EDFA) is used to amplify the pulse train up to 1.5 W average power. The usage of a preamplifier is to reduce the amount of ASE incurred by high gain amplification. The 1.5 W average power pulses were

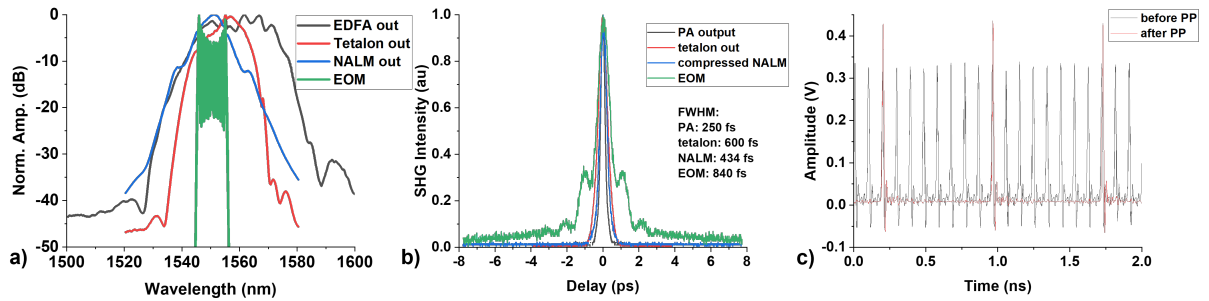


Figure 5.13: Diagnostic traces of the new all fiber approach to generating high contrast ultrashort pulses for supercontinuum generation. a) optical spectrum of OEO EOM comb output (green), NALM 1 output (blue), tunable etalon throughput (red), final EDFA output (black). b) Intensity autocorrelation traces of OEO EOM comb output (green), NALM 1 output (blue), tunable etalon throughput (red), final EDFA output (black). c) Sampling scope traces before pulse-picker (black) and after pulse-picker (red).

then sent through 0.7 m of DCF. The DCF was used to compensate for the chirp incurred by the following fiber circulator, fiber pigtailed on the fiber launchers (for etalon coupling), fiber pigtailed on the high extinction pulse-picker, and other lengths of fiber. Unfortunately, the DCF splice exhibited high losses necessitating amplification to 1.5 W. The tunable etalon used is the same as the ~ 600 finesse tunable etalon shown in fig. 3.9. To ensure the pulse-picker was properly saturated, the output power of the double clad EDFA was set to ensure ~ 24.5 dBm of average power made it to the pulse-picker. The pulse-picker downsampled the repetition rate by a factor of 8 from ~ 10.5 GHz to ~ 1.3 GHz. It is important to note that the pulse-picker has an integrated polarizer that can only handle 15 mW in the orthogonal polarization. To protect the pulse-picker from polarization fluctuations caused by the double clad EDFA, an external fiber polarizer and polarization controller were used. The pulse-picked pulse train was then sent through a final finisar waveshaper to again apply only linear chirp prior to the final EDFAs. We again used two EDFAs to reduce the total incurred ASE from amplification. The optical spectrum is shown in Fig. 5.13a with the OEO EOM comb output (green), NALM 1 output (blue), etalon throughput (red), and the final EDFA

output (black). The intensity autocorrelation is shown in Fig. 5.13b with the OEO EOM comb output (green), NALM 1 output (blue), etalon throughput (red), and the final EDFA output (black). The sampling scope trace before the pulse-picker (black) and after the pulse-picker (red) is shown in Fig. 5.13c. We observe after output of the NALM, the output of the tunable etalon exhibits a much broader optical spectrum but shifted towards longer wavelengths. At first, the runs contrary to the previously mentioned issue of gain narrowing. Since we started with less optical spectra when entering the double clad EDFA, the effect of gain narrowing was reduced. In addition, we observe the shorter wavelength side to have been reduced after the double clad EDFA while the longer wavelengths have been added. This effect has been observed in [77] where the combination of a normal dispersion gain medium and SPM resulted in generating broad optical spectrum on the longer wavelength side of a pulse whereas the shorter wavelength side gained no additional spectra. We also observed the output pulses after the double clad EDFA to be linearly chirped. In [77], it's shown that significantly broader optical spectra can be obtained by simply amplifying the pulse train to higher output powers. The condition for generating such clean broadening are to start with a center wavelength close to the peak absorption & gain wavelengths of the amplifier and normal dispersion gain fiber. The highly linear chirp is also reflected in the intensity autocorrelation trace after the etalon in Fig. 5.13b. The output of the etalon pulses are linearly chirped with no sidelobes incurred by higher order dispersion.

The final EDFA again uses normal dispersion gain fiber and is used for additional spectral broadening. The gain fiber in the final EDFA is spliced to SMF28 which is capable of compressing the pulses closer to the transform limit. We measured an intensity autocorrelation FWHM of 250 fs after the final EDFA. We note that increasing the output power of the final EDFA would result in even shorter pulses with higher average power. Finally, the new electrical pulse generator is found to suppress the adjacent ~ 10.5 GHz pulses. The newly generated pulses are sufficiently short and powerfully enough for supercontinuum generation in waveguides.

In this chapter, we discussed amplification of ultrashort pulses in fiber amplifiers. We started the discussion with parameters on EDF. We covered the different pump sources that are used in these Watt class EDFA's as well as the types of fibers. Then, we discussed practicalities associated with such high power amplifiers and shifted our focus to reducing the necessary powers using pulse-picking. Through pulse-picking, we have demonstrated an approach for generating 1 nJ pulse energies shorter than 100 fs. We have also demonstrated a lower noise approach for generating 200 pJ pulse energies shorter than 200 fs which are sufficient for coherent octave spanning supercontinuum generation through nonlinear waveguides (as opposed to fiber). The next chapter will discuss coherent octave spanning supercontinuum generation in more detail.

CHAPTER 6: COHERENT OCTAVE SPANNING SUPERCONTINUUM GENERATION FOR CARRIER-ENVELOPE-OFFSET FREQUENCY DETECTION

Supercontinuum generation, also known as white light generation, is a process where the spectral bandwidth of a source significantly increases. Several research articles have been published on this process using various optical media and various sources. However, for our purposes, we require an octave of coherent spectral bandwidth ($1 - 2\mu m$) to measure the carrier-envelope-offset frequency. An excellent review on the desirable pulse properties for generating a coherent supercontinuum can be found in [78]. Although the literature has stated the need for pulse energies of 1 nJ and sub-100 fs pulse durations [79], this is applicable to solid core highly nonlinear fiber and photonic crystal fiber. Nonlinear waveguides have been used to generate coherent octave spanning supercontinuum generation with only a fraction of the pulse energies required for fiber [80], [81]. Despite the wealth of research on the topic, it is important to know how it works.

Theoretical background: Supercontinuum Generation

The master equation for simulating supercontinuum generation is known as the Nonlinear Schrodinger equation (NLSE). It is simply a pulse propagation equation which takes into account the dispersion of the guiding medium and the nonlinearity of the medium. Eq. 6.1 is the generalized NLSE for optical fiber. However, nonlinear waveguides use a similar equation for simulating supercontinuum generation.

$$\frac{\partial A}{\partial z} + \frac{\alpha A}{2} - \sum_{k \geq 2} \frac{i^{k+1}}{k!} \beta_k \frac{\partial^k A}{\partial T^k} = i\gamma(1 + i\tau_{shock} \frac{\partial}{\partial T})(A(z, T) \int_{-\infty}^{\infty} R(T') |A(z, T - T')|^2 dT' + i\Gamma_R(z, T)) \quad (6.1)$$

Equation 6.1 is the generalized NLSE with all the dispersion and nonlinear terms in fiber incorporated [79]. Given the pulse properties, fiber nonlinear coefficient, loss, and full dispersion profile of the fiber, it is possible to numerically solve this equation using the split-step Fourier method or the ODE45 solver in MATLAB. Experimental data will be discussed in the next section. The coherence and spectral broadening in supercontinuum generation is heavily dependent on the dispersion properties of the fiber. Significant work in literature has been dedicated towards discussing the different mechanisms behind spectral broadening in various regimes. Pumping with pulse widths shorter than 100 fs has been shown to produce coherent spectral broadening while pumping with pulse widths greater than 100 fs has been shown to produce less coherent spectra. In the literature, soliton order or soliton number have been used to describe the pulse contrast. With higher soliton orders referring to pulses with greater pedestal energy as opposed to energy in the peak. It has also been shown that higher soliton orders produce incoherent supercontinuum, hence the need for low pedestal ultrashort pulses with sufficient pulse energy.

The form of spectral broadening is most affected by the dispersion properties of the fiber. Pumping in the normal dispersion regime gives rise to broadening dictated almost solely by SPM. This is because both normal dispersion and SPM act as mechanisms to stretch the pulse along propagation; reducing the pulse peak power and nonlinear effects associated. The result is a continuum with significantly less spectral broadening per unit length with high coherence. Pumping in the anomalous dispersion regime gives rise to a host of nonlinear effects due to soliton propagation. Soliton propagation occurs because SPM generates additional colors and a linear chirp at the center of the pulse. The anomalous dispersion of the medium acts to compensate the linear chirp while the pulse

propagates. When considering supercontinuum generation, the dispersion of the medium and the nonlinearity act to constantly compress the pulse while it propagates through fiber. Since the pulse duration is decreasing while propagating, the peak power is increasing during propagation along the fiber. The peak power induced by soliton effects allows for a host of various other nonlinear effects such as stimulated Raman scattering, optical shock, modulation instability, and more to occur. As a result, the spectral broadening per unit length is much larger but the coherence is typically much worse. Pumping at the zero-dispersion regime gives rise a mix of the aforementioned nonlinear effects. The normal dispersion side experiences little broadening due to the reduced peak power while the anomalous dispersion side experiences significant nonlinear effects due to soliton propagation. These effects are the same as mentioned in chapter 4 using a shorter length and even higher nonlinearity.

The spectral broadening associated with different dispersion parameters in fiber is shown in Fig. 6.1, 6.2, and 6.3. These figures are generated in Matlab using code from [79]. The fiber properties such as dispersion, attenuation, and nonlinear fiber coefficient are obtained from commercially available HNLF from Thorlabs. The dispersion parameter was obtained by applying polynomial fit curves to compute the higher order dispersion terms from the raw data provided on their website. The input pulse parameters to each of these fibers are the same with 10 kW of peak power, pulse profile of $sech^2$, and a pulse duration of ~ 70 fs. We stress that dispersion is the only parameter changing and that γ & α are the same in each simulation.

Fig. 6.1 shows a spectrogram of the aforementioned pulses propagating in 0.5 m of Thorlabs HN1550. The dispersion terms used are as follows: $\beta_2 = 1.311094521886622 * 10^{-27} \frac{s^2}{m}$, $\beta_3 = 6.851657004159531 * 10^{-42} \frac{s^3}{m}$, $\beta_4 = 2.597946354769162 * 10^{-55} \frac{s^4}{m}$, $\beta_{5-10} = 0$. Although normal dispersion HNLFs have been shown to produce purely coherent spectra, the spectral broadening is extremely limited. This can be seen in Fig. 6.1 where the generated optical spectrum doesn't even reach $1.2\mu m$. This makes the normal dispersion HNLF unsuitable for measuring f_{ceo} . We

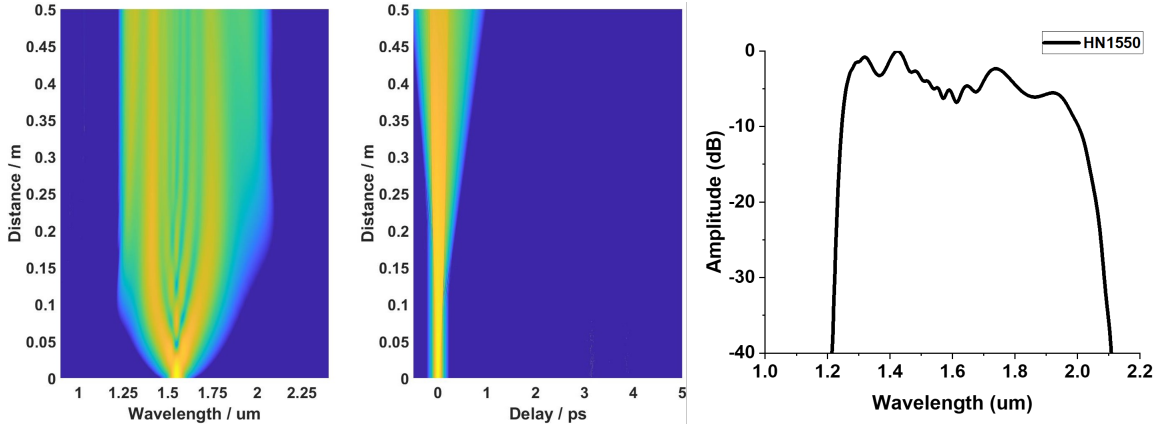


Figure 6.1: Supercontinuum generation simulation pumping .5 m of Thorlabs HN1550 with sech pulses of 10 kW peak power and ~ 70 fs. Left: Spectral evolution of pulse, middle: temporal evolution of pulse, right: spectrum of pulse after .5 m in HNLF.

also observe the shape of the output spectrum to resemble a parabola. This is caused by the previously stated effects where the normal dispersion coupled with SPM act to constantly stretch the pulse along propagation of the fiber. At the same time, SPM generates nonlinear phase which is proportional to the intensity profile of the pulse.

Fig. 6.2 shows a spectrogram of the aforementioned pulses propagating in 0.5 m of Thorlabs HN1550P. The dispersion terms used are as follows: $\beta_2 = -1.664270314152531 * 10^{-27} \frac{s^2}{m}$, $\beta_3 = 1.722728270634876 * 10^{-41} \frac{s^3}{m}$, $\beta_4 = 3.140721702898135 * 10^{-55} \frac{s^4}{m}$, $\beta_{5-10} = 0$. We observe far more spectral broadening in Fig. 6.2 compared to Fig. 6.1. The spectral broadening also occurs on a much shorter length. As previously stated, this is caused by the dispersion parameter as opposed to the nonlinear coefficient. Although the spectral broadening using the anomalous dispersion HNLF improved, it still does not span a full octave. This leads us to try another HNLF with a different dispersion parameter.

Fig. 6.2 shows a spectrogram of the aforementioned pulses propagating in 0.5 m of Thorlabs

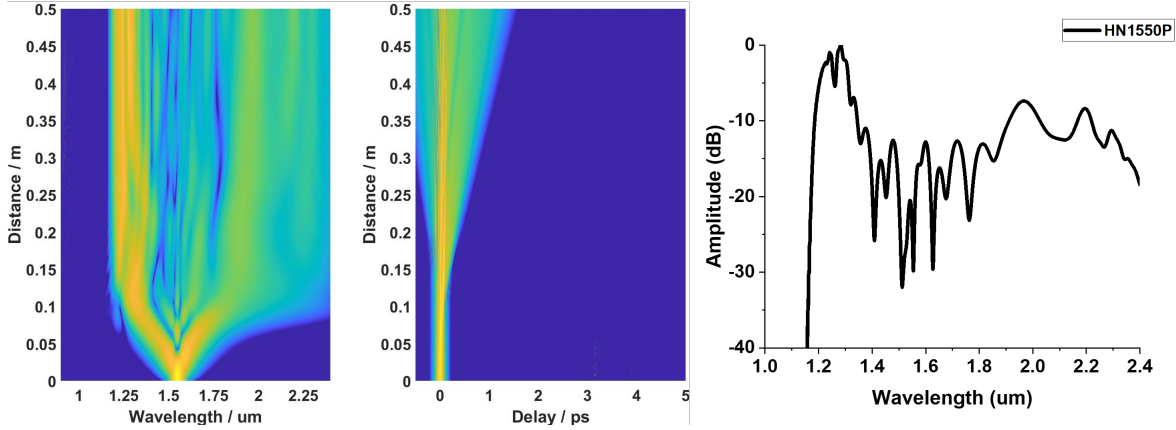


Figure 6.2: Supercontinuum generation simulation pumping .5 m of Thorlabs HN1550P with sech pulses of 10 kW peak power and ~ 70 fs. Left: Spectral evolution of pulse, middle: temporal evolution of pulse, right: spectrum of pulse after .5 m in HNLF.

PMHN5. Unlike the previously mentioned fibers, the raw dispersion data was not available. We used experimentally measured supercontinuum spectra from PMHN5 and adjusted the dispersion terms to match our experimental data. The dispersion terms used are as follows: $\beta_2 = -1.1830 * 10^{-26} \frac{s^2}{m}$, $\beta_3 = 8.1038 * 10^{-41} \frac{s^3}{m}$, $\beta_4 = -9.5205 * 10^{-56} \frac{s^4}{m}$, $\beta_5 = 2.0737 * 10^{-70} \frac{s^5}{m}$, $\beta_6 = -5.3943 * 10^{-85} \frac{s^6}{m}$, $\beta_7 = 1.3486 * 10^{-99} \frac{s^7}{m}$, $\beta_8 = -2.5495 * 10^{-114} \frac{s^8}{m}$, $\beta_9 = 3.0524 * 10^{-129} \frac{s^9}{m}$, $\beta_{10} = -1.7140 * 10^{-144} \frac{s^{10}}{m}$. From these simulations, we observe that careful selection of the dispersion properties of the HNLF are required to obtain the full octave. Simply choosing anomalous dispersion HNLF will not yield the desired spectral bandwidth.

Typically, the blue colors used in self-referencing are a result dispersive wave generation while the red colors used for SHG are a result of the soliton self-frequency shift. Again, these effects are dependent on the dispersion properties of the fiber. The ideal properties of a HNLF for f-2f interferometry include: generation of significant power at 1 & 2 μm and low splice loss to SMF. In summary, the dispersion properties of the fiber affect the spectral broadening in supercontinuum generation. The dependence on pulse parameters boils down to using high contrast, sub ~ 100 fs

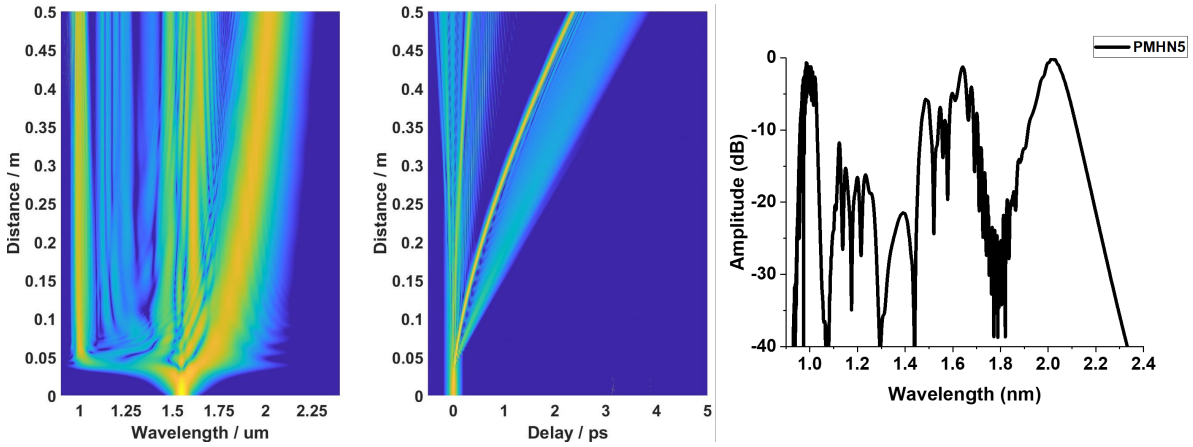


Figure 6.3: Supercontinuum generation simulation pumping .5 m of Thorlabs PMHN5 with sech pulses of 10 kW peak power and ~ 70 fs. Left: Spectral evolution of pulse, middle: temporal evolution of pulse, right: spectrum of pulse after .5 m in HNLf.

pulses with sufficient peak power in the fiber.

Experimental Work: Supercontinuum generation

To observe the spectral broadening in the HNLf, we used a commercial FMLL with a repetition rate of 20 MHz, average power of 3 mW, and emitting 300 fs pulses directly from the oscillator. As previously discussed, these pulses are too long and weak to generate an octave via supercontinuum generation in fiber. Therefore, we constructed an EDFA for nonlinear spectral broadening and pulse compression. The schematic and diagnostic traces of this approach can be seen in Fig. 6.4 & 6.5. We used 19 cm of dispersion compensating fiber (DCF) to pre-chirp the pulses prior to entry into the EDFA. The EDFA was constructed with short lengths of input and output SMF28 fiber to reduce dispersion and nonlinear effects. This is because the pulse energy of the MLL output is still high enough to yield considerable SPM in SMF28 before entering the EDFA. The erbium doped fiber (EDF) used was a highly doped EDF (Liekki Er110-4/125) pumped by a 1 W 976 nm laser.

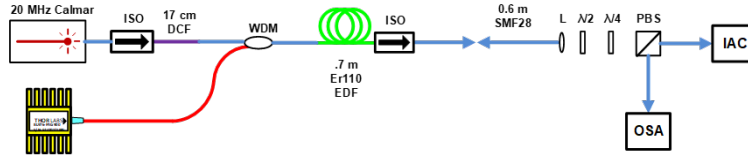


Figure 6.4: Setup for generating sub \sim 100 fs pulses for supercontinuum generation

We note that the splices between EDF and SMF were not optimized, optimized splice recipes would yield lower losses. After the EDFA, pulse energies exceeding 1 nJ were obtained which gives rise to significant amounts of SPM in the SMF28 used after the gain section. We measured \sim 30 mW average power in the amplified pulse train. The amplified pulses were then compressed in a short length of SMF28 pigtailed on the fiber isolator. We observed soliton compression on the output pulse in the short length of SMF28 used as pigtailed on the fiber isolator and 0.5 m patch cord leading into the SHG autocorrelator. It is important to note how the intensity autocorrelation and OSA are measured. Before entering the intensity autocorrelator, a 60 cm SMF28 patch cord with an 8 mm focal length aspheric lens acting as a collimator is used. A quarter wave plate and half wave plate are used to adjust the polarization while a PBS is used to ensure p-polarized light entering the autocorrelator for efficient phase matching. The s-polarized light (reflected from the PBS) is then coupled into another fiber to measure the optical spectrum. By using the tapped off light from the PBS to measure the optical spectrum, we are significantly reducing the peak power of the pulse entering the SMF28 fiber leading to the OSA. Had we placed the output of the EDFA directly into the OSA, our measurement would show the amplified pulse after significant spectral broadening. As a standard, all intensity autocorrelation measurements are taken with a 60 cm long SMF28 patch cord.

We spliced SMF28 to both ends of HNLF to measure the generated supercontinuum on an optical spectrum analyzer. We ensured the input length of SMF spliced to the HNLF matches that of the

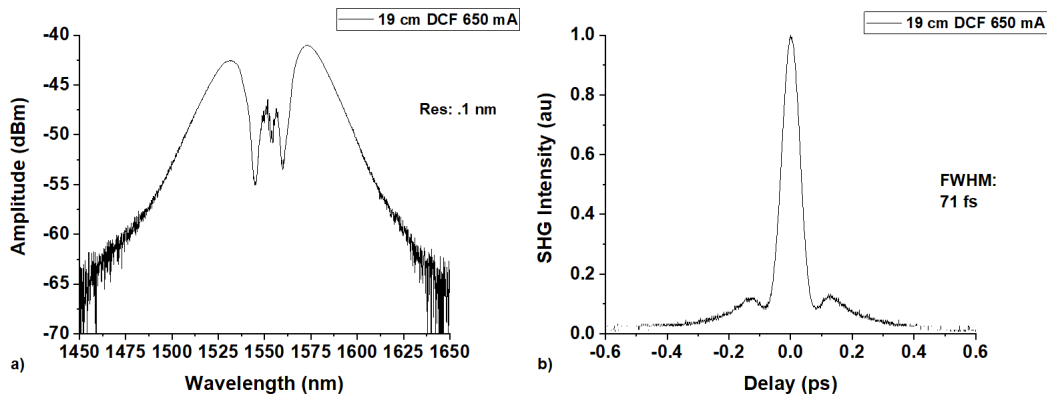


Figure 6.5: Diagnostic traces of amplified 20 MHz fiber laser used for supercontinuum generation experiments: a) intensity autocorrelation after the home-built EDFA, b) optical spectrum after the home-built EDFA

SMF into our SHG intensity autocorrelator (60 cm). Since our optical spectrum analyzer can only measure light from 600-1750 nm, another spectrum analyzer was used to record 1200-2400 nm. The generated continuum for various HNLFs can be seen in Fig. 6.6-6.10. Supercontinuum was measured for various types of HNLF; 10 cm of anomalous dispersion with near zero dispersion slope from OFS (OFS $D=1.25$ ps/nm/km and $S = .0093$ ps/nm²/km), 15 cm of anomalous dispersion HNLF ($D=2.5$ ps/nm/km and $S=.017$ ps/nm/km), 47 cm of anomalous dispersion HNLF ($D=2.5$ and $S=.017$), and 50 cm of polarization maintaining anomalous dispersion (PM-HNLF). From the plots, we observe that the HNLF that produced the best spectral broadening was the PM-HNLF (purchased from Thorlabs, dispersion estimated ~ 5 ps/nm/km and $S = .025$ ps/nm/km²). It is important to note that a low loss splice at the input end of the HNLF is employed to ensure efficient nonlinear spectral broadening. Typically, the mode field diameter (MFD) of a nonlinear fiber is significantly lower than the MFD of single mode fiber such as SMF28. Butt coupling loss from SMF28 to HNLF is on the order of 3.6 dB. This loss can be significantly reduced by building a custom splice recipe. We have built a splice recipe for each of the HNLFs and demonstrated

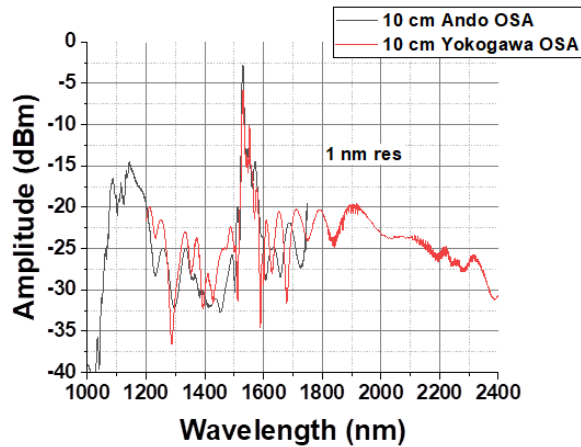


Figure 6.6: Optical spectrum of supercontinuum generation 10 cm of anomalous dispersion HNLF ($D = 1.25 \text{ ps/nm/km}$ and $S = .0093 \text{ ps/nm}^2/\text{km}$)

splice losses of $\leq .5$ dB.

From the optical spectrum, we observe drastically different output spectra. The HNLF that produces the most broadening is the PMHN5 from Thorlabs. Not only is there a good amount of spectra at $1 \mu\text{m}$, there is also a good amount of spectra at $2 \mu\text{m}$ which can be used for SHG. With the PM-HNLF, the two polarization axes exhibit slightly different dispersion characteristics which gives rise to slightly different wavelengths for the dispersive wave. The HNLF with $D = 2.5 \text{ ps/nm/km}$ produces a good amount of spectra around 1040 nm but the $2 \mu\text{m}$ spectra is lacking. For f-2f interferometry, we need lots of power at $2 \mu\text{m}$ so that we can double the frequency to $1 \mu\text{m}$ using SHG. Less power entails less SHG light. With less SHG light, less power would be available for the measurement of a f_0 beat note. This leads to a reduction in the SNR of f_0 beat note or even not being able to measure f_0 .

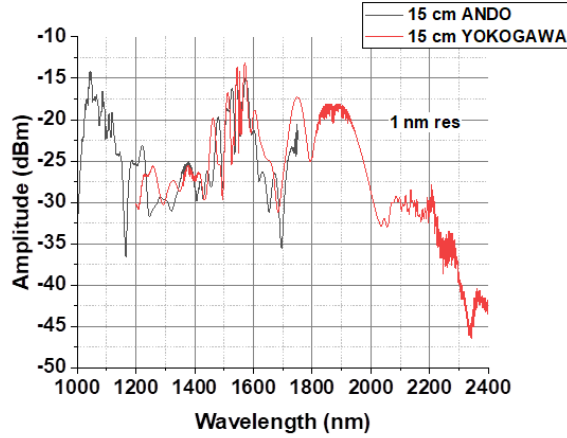


Figure 6.7: Optical spectrum of supercontinuum generation using 15 cm of anomalous dispersion ($D = 2.5 \text{ ps/nm/km}$ and $S = .017 \text{ ps/nm}^2/\text{km}$)

Carrier-Envelope-Offset Frequency Detection

In this section, we cover detection of the carrier-envelope-offset frequency of the 20 MHz fiber MLL. To detect the carrier-envelope-offset frequency, not only is a coherent octave spanning spectrum required, but some form of nonlinear interaction is required in the interferometer. The simplest of which is called the f - $2f$ interferometer [18], where the low frequency end of the spectrum is doubled via SHG so that it can interfere with the high frequency portion of the spectrum. Since SHG is a second order nonlinear effect, a second order nonlinear crystal is required. Typically periodically poled Lithium Niobate (PPLN) is used for SHG because of its high $\chi^{(2)}$ as well as the increased phase matching efficiency due to quasi-phase matching. It is important to note that for an optimum f_{ceo} beat note, one would need to know the spectral features of the supercontinuum before acquiring a PPLN. For a supercontinuum that reaches 775 nm, it would be ideal to order a PPLN that is poled for SHG at 775 nm. Consequently, for a supercontinuum that reaches 1000 nm, it would be ideal to order a PPLN that is poled for SHG at 1000 nm. After selecting a proper

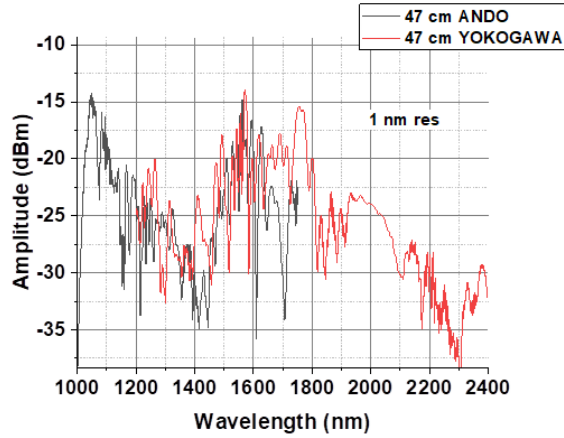


Figure 6.8: Optical spectrum of supercontinuum generation using 47 cm of anomalous dispersion ($D = 2.5 \text{ ps/nm/km}$ and $S = .017 \text{ ps/nm}^2/\text{km}$)

PPLN, the correct optics would need to be selected for the interferometer. In our experiment, a bulk 10 mm PPLN crystal with four separate poled regions for 1018-1125 nm is used for SHG.

There are three common configurations of the f-2f interferometer used to detect f_0 shown in Fig 6.11 [18] which include the non-common path, quasi-common path, and common path f-2f interferometer. In general, the concept of f-2f interferometry is to ensure that the frequency doubled 1 μm light and the supercontinuum 1 μm light spatially, spectrally, temporally, and polarization overlap. Previous work in detecting f_0 has shown that the inline interferometer offers superior noise performance compared to other f-2f interferometer implementations. This difference can be attributed to the non-correlated noise fluctuations between the 1 μm SHG light and the 1 μm supercontinuum light. For supercontinuum generation in fiber, the in-line interferometer is most common because of the availability of fiber. As previously mentioned, the doubled light and the SCG light must overlap spectrally and temporally. Spectral overlap is achieved by generating the correct continuum in which the SHG signal overlaps with the short wavelength section of the continuum. This was achieved by proper selection of HNLF and additional optical bandpass fil-

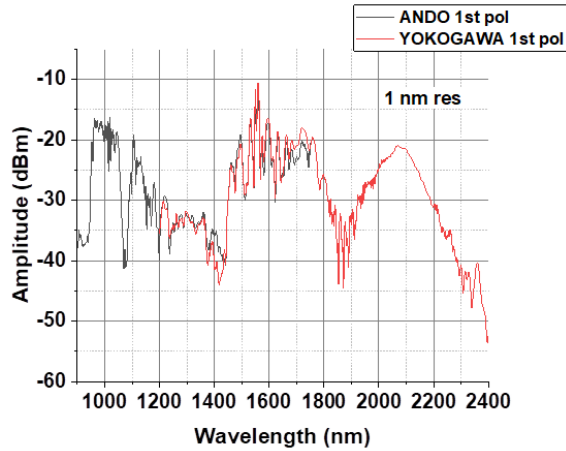


Figure 6.9: Optical spectrum of supercontinuum generation using 50 cm of anomalous dispersion PM-HNLF on one polarization axis

ters placed in the interferometer. For temporal delay, the non-common path interferometer uses a physical delay while the common path interferometer uses fiber. For the in-line interferometer, dispersion is used to delay the color components to overlap the pulses. Characteristics of the materials used must be considered when using the in-line interferometer. Dispersion characteristics computed using the Sellmeier equations of CaF₂, SiO₂, and LiNbO₃ are shown below in Fig. 6.12.

Lithium Niobate has an extremely strong normal dispersion at 1 μm compared to most common materials used which causes the 1 μm light to be significantly delayed compared to the 2 μm light. For the two wavelength regions to temporally overlap, an additional delay for the 2 μm light must be done without separating the colors. This can be done using fused silica or SMF28 spliced on to the end of a HNLF or by physically delaying it using a delay arm. The amount of SMF28 required to ensure perfect temporal overlap depends on the length of HNLF, dispersion properties of the HNLF, and the chirp properties of the SCG light. In our experiment, we employed the non-common path interferometer to ensure that the pulses overlap in time, space, frequency, and polarization. From the previous section, we have already determined the length of PM-HNLF re-

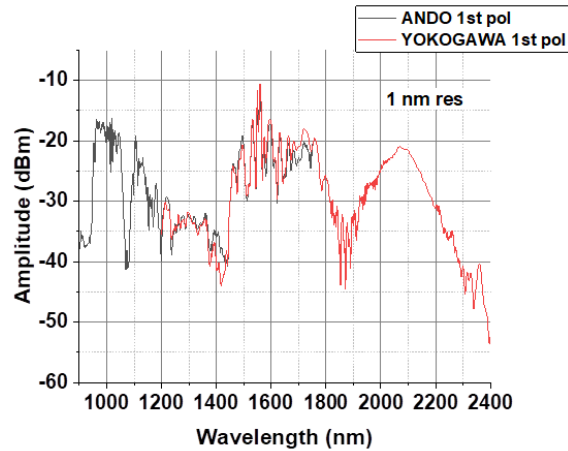


Figure 6.10: Optical spectrum of supercontinuum generation using 50 cm of anomalous dispersion PM-HNLF on a second polarization axis

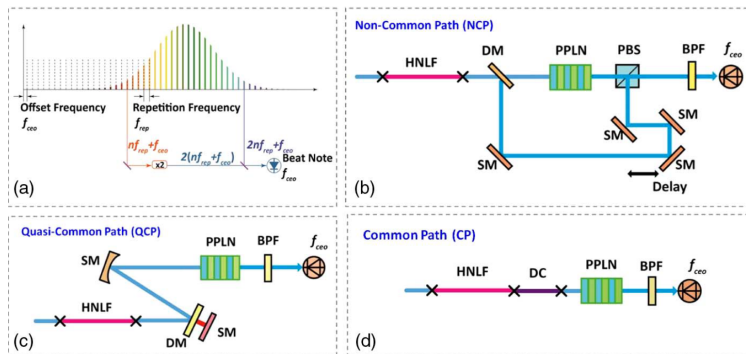


Figure 6.11: a) Conceptual diagram of f-2f interferometry, b) non-common path f-2f interferometer schematic, c) quasi-common path f-2f interferometer schematic, d) common path (in line) f-2f interferometer schematic.

quired to generate sufficient power at 1 and 2 μm . We then connectorized the HNLF and polished the facet till it was flat to ensure that the outgoing light would have no chromatic angular dependence. Future iterations could use an APC connectorized HNLF for simplicity. A schematic of the f-2f interferometer is shown below in Fig. 6.13.

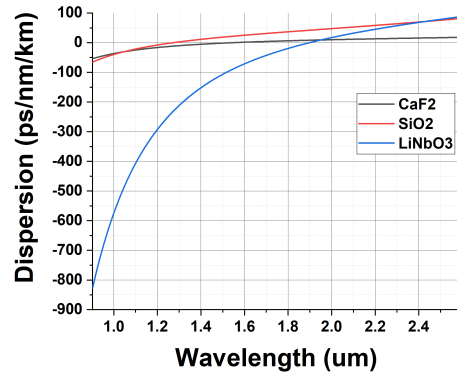


Figure 6.12: Calculated dispersion parameter for common materials used for f-2f interferometry

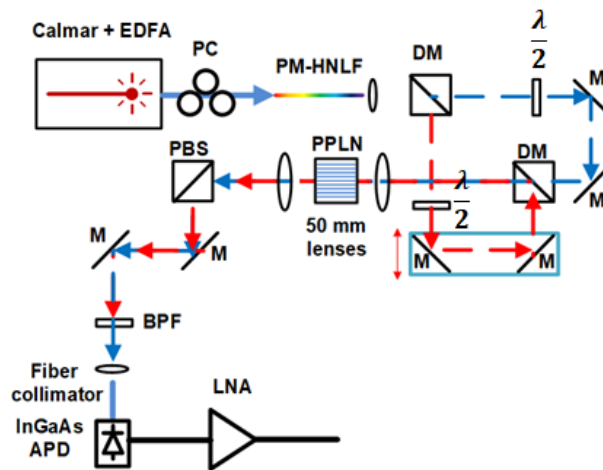


Figure 6.13: Experimental implementation of non-common path f-2f interferometer. PC: fiber polarization controller, PM-HNLF: 0.5 m of Thorlabs PMHN5, DM: dichroic mirror, $\frac{\lambda}{2}$: half waveplate, M: metallic mirror, $\frac{\lambda}{2}$: half waveplate, PPLN: periodically poled Lithium Niobate, PBS: polarizing beam splitter, BPF: 1030 nm optical bandpass filter, LNA: Wenzel low noise amplifier.

The non-common path interferometer in Fig. 6.13 uses dichroic mirrors to split and recombine the 1 μm and 2 μm such that temporal overlap is achieved using the tunable delay stage. By aligning the polarization of the input pulse along one of the principle polarization axes of the PM-HNLF, it is possible to ensure no coupling between the orthogonal polarization modes. The half waveplate

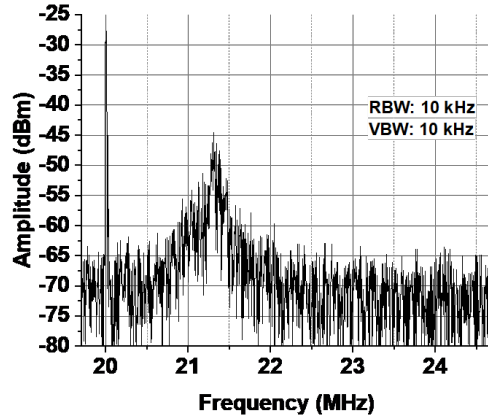


Figure 6.14: Carrier-envelope-offset frequency detection using commercial FMLL

at $2 \mu\text{m}$ is used to ensure efficient SHG through phase-matching while the $1 \mu\text{m}$ waveplate is used to match the polarization of the SHG light, this enables the f and $2f$ light to match in polarization. The PPLN is inside a small temperature-controlled oven, allowing for temperature tuning of the poling period. The confocal approximation was used to calculate the needed focal length of lenses to ensure maximum SHG efficiency. This is done by having $L_c = 2z_R$, where L_c is the length of the crystal and Z_R is the Rayleigh range. For our experiment, a $f=3.1 \text{ mm}$ aspheric lens used to collimate the supercontinuum from a $\sim 4 \mu\text{m}$ mode field diameter fiber would need 50 mm lenses for focusing into the PPLN. We selected CaF_2 lenses due to the low loss at $2 \mu\text{m}$ for focusing into the PPLN. A PBS is used to further enforce the electric field orientation ensuring alignment of the electric field of both f and $2f$ spectra. A bandpass filter centered at 1030 nm is rotated to ensure only the f and $2f$ light interferes: ensuring spectral overlap. Finally, the light is focused on an InGaAsP APD. The APD was placed on a three-axis stage to measure the interference. The beat note was then amplified by a Wenzel low noise RF amplifier. The resulting f_0 beat note for the 20 MHz fiber MLL is shown in Fig. 6.14.

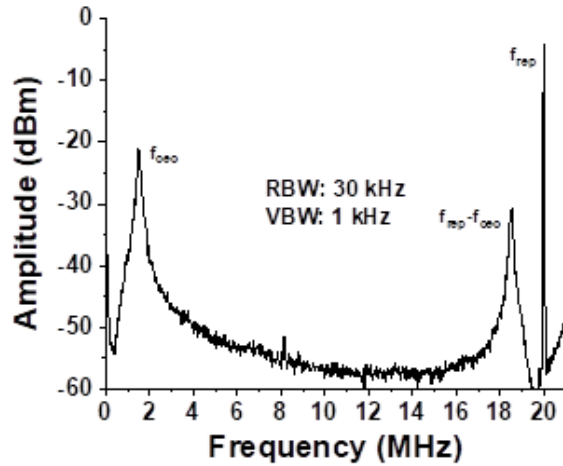


Figure 6.15: Improved f_0 beat note for commercial fiber mode-locked laser.

Fig. 6.14 shows the measured f_0 beat note using our interferometer. The first iteration of our interferometer used an aspheric lens to couple the light into HI1060 fiber for spatial overlap of the f and $2f$ components. The output of the fiber was then connected to a fiber connector on the input of the APD. For this measurement of f_{ceo} , we were able to couple $\sim 17 \mu\text{W}$ of SHG power and $\sim 7 \mu\text{W}$ of $1 \mu\text{m}$ power into the HI1060 fiber. We observed an SNR of ~ 20 dB at a resolution bandwidth (RBW) and video bandwidth (VBW) of 10 kHz. Decreasing the RBW did not increase the SNR of the f_0 beat note, indicating that the beat note has a broad spectral distribution. This indicates that the linewidth of the f_0 beatnote is larger than the resolution bandwidth of 10 kHz. We replaced the fiber collimator with an 8 mm focal length aspheric lens focusing onto the APD and observed a much larger SNR. We measured $\sim 150 \mu\text{W}$ of power at 1030 nm and in the SHG light. The improved beat note can be seen in Fig. 6.15.

Nonlinear waveguides for coherent octave spanning supercontinuum generation

Nonlinear waveguides have attracted significant attention for generating coherent octave spanning supercontinuum generation. Owing to the significantly smaller waveguide dimensions, the nonlinear coefficient (consequently the supercontinuum threshold) is significantly higher. In addition to the high nonlinear coefficient, the dispersion profile is also controllable by adjusting the waveguide dimensions [82]. The benefit to generating supercontinuum in a waveguide compared to fiber consist of the following: reduced pulse energies required (~ 200 pJ as opposed to \sim nJ), significantly smaller footprint, and broader spectral coverage. Historically, waveguide coupling was extremely loss due to the severe mode mismatch between SMF28 (MFD= $10 \mu m$) and waveguide modes ($< \mu m$). Advancements in waveguide coupling by use of small core fibers [83], tapered fibers [84], and inverse tapered waveguides have brought coupling losses into waveguides to ~ 1 dB. Waveguide losses were another issue that have been improved upon by improvement in fabrication. These improvements have enabled commercialization of waveguide-based supercontinuum devices. To simplify the pulse requirements for producing a coherent octave through supercontinuum generation, we have purchased a comb offset stabilization module (COSMO) from octave photonics. The COSMO uses dispersion engineered Tantalum waveguides for supercontinuum generation [80], PPLN for SHG, and a photodetector with integrated transimpedance amplifier. The COSMO uses a 0.5 m PM1550 fiber pigtail as the input which matches our patch cord length into the autocorrelator. The waveguides are engineered so that the dispersive wave from the supercontinuum spectrally ends up at 775 nm ($\frac{1550}{2} = 775$ nm). Significant pulse energy at 1550 nm remains even after supercontinuum which lends itself to high power SHG at 775 nm. The usage of a dispersion engineered waveguide for f-2f interferometry at 775 nm was also done in [14]. In contrast with our work in measuring f_0 using fiber for supercontinuum, the COSMO requires only pulses shorter than 200 fs with pulse energies of 200 pJ. We have also measured the f_0 beat note of the 20 MHz FMLL using the COSMO. Fig. 6.16a shows the schematic for measuring f_0 of the 20 MHz FMLL using the

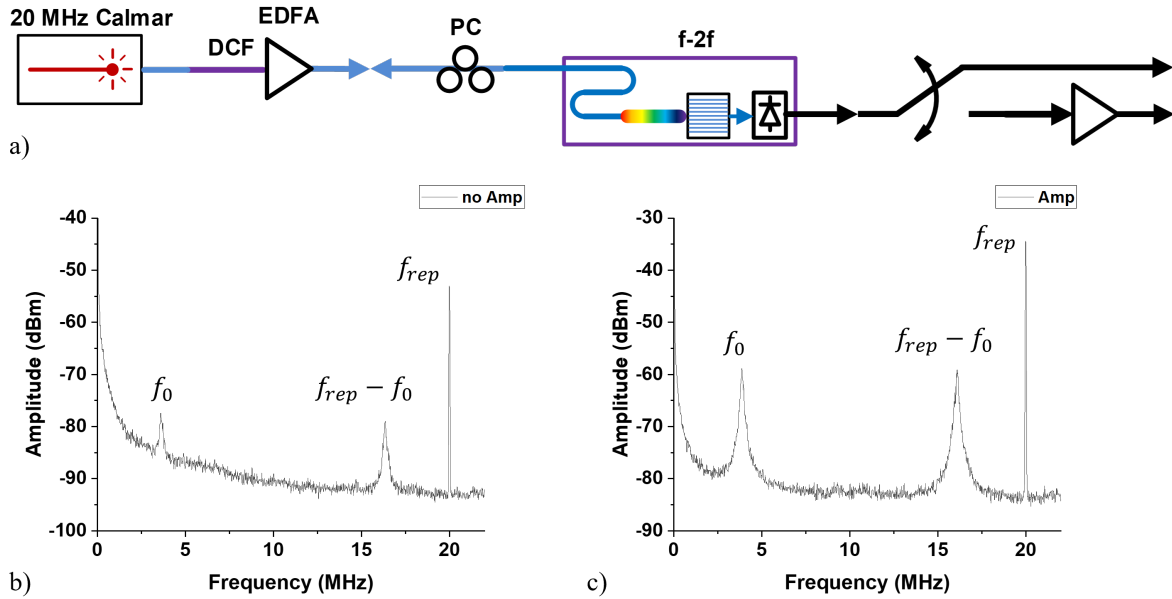


Figure 6.16: a) Schematic for measuring the carrier-envelope-offset frequency of a 20 MHz repetition rate fiber mode-locked laser using the COSMO, b) Measured carrier-envelope-offset frequency without post amplification, c) Measured carrier-envelope-offset frequency with low noise Wenzel RF amplifier.

COSMO. The FMLL is amplified up to a few mW and the pulses are sent into the COSMO. The measured f_0 beat note without the Wenzel RF amplifier is shown in Fig. 6.16b while f_0 measured with the Wenzel RF amplifier is shown in Fig. 6.16c.

In this chapter, we discussed coherent octave spanning supercontinuum generation. We started the discussion with supercontinuum generation in fiber and showed simulations for various commercially available HNLFs. We then showed experimental data using various HNLFs pumped by an amplified 20 MHz repetition rate FMLL which helped us in selecting a HNLF. An f-2f interferometer was constructed to measure f_0 of the FMLL using the proper HNLF. Finally, we discussed waveguide-based supercontinuum generation and measured f_0 using a commercially available waveguide-based f-2f interferometer. In doing this, we have experimentally obtained the

pulse parameters needed to measure f_0 using our OEO EOM comb system. The next chapter will discuss the measurement of f_0 for our OEO EOM comb system.

CHAPTER 7: CARRIER ENVELOPE OFFSET FREQUENCY

EXPERIMENTS

As previously mentioned, a fully stabilized optical frequency comb requires knowledge and control over both f_0 and f_{rep} . If $f_{rep} < 100$ GHz, then a high-speed photodetector & high bandwidth RFSA can easily measure f_{rep} . To measure f_0 , a coherent octave of bandwidth is required. Since most gain media do not support octave spanning spectra, coherent supercontinuum generation is employed. In the preceding chapters, we have designed, characterized, and constructed a 10.5 GHz repetition rate oscillator. Since the oscillator's output pulse characteristics were unsuitable for coherent octave spanning supercontinuum generation, we demonstrated an alternative method to conditioning the pulses to meet the necessary requirements. We came up with two different systems for producing ultrashort pulses using two different pulse-pick rates and a tunable etalon. We have also experimentally characterized different highly nonlinear fibers for octave spanning supercontinuum generation and determined the optimal fiber parameters. Finally, we have also characterized the use of nonlinear waveguides (COSMO) to measure f_0 . In this chapter, we show how different system architectures affect the ability to measure an f_0 beat note.

Pulse-picking By 64 Experiments

In the previous chapters, we constructed a system that produces ultrashort pulses with 1.5 nJ pulse energies using an EOM comb, a pulse-picker, a 50/50 NALM, and an EDFA. The pulse-picker was used to downsample the repetition rate by a factor of 64, thereby reducing the power requirements on the EDFA to ~ 250 mW. This is shown in Fig. 5.10. We now seek to measure f_0 of the EOM comb.

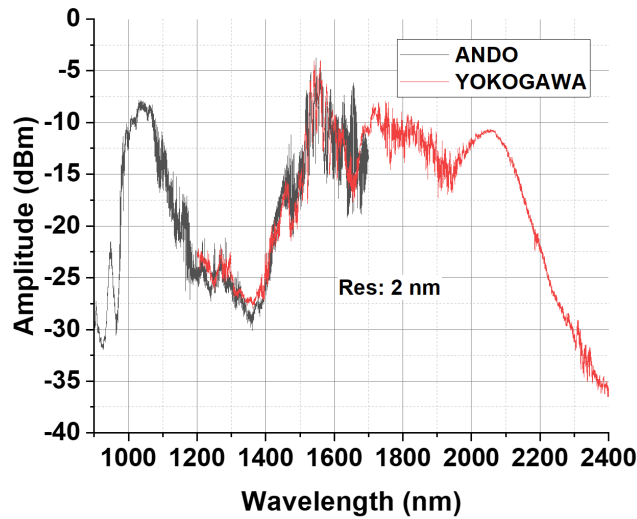


Figure 7.1: Optical spectrum of supercontinuum generated using 50 cm of PMHN5 seeded by the EOM comb downsampled by 64 and then amplified to 1.5 nJ.

Fig. 7.1 shows the optical spectrum of the supercontinuum generated by 50 cm of PMHN5 and seeded by Fig. 5.10. We again observe spectral peaks at 1 & 2 μm that are used for the f-2f interferometer. We measured $\sim 250 \mu\text{W}$ power in both the fundamental and SHG components as well. Despite all of this work, we did not measure an f_0 beat note. However, we observed that when the interferometer was aligned, the noise floor would drastically increase. When the interferometer was misaligned, the noise floor would drop again. This effect was also mentioned in [35] when trying to measure f_0 . This effect was initially attributed to seeded supercontinuum with pulses that were longer than 100 fs. However, our pulses are much shorter than 100 fs. This leads us to believe that the coherence of the comb itself has degraded somewhere.

To gain additional insight into our problem, we performed several heterodyne beat measurements in various parts of the system. We used a 100 Hz linewidth CW laser centered at 1546 nm as our local oscillator for the heterodyne beat notes. Since our EOM comb system uses a 7 Hz linewidth

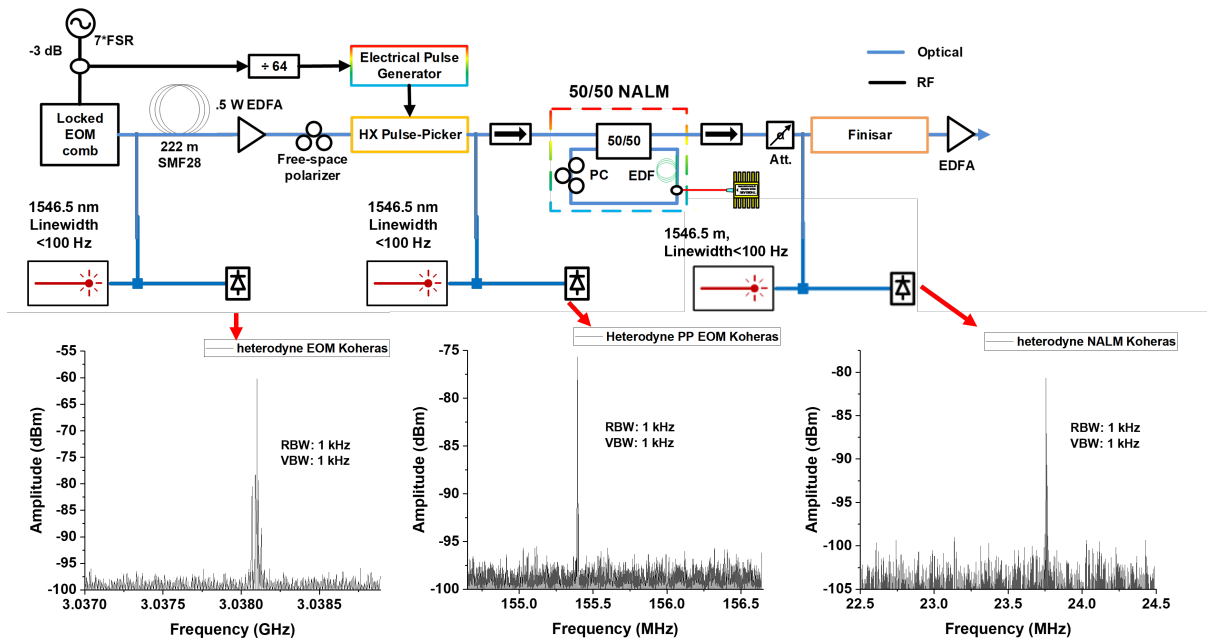


Figure 7.2: Top: Schematic for measuring heterodyne beat notes in each part of our locked EOM comb system. Bottom: Measured heterodyne beat notes after the 100k finesse etalon, pulse-picker, and NALM using a <100 Hz linewidth laser.

CW laser, we are unable to obtain linewidth information in the heterodyne beat notes, but we can still measure SNR of the comb lines.

Fig. 7.2 shows four heterodyne beat measurements that were taken using the 100 Hz linewidth CW laser centered at 1546 nm. We observe the SNR of the heterodyne beat note significantly decreases after each stage. Most notably, the SNR decreases by over 20 dB after pulse-picking! Why is there such a massive decrease in SNR after pulse-picking? When pulse-picking, we observe a decrease in power by two factors: 1) the insertion loss and 2) the pulse-picking rate. Our pulse-picker has an insertion loss of 4.2 dB and we pulse-picked by a factor of 64, which is an additional 18 dB of loss. This gives us a total loss of 22.2 dB after pulse-picking. In addition, the 50/50 NALM that was used to shorten our pulse and improve pulse-picker extinction seems to have reduced the

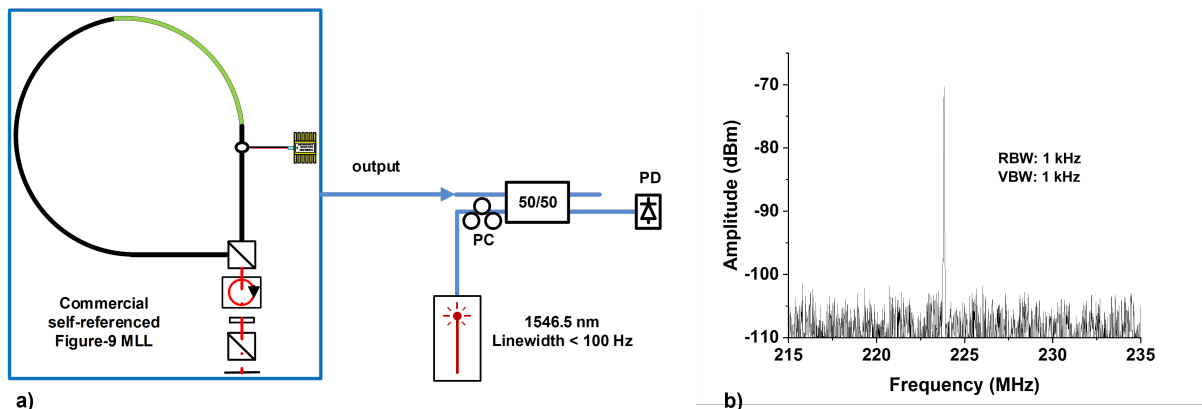


Figure 7.3: Heterodyne beat measurement with Menlo fiber mode-locked laser and CW laser.

SNR of our comb even further. It is also important to note that losses can only reduce the SNR of a combline. The only way to increase the SNR of a combline would be to amplify and filter it.

We also performed a heterodyne beat measurement with the same CW laser and a Menlo systems fiber mode-locked laser. This is shown in Fig. 7.3. The Menlo fiber mode-locked laser has a repetition rate of ~ 250 MHz. The repetition rate of our pulse-picked EOM comb and the Menlo laser is close, this means that a heterodyne beat measurement with the commercial fiber mode-locked laser should be on the same order of magnitude in terms of SNR.

We observe in Fig. 7.3 & 7.2 that not only is the SNR of the heterodyne beat measurement of the EOM comb low, it's also far worse than the commercial fiber mode-locked laser! This leads us to believe that pulse-picking and the NALM is the cause of our incoherent continuum. With this in mind, how would it be possible to measure f_0 with an EOM comb? We observed that the degradation in SNR was a result of heavy losses from the pulse-picker and the NALM. If we reduce the pulse-pick factor and removed the NALM, we may see something else. As such, we attempt this experiment again using a lower pulse-pick rate.

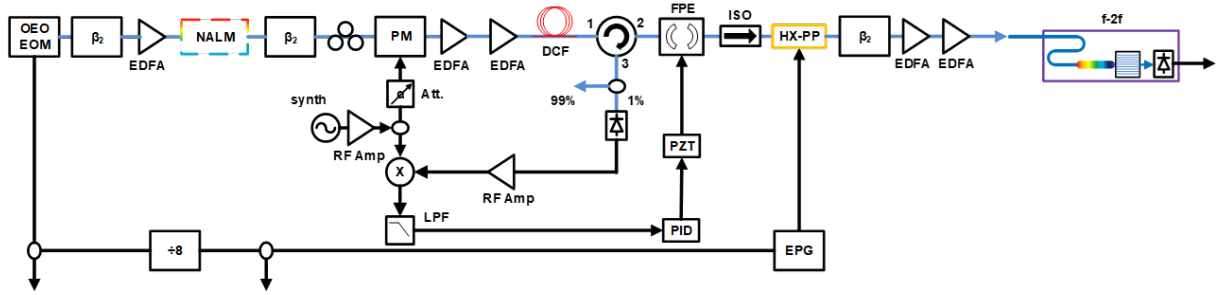


Figure 7.4: Experimental schematic of measuring f_0 using our OEO EOM comb using the COSMO. β_2 : linear chirp applied by waveshaper, EDFA: erbium doped fiber amplifier, NALM: nonlinear amplifying loop mirror, PM: phase modulator, DCF: 0.7 m dispersion compensating fiber, FPE: tunable ~ 600 finesse Fabry-Perot etalon, ISO: fiberized isolator, f-2f: COSMO, PZT: high voltage piezo driver, RF Amp: RF amplifier, LPF: low pass filter, PID: proportional-integral-derivative controller, EPG: electrical pulse generator.

Pulse-picking by 8 Experiments

From the previous section, we were unsuccessful in measuring f_0 with an EOM comb when we pulse-picked by a factor of 64. We attribute the failure to the following issues: insufficiently short pulse-pick gate, too much ASE noise as a result of repeated amplification, and pulse-picking too aggressively. By reducing the pulse-pick rate from 64 to 8, we reduced our pulse-picking losses from 18 dB to 9 dB. Even if pulse-pick factor alone is not an issue, the loss incurred by pulse-picking is still an issue. If the pulse-pick rate is too high, then there wouldn't be enough optical power to saturate the final amplifier. We also used nonlinear waveguides for supercontinuum generation as opposed to nonlinear fiber. This allowed us to reduce the needed average power by a factor of 5. In addition, we constructed a tunable etalon to filter the noise in between combines right before pulse-picking. The usage of the tunable etalon also reduces the amount of ASE that we incurred through repeated steps of amplification. The experimental schematic of this is shown in Fig. 7.4 along with associated data in Fig. 5.13 prior to measuring f_0 .

The system in fig. 7.4 is the same schematic found in Fig. 5.12 for generating ultrashort pulses. The output of this system is then fed into the COSMO for measuring f_0 . Unlike the pulse-pick by 64 case where we used fiber for supercontinuum generation, the nonlinear waveguides we purchased are prepackaged with a PPLN (for SHG), and an APD (for f_0 detection). Unfortunately, there is no optical output that allows us to measure the generated continuum. However, we demonstrate in Fig. 7.5 the detection of the carrier-envelope-offset frequency of our OEO EOM comb. We note that we were only able to measure the beat note when we used two optical amplifiers after pulse-picking as opposed to one. This indicates to us that the coherency of the beat note is extremely sensitive to ASE and that a low noise EDFA designed for pulsed amplification is required. It is also important to note that the polarization of the output pulses must be perfectly matched to measure a beat note. In our experiment, we used a short fiber length polarization controller in between the output of the EDFA and the input to the nonlinear waveguide. We also measured the intensity autocorrelation after the fiber polarization controller to ensure we correctly measured the pulses entering the nonlinear waveguide. Finally, it is important to note that the measured f_0 beat note fluctuated in amplitude. This is caused by the unstable polarization output after the NALM and EDFA prior to pulse-picking.

Fig. 7.5 shows the measured f_0 data before and after the Miteq RF amplifier. Unfortunately, we could not locate the Wenzel amplifier used in Fig. 6.16 to increase the SNR of the f_0 beat note.

In this chapter, we attempted to measure f_0 using two different EOM comb systems. In the first system, we used an external RF synthesizer to drive the EOM comb, pulse-picked by 64, amplified the pulse-picked pulse train with a NALM, amplified the pulses again, and then sent the amplified pulses into our home-built f-2f interferometer using HNLF. We could not measure an f_0 beat note with this first system. Our second system addressed several issues in the first system such as externally filtering the pulse train and reducing the number of amplifiers after the optical filter. With these changes, we successfully measured an f_0 beat note of the OEO EOM comb system.

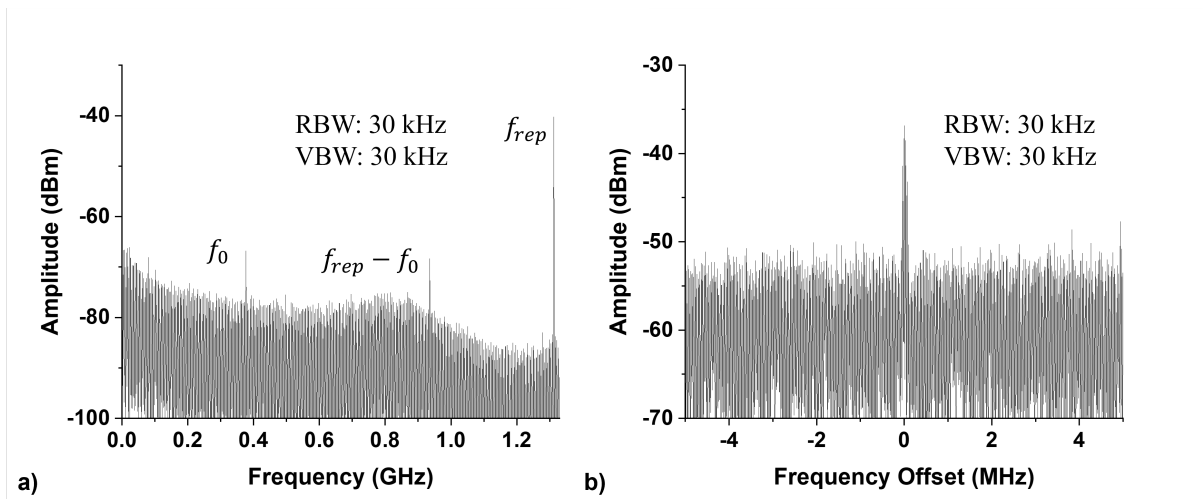


Figure 7.5: Measured carrier-envelope-offset beat note using OEO EOM comb. a) Without Miteq RF amplifier, b) with Miteq RF amplifier.

CHAPTER 8: CONCLUSION

In this thesis, we have presented significant advancements in high repetition rate (>10 GHz) self-referenced optical frequency combs in the telecommunications band. Due to the limitations imposed by cavity size and available gain media, passively mode-locked laser based high repetition rate comb sources are sparse. This has necessitated the use of an external low noise RF source for electro-optic modulation in generating high repetition rate comb sources. In addition, coherent octave spanning supercontinuum generation is challenging for high repetition rate sources. An opto-electronic oscillator driven electro-optic modulated comb was constructed using a 100k finesse Fabry-Perot etalon. The etalon was used as the high Q element in an opto-electronic oscillator for stabilizing the CW laser and generating a spectrally pure 10 GHz RF signal. The 10 GHz signal was then used to drive a cascade of electro-optic phase modulators generating an electro-optic modulated comb. The comb bandwidth spans 10 nm centered at 1550 nm and generates pulses that are compressible to 840 fs. Using the etalon for the opto-electronic oscillator eliminates the need for a costly external low noise RF source. The resulting pulses generated from our comb has significant excess chirp. By using a nonlinear amplifying loop mirror, the low contrast 840 fs pulses are reshaped into pedestal free 300 fs pulses. An external tunable etalon was also constructed for filtering noise in between comb lines. We also constructed erbium doped fiber amplifiers for nonlinear spectral broadening. The combination of our home-built nonlinear amplifying loop mirror and optical amplifiers eliminated the need for expensive and lossy grating-based pulse shapers. Finally, we measured the carrier-envelope-offset frequency of our high repetition rate comb source. The usage of nonlinear waveguides reduced the pulse requirements for generating a coherent octave through supercontinuum generation. By addressing the difficulties in generating a high repetition rate comb source with high pulse contrast and sufficient pulse energy, we have demonstrated the first self-referenced opto-electronic oscillator driven electro-optic modulated op-

tical frequency comb. Moreover, our improvements are capable of scaling into higher repetition rates and provide a path towards integration.

Future work

We have demonstrated a self-referenced high repetition rate comb source in the telecommunications band. Several improvements to the current architecture can still be made to simplify or improve the system. Photonically filtered opto-electronic oscillators are still largely unexplored and the phase noise performance still lags the theoretical phase noise estimations. Improving the phase noise of the opto-electronic oscillator would result in a lower phase noise RF signal for various applications and improve the SNR of the f_0 beat note. In our fiber-based pulse compressor, we used non-polarization maintaining fibers due to availability. Future experiments can envision using polarization maintaining highly nonlinear fibers and polarization maintaining erbium doped fibers to eliminate polarization fluctuations (increasing long term stability for measuring f_0). The improved polarization stability would also allow the system to operate in a wider range of environments outside of the laboratory. Although we used a nonlinear amplifying loop mirror to shorten the pulse and improve the contrast, it is possible to generate an electro-optic modulated comb with lower pedestal energy. This can be achieved by adding additional intensity modulators, driving the intensity modulator with a shorter pulse, or employing a time lens approach and stretching phase modulation using dispersion compensating fiber. By reducing the pedestal energy in an EOM comb, pulse shaping may not be required. Instead, the pulse can be directly amplified to nanojoule levels and be spectrally broadened inside the amplifier with highly linear chirp. We have demonstrated the feasibility of spectral broadening inside an optical amplifier for producing ultra-short pulses. Additionally, we used a tunable low finesse etalon for externally filtering the noise in between comb lines. A higher finesse cavity would improve the SNR of the detected f_0 beat note.

Although briefly discussed, the filtered opto-electronic oscillator driven electro-optic modulated comb source still merits further investigation. Combining the improvements could conceivably enhance the performance of the system while reducing the complexity.

LIST OF REFERENCES

- [1] Peter J. Delfyett, Sangyoun Gee, Myoung Taek Choi, Hossein Izadpanah, Wangkuen Lee, Sarper Ozharar, Franklyn Quinlan, and Tolga Yilmaz. Optical frequency combs from semiconductor lasers and applications in ultrawideband signal processing and communications. *Journal of Lightwave Technology*, 24:2701–2719, 7 2006.
- [2] S. A. Diddams, J. C. Bergquist, S. R. Jefferts, and C. W. Oates. Standards of time and frequency at the outset of the 21st century. *Science*, 306:1318–1324, 2004.
- [3] L. Hollberg, S. Diddams, A. Bartels, T. Fortier, and K. Kim. The measurement of optical frequencies. *Metrologia*, 42:105–124, 2005.
- [4] M. T. Murphy, Th Udem, R. Holzwarth, A. Sismann, L. Pasquini, C. Araujo-Hauck, H. Dekker, S. D’Odorico, M. Fischer, T. W. Hänsch, and A. Manescau. High-precision wavelength calibration of astronomical spectrographs with laser frequency combs. *Monthly Notices of the Royal Astronomical Society*, 380:839–847, 2007.
- [5] Andrew J. Metcalf, Tyler Anderson, Chad F. Bender, Scott Blakeslee, Wesley Brand, David R. Carlson, William D. Cochran, Scott A. Diddams, Michael Endl, Connor Fredrick, Sam Halverson, Daniel D. Hickstein, Fred Hearty, Jeff Jennings, Shubham Kanodia, Kyle F. Kaplan, Eric Levi, Emily Lubar, Suvrath Mahadevan, Andrew Monson, Joe P. Ninan, Colin Nitroy, Steve Osterman, Scott B. Papp, Franklyn Quinlan, Larry Ramsey, Paul Robertson, Arpita Roy, Christian Schwab, Steinn Sigurdsson, Kartik Srinivasan, Gudmundur Stefansson, David A. Sterner, Ryan Terrien, Alex Wolszczan, Jason T. Wright, and Gabriel Ycas. Stellar spectroscopy in the near-infrared with a laser frequency comb. *Optica*, 6:233, 2019.
- [6] F Quinlan, TM Fortier, MS Kirchner, JA Taylor, JC Bergquist, T Rosenband, N Lemke, A Ludlow, Y Jiang, CW Oates, et al. Optical frequency combs for low phase noise microwave

- generation. In *2011 XXXth URSI General Assembly and Scientific Symposium*, pages 1–3. IEEE, 2011.
- [7] Mohammad Umar Piracha, Dat Nguyen, Dimitrios Mandridis, Tolga Yilmaz, Ibrahim Ozdur, Sarper Ozharar, and Peter J Delfyett. Range resolved lidar for long distance ranging with sub-millimeter resolution. *Optics Express*, 18:7184, 2010.
- [8] Scott A Diddams. The evolving optical frequency comb invited. *J. Opt. Soc. Am. B*, 27:B51–B62, 11 2010.
- [9] Steven T. Cundiff. Phase stabilization of ultrashort optical pulses. *Journal of Physics D: Applied Physics*, 35, 2002.
- [10] Sebastian Koke, Christian Grebing, Harald Frei, Alexandria Anderson, Andreas Assion, and Günter Steinmeyer. Direct frequency comb synthesis with arbitrary offset and shot-noise-limited phase noise. *Nature Photonics*, 4:462–465, 2010.
- [11] Atsushi Ishizawa, Tadashi Nishikawa, Akira Mizutori, Hidehiko Takara, Hidetoshi Nakano, Tetsuomi Sogawa, Atsushi Takada, and Masafumi Koga. Generation of 120-fs laser pulses at 1-ghz repetition rate derived from continuous wave laser diode. *Optics Express*, 19:22402, 2011.
- [12] Dae Sik Kim, Masato Arisawa, Akihiro Morimoto, and Tetsuro Kobayashi. Femtosecond optical pulse generation using quasivelocitly-matched electrooptic phase modulator. *IEEE Journal on Selected Topics in Quantum Electronics*, 2:493–499, 1996.
- [13] Andrew J. Metcalf, Victor Torres-Company, Daniel E. Leaird, and Andrew M. Weiner. High-power broadly tunable electrooptic frequency comb generator. *IEEE Journal on Selected Topics in Quantum Electronics*, 19, 2013.

- [14] David R. Carlson, Daniel D. Hickstein, Wei Zhang, Andrew J. Metcalf, Franklyn Quinlan, Scott A. Diddams, and Scott B. Papp. Ultrafast electro-optic light with subcycle control. *Science*, 361:1358–1363, 2018.
- [15] Michael E. Plascak, Ricardo Bustos Ramirez, Kristina Bagnell, and Peter J. Delfyett. Tunable broadband electro-optic comb generation using an optically filtered optoelectronic oscillator. *IEEE Photonics Technology Letters*, 30:335–338, 2 2018.
- [16] Atsushi Ishizawa, Tadashi Nishikawa, Akira Mizutori, Hidehiko Takara, Atsushi Takada, Tetsuomi Sogawa, and Masafumi Koga. Phase-noise characteristics of a 25-ghz-spaced optical frequency comb based on a phase- and intensity-modulated laser. *Optics Express*, 21:29186, 2013.
- [17] Katja Beha, Daniel C. Cole, Pascal Del’Haye, Aurélien Coillet, Scott A. Diddams, and Scott B. Papp. Electronic synthesis of light. *Optica*, 4:406, 4 2017.
- [18] Jungwon Kim and Youjian Song. Ultralow-noise mode-locked fiber lasers and frequency combs: principles, status, and applications. *Advances in Optics and Photonics*, 8:465, 2016.
- [19] Brian R. Washburn, Scott A. Diddams, Nathan R. Newbury, Jeffrey W. Nicholson, Man F. Yan, and Carsten G. Jørgensen. Phase-locked, erbium-fiber-laser-based frequency comb in the near infrared. *Optics Letters*, 29:250, 2004.
- [20] Yoshiaki Nakajima, Yuya Hata, and Kaoru Minoshima. All-polarization-maintaining er-fiber-based dual optical frequency combs with nonlinear amplifying loop mirror. *2018 Conference on Lasers and Electro-Optics Pacific Rim, CLEO-PR 2018*, 24:8160–8167, 2018.
- [21] Ivan Hernandez-Romano, Dimitrios Mandridis, Daniel A. May-Arrijoja, Jose J. Sanchez-Mondragon, and Peter J. Delfyett. Mode-locked fiber laser using an su8/swcnt saturable absorber. *Optics Letters*, 36:2122, 2011.

- [22] David Chao et al. *Self-referenced 1.5 [mu] m fiber frequency combs at GHz repetition rates*. PhD thesis, Massachusetts Institute of Technology, 2012.
- [23] A. Cingöz, D. C. Yost, T. K. Allison, A. Ruehl, M. E. Fermann, I. Hartl, and J. Ye. Broadband phase noise suppression in a yb-fiber frequency comb. *Optics Letters*, 36:743, 2011.
- [24] Peng Qin, Youjian Song, Hyoji Kim, Junho Shin, Dohyeon Kwon, Minglie Hu, Chingyue Wang, and Jungwon Kim. Reduction of timing jitter and intensity noise in normal-dispersion passively mode-locked fiber lasers by narrow band-pass filtering. *Optics Express*, 22:28276, 2014.
- [25] Chan Gi Jeon, Shuangyou Zhang, Junho Shin, and Jungwon Kim. Highly tunable repetition-rate multiplication of mode-locked lasers using all-fibre harmonic injection locking. *Scientific Reports*, 8:1–9, 2018.
- [26] N. Onodera. Supermode beat suppression in harmonically mode-locked erbium-doped fibre ring lasers with composite cavity structure. *Electronics Letters*, 33:962–963, 1997.
- [27] Kun Xu, Ruixin Wang, Yitang Dai, Feifei Yin, Jianqiang Li, Yuefeng Ji, and Jintong Lin. Supermode noise suppression in an actively mode-locked fiber laser with pulse intensity feed-forward and a dual-drive mzm. *Laser Physics Letters*, 10, 2013.
- [28] Peter J. Delfyett, Leigh Thirion Florez, N. Stoffel, T. Gmitter, Nicholas C. Andreadakis, Yaron Silberberg, Jonathan P. Heritage, and Gerard A. Alphonse. High-power ultrafast laser diodes. *IEEE Journal of Quantum Electronics*, 28:2203–2219, 1992.
- [29] Bojan Resan and Peter J. Delfyett. Dispersion-managed breathing-mode semiconductor mode-locked ring laser: Experimental characterization and numerical simulations. *IEEE Journal of Quantum Electronics*, 40:214–221, 2004.

- [30] Kyungbum Kim, Shinwook Lee, and Peter J. Delfyett. 1.4kw high peak power generation from an all semiconductor mode-locked master oscillator power amplifier system based on extreme chirped pulse amplification(x-cpa). *Optics Express*, 13:4600, 2005.
- [31] Kristina Bagnell, Anthony Klee, Peter J. Delfyett, Jason J. Plant, and Paul W. Juodawlkis. Demonstration of a highly stable 10 ghz optical frequency comb with low timing jitter from a scowa-based harmonically mode-locked nested cavity laser. *Optics Letters*, 43:2396, 2018.
- [32] P. J. Delfyett, A. Dienes, J. P. Heritage, M. Y. Hong, and Y. H. Chang. Femtosecond hybrid mode-locked semiconductor laser and amplifier dynamics. *Applied Physics B Laser and Optics*, 58:183–195, 1994.
- [33] Dominik Waldburger, Sandro M. Link, Mario Mangold, Cesare G. E. Alfieri, Emilio Gini, Matthias Golling, Bauke W. Tilma, and Ursula Keller. High-power 100 fs semiconductor disk lasers. *Optica*, 3:844, 2016.
- [34] Franklyn Quinlan, Charles Williams, Sarper Ozharar, Sangyoun Gee, and Peter J Delfyett. Self-stabilization of the optical frequencies and the pulse repetition rate in a coupled opto-electronic oscillator. *Journal of lightwave technology*, 26(15):2571–2577, 2008.
- [35] Mehmetcan Akbulut, Josue Davila-Rodriguez, Ibrahim Ozdur, Franklyn Quinlan, Sarper Ozharar, Nazanin Hoghooghi, and PJ Delfyett. Measurement of carrier envelope offset frequency for a 10 ghz etalon-stabilized semiconductor optical frequency comb. *Optics express*, 19(18):16851–16865, 2011.
- [36] Edris Sarailou, Abhijeet Ardey, and Peter J Delfyett. Low noise ultrashort pulse generation by direct rf modulation at 22 ghz from an algainas multiple quantum-well laser at $1.55 \mu\{m\}$. *IEEE Photonics Technology Letters*, 24:1561–1563, 2012.

- [37] Nayara Jornod, Kutun Guřrel, Valentin J. Wittwer, Pierre Brochard, Sargis Hakobyan, Ste´phane Schilt, Dominik Waldburger, Ursula Keller, and Thomas Suřdmeyer. Carrier-envelope offset frequency stabilization of a mode-locked semiconductor laser. *Optics InfoBase Conference Papers*, Part F75-A, 2017.
- [38] Tobias J. Kippenberg, Alexander L. Gaeta, Michal Lipson, and Michael L. Gorodetsky. Dissipative kerr solitons in optical microresonators. *Science*, 361, 2018.
- [39] P. Del’Haye, T. Herr, E. Gavartin, M. L. Gorodetsky, R. Holzwarth, and T. J. Kippenberg. Octave spanning tunable frequency comb from a microresonator. *Physical Review Letters*, 107:1–4, 2011.
- [40] T. J. Kippenberg, R. Holzwarth, and S. A. Diddams. Microresonator-based optical frequency combs. *Science*, 332:555–559, 2011.
- [41] Martin H. P. Pfeiffer, Clemens Herkommer, Junqiu Liu, Hairun Guo, Maxim Karpov, Erwan Lucas, Michael Zervas, and Tobias J. Kippenberg. Octave-spanning dissipative kerr soliton frequency combs in si_3n_4 microresonators. *Optica*, 4:684, 2017.
- [42] J. D. Jost, E. Lucas, T. Herr, C. Lecaplain, V. Brasch, M. H. P. Pfeiffer, and T. J. Kippenberg. All-optical stabilization of a soliton frequency comb in a crystalline microresonator. *Optics Letters*, 40:4723, 2015.
- [43] T. Kobayashi, H. Yao, K. Amano, Y. Fukushima, A. Morimoto, and T. Sueta. Optical pulse compression using high-frequency electrooptic phase modulation. *IEEE Journal of Quantum Electronics*, 24:382–387, 1988.
- [44] Ulrich L Rohde, Enrico Rubiola, and Jerry C Whitaker. *Microwave and wireless synthesizers: theory and design*. John Wiley & Sons, 2021.

- [45] Gianni Di Domenico, Stéphane Schilt, and Pierre Thomann. Simple approach to the relation between laser frequency noise and laser line shape. *Applied optics*, 49(25):4801–4807, 2010.
- [46] R W P Drever, J. L. Hall, F. V. Kowalski, J. Hough, G. M. Ford, A. J. Munley, and H. Ward. Laser phase and frequency stabilization using an optical resonator. *Applied Physics B*, 31:97–105, 1983.
- [47] Eric D. Black. An introduction to pound–drever–hall laser frequency stabilization. *American Journal of Physics*, 69:79–87, 2001.
- [48] Lawrence Trask, Ricardo Bustos-Ramirez, Michael Plascak, and Peter Delfyett. Noise performance of filtered optical frequency combs. In *CLEO: Applications and Technology*, pages JW2A–74. Optica Publishing Group, 2019.
- [49] Lawrence Trask, R Bustos-Ramirez, C Shipurkar, SV Pericherla, and Peter J Delfyett. Hyperfine filtering of an electro-optic modulated comb. In *2020 IEEE Photonics Conference (IPC)*, pages 1–2. IEEE, 2020.
- [50] X Steve Yao and Lute Maleki. Optoelectronic microwave oscillator. *J. Opt. Soc. Am. B*, 13:1725–1735, 8 1996.
- [51] Etgar C Levy, Moshe Horowitz, and Curtis R Menyuk. Modeling optoelectronic oscillators. *JOSA B*, 26(1):148–159, 2009.
- [52] X. Steve Yao and Lute Maleki. Multiloop optoelectronic oscillator. *IEEE Journal of Quantum Electronics*, 36:79–84, 2000.
- [53] Danny Eliyahu, Kouros Sariri, Joseph Taylor, and Lute Maleki. Optoelectronic oscillator with improved phase noise and frequency stability. *Photonic Integrated Systems*, 4998:139, 2003.

- [54] Danny Eliyahu, David Seidel, and Lute Maleki. Rf amplitude and phase-noise reduction of an optical link and an opto-electronic oscillator. *IEEE Transactions on Microwave Theory and Techniques*, 56:449–456, 2008.
- [55] Marcus Bagnell, Josue Davila-Rodriguez, and Peter J. Delfyett. Millimeter-wave generation in an optoelectronic oscillator using an ultrahigh finesse etalon as a photonic filter. *Journal of Lightwave Technology*, 32:1063–1067, 3 2014.
- [56] Dmitry Strekalov, David Aveline, Nan Yu, Robert Thompson, Andrey B. Matsko, and Lute Maleki. Stabilizing an optoelectronic microwave oscillator with photonic filters. *Journal of Lightwave Technology*, 21:3052–3061, 12 2003.
- [57] Lawrence Robert Trask, Srinivas Varma Pericherla, Chinmay Shirpurkar, and Peter J Delfyett. Generation and stabilization of a terahertz spanning electro-optic modulated oscillator comb. *IEEE Photonics Technology Letters*, 2023.
- [58] Ryan C Terrien, Joe P Ninan, Scott A Diddams, Suvrath Mahadevan, Samuel Halverson, Chad Bender, Connor Fredrick, Fred Hearty, Jeff Jennings, Andrew J Metcalf, et al. Broad-band stability of the habitable zone planet finder fabry–pérot etalon calibration system: Evidence for chromatic variation. *The Astronomical Journal*, 161(6):252, 2021.
- [59] Dimitrios Mandridis, Ibrahim Ozdur, Marcus Bagnell, and Peter J Delfyett. Free spectral range measurement of a fiberized fabry–perot etalon with sub-hz accuracy. *Optics Express*, 18(11):11264–11269, 2010.
- [60] Ibrahim Ozdur, Sarper Ozharar, Franklyn Quinlan, Sangyoun Gee, and Peter Delfyett Jr. Improved technique for high precision fsr measurement. In *Enabling Photonics Technologies for Defense, Security, and Aerospace Applications IV*, volume 6975, pages 57–67. SPIE, 2008.

- [61] Takashi Inoue and Shu Namiki. Pulse compression techniques using highly nonlinear fibers. *Laser & Photonics Reviews*, 2(1-2):83–99, 2008.
- [62] Linn F Mollenauer, Roger H Stolen, and James P Gordon. Experimental observation of picosecond pulse narrowing and solitons in optical fibers. *Physical Review Letters*, 45(13):1095, 1980.
- [63] Govind P Agrawal. Nonlinear fiber optics. In *Nonlinear Science at the Dawn of the 21st Century*, pages 195–211. Springer, 2000.
- [64] Christophe Finot, John M Dudley, Bertrand Kibler, David J Richardson, and Guy Millot. Optical parabolic pulse generation and applications. *IEEE Journal of Quantum Electronics*, 45(11):1482–1489, 2009.
- [65] Dan Anderson, M Desaix, M Lisak, and Manuel L Quiroga-Teixeiro. Wave breaking in nonlinear-optical fibers. *JOSA B*, 9(8):1358–1361, 1992.
- [66] N J Doran and David Wood. Nonlinear-optical loop mirror. *Opt. Lett.*, 13:56–58, 1 1988.
- [67] M E Fermann, F Haberl, M Hofer, and H Hochreiter. Nonlinear amplifying loop mirror. *Opt. Lett.*, 15:752–754, 7 1990.
- [68] B-E Olsson and Peter A Andrekson. Extinction ratio improvement using the nonlinear optical loop mirror. *IEEE photonics technology letters*, 7(1):120–122, 1995.
- [69] Andrew M Weiner. *Ultrafast optics*. John Wiley & Sons, 2011.
- [70] William S Wong, Shu Namiki, Mordechai Margalit, Hermann A Haus, and Erich P Ippen. Self-switching of optical pulses in dispersion-imbalanced nonlinear loop mirrors. *Optics letters*, 22(15):1150–1152, 1997.

- [71] Lawrence Robert Trask, Srinivas Varma Pericherla, and Peter J Delfyett. Towards an all-fiberized ghz self-referenced electro-optic-modulated comb. In *2022 Conference on Lasers and Electro-Optics (CLEO)*, pages 1–2. IEEE, 2022.
- [72] L Stampoulidis, K Vyrsoinos, P Bakopoulos, G Guekos, and H Avramopoulos. Optical pulse compression in a polarization insensitive non-linear loop mirror. *Optics communications*, 238(1-3):105–111, 2004.
- [73] KR Tamura and M Nakazawa. A polarization-maintaining pedestal-free femtosecond pulse compressor incorporating an ultrafast dispersion-imbalanced nonlinear optical loop mirror. *IEEE Photonics Technology Letters*, 13(5):526–528, 2001.
- [74] VR Supradeepa, Yan Feng, and Jeffrey W Nicholson. Raman fiber lasers. *Journal of Optics*, 19(2):023001, 2017.
- [75] Vincent Kuhn. Near diffraction limited high-power narrow-linewidth er3+-doped fiber amplifiers: developments towards laser sources at 1.5 [μ m] wavelength for gravitational wave astronomy. 2011.
- [76] Daniel C Cole, Scott B Papp, and Scott A Diddams. Downsampling of optical frequency combs. *JOSA B*, 35(7):1666–1673, 2018.
- [77] Pavel Sidorenko, Walter Fu, and Frank Wise. Nonlinear ultrafast fiber amplifiers beyond the gain-narrowing limit. *Optica*, 6(10):1328–1333, 2019.
- [78] Goëry Genty, Ari T Friberg, and Jari Turunen. Coherence of supercontinuum light. *Progress in Optics*, 61:71–112, 2016.
- [79] John M. Dudley, Goery Genty, and Stephane Coen. Revmodphys.78.1135. *American Physical Society*, 78:1135–1184, 2006.

- [80] Kieran F Lamee, David R Carlson, Zachary L Newman, Su-Peng Yu, and Scott B Papp. Nanophotonic tantalum waveguides for supercontinuum generation pumped at 1560 nm. *Optics Letters*, 45(15):4192–4195, 2020.
- [81] David R Carlson, Daniel D Hickstein, Alex Lind, Judith B Olson, Richard W Fox, Roger C Brown, Andrew D Ludlow, Qing Li, Daron Westly, Holly Leopardi, et al. Photonic-chip supercontinuum with tailored spectra for counting optical frequencies. *Physical Review Applied*, 8(1):014027, 2017.
- [82] Yoshitomo Okawachi, Mengjie Yu, Jaime Cardenas, Xingchen Ji, Michal Lipson, and Alexander L Gaeta. Coherent, directional supercontinuum generation. *Optics Letters*, 42(21):4466–4469, 2017.
- [83] Arslan S Raja, Junqiu Liu, Nicolas Volet, Rui Ning Wang, Jijun He, Erwan Lucas, Romain Bouchandand, Paul Morton, John Bowers, and Tobias J Kippenberg. Chip-based soliton microcomb module using a hybrid semiconductor laser. *Optics Express*, 28(3):2714–2721, 2020.
- [84] TG Tiecke, KP Nayak, Jeffrey Douglas Thompson, T Peyronel, Nathalie P de Leon, V Vuletić, and MD Lukin. Efficient fiber-optical interface for nanophotonic devices. *Optica*, 2(2):70–75, 2015.